The Ceiling Method for the Growth of High Resolution Protein Crystals

PROEFSCHRIFT

ter verkrijging van de graad van doctor
aan de Radboud Universiteit Nijmegen,
op gezag van de rector magnificus prof. mr. S.C.J.J. Kortmann,
volgens besluit van het college van decanen in het openbaar te verdedigen
op woensdag 4 juni 2014
om 13.30 uur precies

door

Alaa Adawy Mohamed Hassan

Geboren op 24 augustus 1982
te Al-Dammam, Koninkrijk Saoedi-Arabië

Promotoren:	Prof. dr. Elias Vlieg Prof. dr. Willem J. de Grip
Copromotor:	Dr. Willem J. P. van Enckevort
Manuscriptcommissie:	Prof. dr. ir. Jan C.M. van Hest Prof. dr. Piet Gros (Utrecht Universiteit) Dr. Dominique Maes (Vrije Universiteit Brussel, België)

Afgedrukt door: Ipskamp Drukkers, Enschede, Nederland.

The Ceiling Method for the Growth of High Resolution Protein Crystals

Doctoral Thesis

to obtain the degree of doctor
from Radboud University Nijmegen
on the authority of the Rector Magnificus prof. dr. S.C.J.J. Kortmann,
according to the decision of the Council of Deans
to be defended in public
on Wednesday, June 4, 2014
at 13.30 hours

by

Alaa Adawy Mohamed Hassan

Born on August 24, 1982
in Al-Dammam, Kingdom of Saudi Arabia

Supervisors:	Prof. dr. Elias Vlieg Prof. dr. Willem J. de Grip
Co-supervisor:	Dr. Willem J. P. van Enckevort
Doctoral Thesis committee:	Prof. dr. ir. Jan C.M. van Hest Prof. dr. Piet Gros (Utrecht University) Dr. Dominique Maes (Free University Brussels, Belgium)

The project, upon which this thesis is based, is funded by The Netherlands Foundation for Scientific Research through its Chemical Council (NWO-CW, project 700.57.022).

Cover design by Alaa Adawy:
Confocal laser fluorescence micrographs for Rhombohedral bovine insulin ceiling (front) and batch (back) crystals grown in the presence of fluorescent-labelled monomers (both shown at the same magnification).

Acknowledgement

In my opinion, the method developed in this thesis: "the ceiling method" represents an evidence that Allah created nature for our comfort with all its facilities. But, it is the way how we value and exploit this grace that makes the big difference. So, all my praise goes to Allah for his grace and also for putting me among very nice people who definitely deserve my gratitude, respect and sincere love.

Professor Elias Vlieg, I would like to deeply thank you for all what you have done for me. From the first contact we had together through a very short message. I even for some reason didn't enclose my CV and you replied by asking me to send it! You could have just ignored my message, but you took me seriously and asked me to come for an interview. Far away in Cairo, everyone around told me "don't do it", but I insisted on giving myself this opportunity and I didn't regret! When I saw you on 26-02-09, I felt how a gentleman you are! How much all members of the group appreciate and like you! This was the most apparent thing I observed, which is a very important factor for a good working and friendly atmosphere. You are always very caring about co-workers, very early every morning, executing top quality research, head of two departments and the whole IMM, participating in conferences worldwide and have never been seen complaining! I am proud that I was among your PhD students.

Professor Wim de Grip, we met later in October 2009. You are always very kind and caring. You permitted me to explore more deeply in the biochemistry world. In Egypt, I didn't have the opportunity to perform many of the biochemical experiments which I did under your supervision. Yet, you trusted me and encouraged me to try and retry and turn my theoretical knowledge to a practical one. I will never forget this day 20-05-11, when you accompanied me to the slaughter house to bring cow eyes to start our purification of the membrane protein opsin. The whole day I was wondering, how active and cooperative you are! You did everything with me! A 65+ professor performs all the experiment with his student! Also, you always allow me to be myself and respect my views. I remember it when you sent me, during the weekends or late in the evening, information or answers to my questions or even just suggestions I was always speechless and only wish to have at least few percent's of your faithfulness to your career. Dear professor Wim, I am really

indebted to you and it was a great honour to work under your supervision.

Dr. Willem van Enckevort, the expert! your fond of birds and astronomy actually reflects how much you are attached to the nature. Surely, your contemplation every night through your telescope has widened your horizon not only to be a good observer of nature, but also to be fond of abstracting every phenomenon or process in the form of equations. It was a very special and challenging opportunity to work under your guidance. You were always trying to be kind. Thank you very much!

Having three supervisors and myself from quite different disciplines was really very challenging. I always felt that I have to merge your different perspectives together with mine. This was not always easy, actually sometimes very exacting... Nevertheless, I really appreciate your support. Because of your continual encouragement my dear supervisors, I got great opportunities to attend summer schools In Granada (Spain), Erice (Italy) and Grenoble, France. I also got nice opportunities to present my research in Utrecht and Veldhoven (Netherlands), Glasgow and London (UK) Huntsville (USA), Louvain (Belgium) and Strasbourg (France). These trips as well as all expenses of my research were funded by NWO, to which I am really grateful. For sure, science is not money, but it cannot stand without an adequate financial support. Indeed, these trips had a big impact on my research and I am happy that I extended my network worldwide.

I also appreciate the chance of the scientific collaboration with Dr. Alexander van Driessche from the group of Professor Juan Gavira-Ruiz, Granada University, Spain. Alexander, I wish I could continue our cooperation; it was shortage of time and other project goals that made this difficult. My dear colleagues from the University of Gothenburg, Sweden: Dr. Susanna Törnroth-Horsefield and Dr. Etienne Rebfutte, from the group of Professor Richard Neutze. I did my main cryocrystallography at your laboratories and freely used your diffractometer. I joined your trips to ESRF beamlines. I sincerely thank you for everything! I had another successful collaboration with the group of protein crystallography at the University of Groningen conducted through Johan Hekelaar and Dr. Andy-Mark Thunnissen to whom I am really grateful as well. The collaborations extended outside universities and I had also a collaboration with National Translational Research Center (NTRC), Oss, The Netherlands. I would like to thank Dr. Guido Zaman, Dr. Joost Uitdehaag and Nicole Seegers for this nice work (to be continued).

I have had very nice time at the department of solid state chemistry. I learned that everyone can be helpful and useful for others.

Dr.Hugo, I had very nice discussions with you in the very beginning! You were always there, listening by your heart, not only by ears as most people do. I wish I could run any scientific collaboration with you, perhaps in the future! Thank you very much!

Dr. Rene de Gelder, we rarely talked together, but you offered me my first opportunity to present my project outside our group, I am really indebted to you!

I cannot mention "assistance" without mentioning **Elizabeth**, not only as the department

secretary, but as a very kind friend who cares for others and offer help with love. I had very nice with your family as well: Karim (the very gentleman), Abdulkarim and Amir who gave me the honour of practising my skills as an Arabic language teacher. Thank you all so much!

Jan van Kessel, when I started at VSC, you was the ONE to be asked about any technical issues. Afterwards, we become friends especially with your nice wife Paulien. The three of us had very nice time chit chat and trying meals from each other cultures. Thanks for the great time we had together.

Erik de Ronde, you are a real value-added to your position. I learned a lot from your information and suggestions. Sometimes, I was stressed out and need some support or even need an advice, I always felt comfortable when you were around. Your absence in the period October 2012 -January 2013 was very painful for the whole department. We missed you, and I was extremely happy that you are back, stronger and still with your positive attitude. I am really indebted to you. Thanks for everything.

Wil Corbeek, I don't really know how to express my gratitude to you! Indeed, you are a talented technician. You helped me in PSI setup and the development of the ceiling crystallization growth cell. I wish I could ask for more, "niet want ik ben nooit tevreden", but I really enjoyed dealing with you and watching your golden hands. Thank you very much!

Wiesiek, from the beginning, you were the one who come with very useful ideas and information that others may think that they are obvious, but they were really very helpful. I really appreciate this very much, you were always very kind.

Of course I cannot forget **Jan Smits**! We did one experiment together and he was really great. May he rest in peace.

While working at the solid state chemistry department, I had through the years many colleagues between post docs, PhD students, M.Sc. students and B.Sc. Students. You guys have created a very nice atmosphere at work, but also during all the social activities we had together. We were like a big team in which every player has his magic touch! **Vedran**, your Dutch accent was very good for a beginner like me :D **Wim Noordin**, thanks for the "gezeligheid" and your help in building my first snowman ;) **Paul Tinnemans**, I cannot mention you without Rafke! Thanks for the "gezeligheid" and help! I still remember it when you decided to bike with me to help me carrying more staff home! **Rienk**, the first colleague for me ever with articles published in Nature. **Fieke**, the active athletic cool girl, thanks for the nice time we had together. **Rita**, the modalist:) I enjoyed most of the discussions we had together at breaks or after working time, you are always trying to care and help, thank you very much! **Laura**, we had great time together, chit chat, practising Dutch while learning Arabic, hanging out... We were both patient toward our mistakes in Dutch: no fears, no one laugh at my hilarious pronunciation :) Yours for sure is much more better! **Rene Steendam**, the quietly confident guy who has a lot to offer. **Wester**,

you are always different with your very special sense of humour! *"ha ha haaa..."* **Eline**, the very kind and caring colleague, I still remember it when you gave me a surprise cake and in the heavy time you were always trying to make it easier... **Stelian**, comfortable like a brother, I will never forget the surprise birthday party. **Arno**, the wikiman, I want to tell you that together with your successor **Ellie**, Rita and Eline, we started our football table practice! It is indeed a lot of fun :)

I would like also to thank all the rest of students, especially **Esther**, **Mireille**, **Iris**, **Kess** and **Leyla** for the nice time, discussions and cooperation.

I also learned that the solid state chemistry department is one state of the united states of VSC-AMS. So, I really would like to thank all members of AMS, specially **Dr. John**, **Günther**, **Gerbe** and **Joep**, for the help and de gezeligheid!

I spent long time working at the biochemistry department, RIMLS. I would like to thank all members of the group of Professor Roland Brock for the nice working and cooperative atmosphere. In particular, I would like to sincerely thank **Petra Bovee-Geurts** for all the technical help she offered and the step by step instructions for protein purification.

I would like also to thank **Dr. Elisabeth Pierson** from the department of general instrumentation for all the help she offered during my confocal fluorescence microscopy measurements. She was always very kind and cooperative...

In Egypt I used to have a lot of friends and one family, but in Nijmegen, surprisingly I have few friends, but many families!

As much as I am indebted to Vlieg the Professor, I am also indebted so much to Vlieg the family: **Mrs. Annemieke, Hedwich, Elger and Redmar**. Thank you very much for your great hospitality and care. Professor Elias, your words: *I will come and take you from home and return you back. I won't feel comfortable to let you go alone in the dark*, is my current definition for a man behaviour!

Ciecel Rutten, for me you were more than a lessor! Despite all the differences between us, we managed not only to co-exist, but also to be friends. You offered me a lot of help during my stay at your home, and even after... You introduced me also to you best friends Frans and Hannie, who are also a big value-added to my experience in Nijmegen... I am really indebted to you all.

Ellen Bakker, I wish you could see my words and attend my thesis defence. We had very nice time together... You offered your help and time despite your very busy schedule. I was also so proud to teach you Arabic. I wished that the time would come when you are professional in this language and start teaching it using your fantastic teaching skills. Our last meeting in Amsterdam together with your partner Rien is unforgettable. We planned another appointment, but the fate prevented it... Ellen, I really miss you so much... and hope that you are now resting in peace in a much better place...

The Netherlands is one of the countries with the highest percentage of foreigner residents. This offered me the chance not only to know about the Dutch culture, but also

very many different cultures. I would like to thank all my international acquaintances and friends, whom I met during the attendance of Dutch courses, conferences, social activities and at the university. I really want to sincerely thank **Norbert**, **Sohani**, **Mikhail** and **Therese** ... We were and will be always there for each other.

I cannot also forget the nice time I had with my Egyptian-Dutch acquaintances in Nijmegen: **Rania** and the families of Mr. **Shahin** and Mr. **El-Sharkawy**... Being in your company was always very pleasant and acted as a pain killer against any sense of alienation.

I would like to thank all the professors and colleagues in Egypt who were always supporting and wishing for me success.

In Egypt many friends were always there for me: ready to listen and offer help. **Sarah Abbas, Marwa Farouk, Hend Awad, Eman Aly, Mohamed Ali, Ibraheem Gamal and Mohamed Hussein**, thank you all very much!

Sayed Abo El-Dahab, you offered your time and support to help me achieving one of my delayed goals: memorizing Quran... Thank you very much!

Tarek Elkhooly and **Mohamed Essam**, my colleagues in Germany and Sweden, we were exchanging all ups and downs including the occasional very horrible sense of alienation... I always felt that my brothers were around.

In the very stressful time, I found you! A precious piece of diamond glowing with encouragement and support... **Zakariae**, I am really indebted to you!

I hope that I haven't unintentionally forgotten anyone, but indeed all the nice people I have in my life wouldn't have been existing in good shape without well functioning proteins running in their beings without being crystallized! Generally, I am grateful to them all, in particular, those of which have been welling to crystallize and provide me with nice results :) But also, I am indebted to the other challenging proteins which kept me busy learning and determined to solve their mystery!

All chocolate bars that ended in my belly :D I cannot imagine how these years with all the *downs* would have been without having access to you! Rest in peace my dears :D

All my sincere love and endless gratitude go to my great family. My siblings: **Ayat, Shaymaa, Mohamed, Asmaa, Anas, Basel and Mariam** and my brothers in law: **Hesham and Mohamed Noureldin**, we are a BIG team. Despite the distance, we are in contact on an almost daily basis. We are like open books to each other...Sometimes people claim that in every person life there are a *blood* family and a *soul* family... We indeed are a family with the *dual* meaning of the word.

My nephew **Mohamed Hesham** and my nieces **Layla, Serien and Larien**, when you get older, you will probably read these words and you will know how much you kept me happy in every moment we were together, even online! Mohamed, your smart questions were always inspiring for me... I hope that your generation will succeed in achieving what ours failed to achieve for **Egypt**...

The core, my parents, the real hero's of my life, it would have never been the way it is without you **Mama** and **Papa**... These years had a lot of cheers, but also sadness for us all. Despite everything, I always feel your concrete support which is always full of care, passion and love. I will be indebted to you forever... From the bottom of my heart, I would like to sincerely thank you and ask you to forgive me for any moment passed in my life which didn't meet your great expectations. If I could dedicate this thesis to anyone, I would indeed write:

This thesis is dedicated to my lovely parents.

Alaa

Contents

Chapter 1

Introduction

1.1 Motivation

Studying living tissues and how they undergo their development and maintenance, how the molecules in these processes are actually formed, how their structures look like and how they function, are questions addressed by the disciplines biochemistry, biophysics and structural biology. Precise answers to these queries are not possible without complete determination of the three-dimensional structure of the involved biological macromolecules. Otherwise, the structure-function relationships would always be ambiguous. Macromolecular crystallographers have been trying to determine precise macromolecular structures since the 1950s. In 1962, Max Perutz and Sir John Cowdery Kendrew were awarded the Nobel prize in Chemistry for their successful attempt to solve the structure of sperm whale myoglobin [1]. This, in turn, encouraged many structural biologists to solve the structure of many other biological macromolecules. According to the protein data bank, PDB, 90611 structures of proteins, nucleic acids and other biological macromolecules have been determined [1]. Most of these structures (92.2%) were solved using X-ray diffraction (XRD). Other methodologies such as nuclear magnetic resonance (NMR), electron microscopy (EM) and neutron diffraction have contributed in solving the remaining structures.

Solution-state NMR - the first alternative for XRD - is restricted to small macromolecules within the range of 70 KDa. For measurements, aqueous samples up to about 300-600 μl of highly purified protein, labelled with stable isotopes (^{15}N,^{13}C), with a relatively low protein concentration (0.1-3 μM) in a buffer solution, adjusted to the desired solvent conditions, are prepared in a thin walled glass tube. The collected data provide information on the structure and dynamics of proteins under investigation. EM (also called

[1] as per 14-05-2013

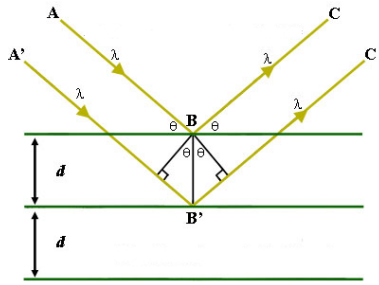

Figure 1.1: Bragg's reflection law. The diffracted X-rays exhibit constructive interference when the distance between paths ABC and A'B'C' differs by an integer number of wavelengths (λ) [2].

Cryo-EM), on the other hand, studies protein samples at cryogenic ($100K$) temperatures without changing their native surroundings. Yet, the accomplished resolution (precision) of cryo-EM maps is not high enough yet to allow for unambiguous model construction of the studied proteins. Because of the size restriction for NMR and low resolution of EM, scientists still rely on collecting data not from single macromolecules, but from an array of this macromolecule identically arranged in all three (or two) spatial dimensions, i.e. a crystal. In this way, the signal is much stronger and the error (so-called noise to signal ratio) is set to a minimum. In order to allow for this 3D (or 2D) assembly of molecules, i.e., crystallisation, the protein is placed in non-physiological environments, which can *occasionally* lead to small conformational changes. A beam of rays can then be directed toward this crystal and because of the interaction with all its elements (electrons or nuclei), the rays undergo *diffraction* into many specific directions if the size of these elements is comparable with the wavelength of the incident beam, such that:

$$n\lambda = 2dsin\theta \tag{1.1}$$

where n is an integer representing the order of diffraction; λ is the wavelength of the incident beam; d is the spacing between the adjacent planes in the crystalline lattice; and θ is the angle between the incident beam and the scattering planes. Equation 1.1 is known as Bragg's law (Fig.1.1).

A *crystallographer* measures the angles and intensities of the diffracted beams, and produces a three-dimensional picture of the electron/nuclei density within the crystal. From this density map, the mean positions of the atoms in the crystal can be determined, as well as their chemical bonds, their disorder and various other properties.

Depending on the beam source, several methods have been accomplished. In neutron diffraction, the least used method, a beam of neutrons interacts directly with the nuclei

within the crystal under investigation. The main advantages of this technique are the sensitivity to light atoms, the ability to distinguish isotopes and absence of radiation damage [3]. For neutron diffraction, relatively large protein crystals (about 0.5-1 mm^3) are required to give good resolution, which are usually challenging to grow.

In X-ray crystallography, fortunately, 10 times smaller crystals (20-100 μm) than those required for neutron diffraction are sufficient. During diffraction, X-rays interact with the electron clouds surrounding the nuclei and, therefore, the diffraction intensity is directly related to the atomic number (Z) of the atoms. Unlike neutron diffraction, XRD is not sensitive to hydrogen atoms, yet their positions within the macromolecule can be estimated during XRD data processing. An intrinsic problem of X-rays is the radiation damage. Cooling the crystals down to cryogenic temperatures (so called cryoprotection) increases the crystal lifetime, but even the prolonged exposure time is often insufficient for the collection of a complete data set from a single crystal. Later, scientists have developed intense and tunable X-ray beams produced by synchrotron radiation facilities, which provide highly intense radiation and thus complete data sets can be collected in one-tenth the time required for achieving this task using a conventional X-ray tube.

Nevertheless, cryoprotection induces long range disorder within the crystals (so called mosaicity) with a concomitant probability of icing. These effects adversely affect the final quality of the resultant diffraction pattern.

Very recently, a very powerful new source known as *the X-ray free-electron laser* (XFEL) has been introduced to overcome the above mentioned problems by providing incredibly intense pulses of X-rays (up to 10^{13} photons) in a duration of about ten femtoseconds (10^{-14} s). These XFEL pulses allow for using nanocrystals and collecting diffraction data at room temperature. Yet, the degree of precision (resolution) for their example (5.7Å) is still far lower than that collected using synchrotron radiation (1.9Å) [4]. Better results are reported when the nancrystals were crystallised *in vivo* [5], which in turn is not yet a widely applicable crystallisation technique.

Therefore, still the large majority of crystallographers rely on X-ray crystallography in their determination of the macromolecular structure of proteins and other biological molecules. For this, the growth of high quality protein crystals ($\approx$ 20-100 μm) is a prerequisite to apply this methodology.

1.2 Protein Crystallisation

Protein crystallisation is the basis for X-ray crystallography. The ultimate aim of macromolecular crystallography is to produce a model of the macromolecule of interest which

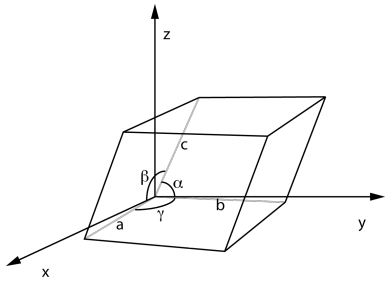

Figure 1.2: Unit cell parameters.

interprets the diffraction images. Proteins, like many molecules, can be prompted to form crystals when placed under the appropriate conditions. During crystallisation, the purified protein undergoes slow precipitation from an aqueous solution. As a result, individual protein molecules align themselves in a repeating series of *unit cells* by adopting a consistent orientation (Fig. 1.2) The resultant crystalline "lattice" is held together by non-covalent interactions [6].

After the growth of a sufficiently big crystal, the crystal is *fished* from its mother liquor, immersed in a cryoprotectant, frozen by being immersed in liquid nitrogen (cryoprotected) and used for XRD experiments. The acquired images of the diffraction patterns are processed by using iMOSFLM [7] or other equivalent software in order to get the Bragg's peaks and the associated integrated intensities (I). An estimate for the crystal lattice parameters ($a, b, c, \alpha, \beta, \gamma$), mosaicity and symmetry elements (how the molecules are related to each other) are provided at this stage. Diffraction results in a set of deflected beams, which are characterised by different amplitudes and phases. The amplitude is easily determined because it is $\propto \sqrt{I}$. By measuring intensities the phase of each Bragg peak is lost, but it can be retreived using for instance the *CCP4* suite [8]. The resultant model can be refined and validated before being deposited in the protein data bank (Fig. 1.3).

The accuracy of the structure determination depends on the maximum scattering angle that still has an acceptable signal to background ratio. Following Bragg's law, a maximum scattering angle θ corresponds to a minimum d spacing, which is the minimum size of the structural details that can be resolved. The larger the θ, the more the details are resolvable. For protein crystallography, the terms *low* (>6 Å), *moderate* (6-2 Å) and *high* (<2 Å) are used for different levels of resolution (Fig.1.4). Resolution is a parameter which depends mainly on the quality of the crystal; it influences and *limits* all the subsequent data processing for building the macromolecular model. Thus, the growth of high quality crystals which eventually provide a high quality X-ray diffraction pattern is the bottleneck for protein structure determination.

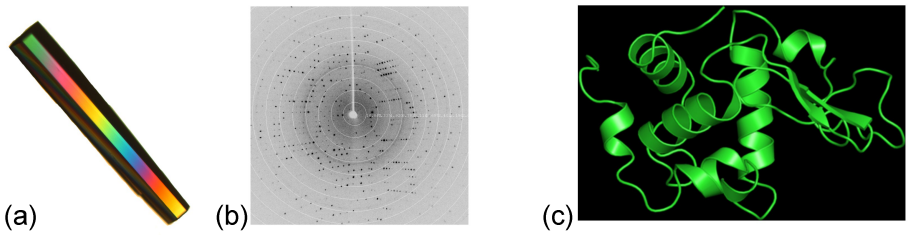

Figure 1.3: Hen egg-white lysozyme (HEWL) crystallised into a high quality monoclinic crystal (a). An X-ray diffractometer was used to record diffractograms (b), which can be used to solve the 3D macromolecule structure as shown in the model built using *Coot* [9] (c).

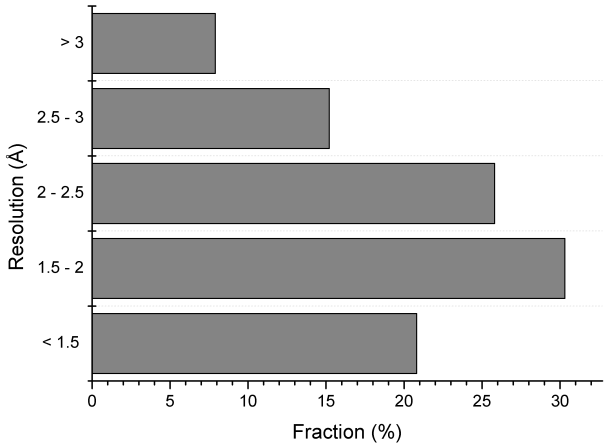

Figure 1.4: The fraction of the solved biological macromolecules (relative to the total number of solved structures) as a function of their accomplished resolution, as per 14-05-2013.

Indeed, protein crystallisation is still an exacting and difficult task compared to many other compounds. The nucleation and growth of protein crystals of high quality requires conditions close to those for getting amorphous aggregates. Good knowledge of the physico-chemical properties of the target protein (its isoelectric point, compatible buffer and precipitant, etc.) is important before proceeding with any crystallisation trials. Most proteins are not available in large quantities and therefore they require being expressed and afterwards isolated from genetically engineered sources at high purification levels in order to be usable for crystallisation trials. The process is twice as difficult for membrane proteins, because of their hydrophobicity and limited stability in detergents. If the factors influencing the target protein are known, controlled supersaturation can be obtained either instantaneously by direct mixing of the protein with the excess precipitant or gradually

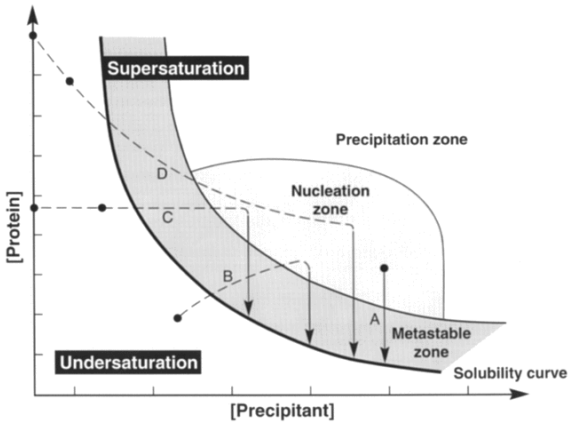

Figure 1.5: A schematic drawing of a protein crystallisation phase diagram based on two of the most commonly varied parameters, protein and precipitant concentrations. The four major crystallisation methods are indicated: (A) Batch crystallisation. (B) Vapour diffusion. (C) Dialysis. (D) Free-interface diffusion (also known as liquid/liquid diffusion). In all cases the system, starting from the black circles, needs to reach the nucleation zone, after which it makes its way through the metastable zone and eventually arrives at the solubility curve. Each method achieves this journey via a different route [11].

by allowing solvent evaporation, salting out, or adding an additive to change the physical environment [10]. In all cases, the aim is to decrease the protein solubility to induce nucleation and subsequent crystal growth, according to the phase diagram (Fig.1.5).

1.3 Crystallisation Methods

Several methods which have been developed to induce crystallisation of biological macromolecules are listed in Table 1.1. The methods vary from those providing predefined crystallisation conditions (bulk and batch methods), to those relying on the gradual variation of the supersaturation at the site of crystallisation (vapour diffusion). The latter can be also accomplished either by manual change of the precipitant concentration, pH or temperature (bulk dialysis and gradual change of temperature), or by slowly mixing of protein solution and precipitant solution, which are designed to be initially apart (free interface diffusion).

Among these methods, the vapour diffusion method is the one which, so far, has yielded the largest number of crystals, followed by the (micro-)batch and the dialysis techniques. This is not a deficiency of the latter two methods, but rather a tendency of the investigators to continue using the vapour diffusion method. This technique, with its different designs

of hanging drop, sitting drop and sandwich drop, has stayed on the throne of protein crystal growth since the sixties [12]. Despite its suspected inability to grow the best crystals, it is popular because of its cheap and easy setup. In addition, various solution parameters can be screened simultaneously using robots against a cost of only 1-10 μl of the valuable purified protein per trial. This explains the continued reliance on this simple and economical technique.

The (micro-)batch method provides the simplest approach to yield high quality crystals if the optimal crystallisation conditions are known. In addition, the micro batch configuration allows for screening at the cost of micro- to nanolitres of the target protein solution. The dialysis method, on the other hand, is only used when the growth of very large crystals for neutron diffraction experiments is required. The possibility of manipulating the conditions to keep the crystal growing is an advantage in this case, yet it is only useful if the crystal surface does not get blocked by impurities or misoriented protein molecules.

Handling protein crystals afterwards is not trivial either. Most protein crystals are small ($<$400 μm). They are very delicate and possess very poor mechanical properties and high solvent content (up to 80%). This watery nature together with their relatively large unit cells make them less ordered compared to e.g. inorganic crystals. In 1934, it was discovered that protein crystals examined in their mother liquor gave better diffraction patterns than dried crystals [13]. Since then, special care is given to maintain their hydration during crystallisation and X-ray measurements.

Despite the development of different techniques to crystallise biological macromolecules, the whole procedure is not always straightforward. The diffraction limit is usually too low to facilitate the determination of the protein macromolecular structure at sufficiently high resolution. Only about 1 % of the human proteins have been structurally studied. Unfortunately, this does not fit with the revolution in the development of X-ray and synchrotron sources, the accompanied data collection and analysis tools. This issue is more dramatic regarding membrane proteins, which represent less than 1.4 % of the solved protein structures [2], despite their importance in the cell proteome. In addition, the structure of almost half of the solved proteins are only determined to a resolution limit $>$2 Å. These challenges and the subsequent difficulty of determining the structures to a reliable level have turned protein crystal growth studies into a new independent discipline.

[2] Protein data bank as per 14-05-13

Table 1.1: Summary of the most common methods used in macromolecular crystallisation

Method	Main characteristic	Advantages	Disadvantages
Bulk crystallisation	Examine whether a protein is crystallisable	Acts as an extra purification step	Always yields microcrystals
Batch crystallisation	Predefined final crystallisation conditions	Easy and reproducible; Has been developed into the micro-batch method	Not suitable for proteins which require slow equilibration to achieve optimal growth
Bulk dialysis	Liquid-liquid interdiffusion with the possibility of continual fine tuning the physical and chemical environment during crystal growth	Growth of very large crystals	Not suitable for screening; Can be twice as slow as other methods when the system is near equilibrium
Free-interface diffusion	Liquid-liquid interdiffusion in capillaries; Suitable for microgravity conditions	Has been further developed to counter-diffusion using gel media and thus no microgravity is required	Not suitable for screening; gel is not suitable for all proteins
Vapour diffusion	Increase saturation of protein solution by evaporation	Extensively used in screening using hanging, sitting and sandwich drop configurations, because small amounts of protein are required	Uncontrolled Marangoni convection

1.4 Growth Kinetics & Impurity Incorporation

The difficulty of growing high quality crystals, capable of diffracting X-rays to high resolution limits is, in part, due to the many solution parameters -both chemical and physical- that must be taken into account. In addition, protein purity is a major factor in the success and reproducibility of crystallisation experiments [14]. Highly pure protein is a prerequisite, which is not easily accomplished even for commercially available globular proteins. The driving force for crystallisation ($\Delta\mu$) is the most important variable controlling the growth rate of crystals. $\Delta\mu$ is determined by the supersaturation, $ln(C/C_{eq})$, with C the actual and C_{eq} the equilibrium solute concentration, such that:

$$\Delta\mu = K_B T ln(C/C_{eq}) = K_B T \sigma \tag{1.2}$$

with K_B is the Boltzmann constant; T the absolute temperature and σ the supersaturation. This parameter needs to be finely tuned until a crystal of sufficient size (preferably $> 100\,\mu m$) is formed.

Unfortunately, protein crystals are also very sensitive to defects, which are formed partly because of fluctuations in the supersaturation in the vicinity of the growing crystals and partly due to the incorporation of impurities. To study quantitatively the impurity incorporation during protein crystal growth, knowledge of the diffusion coefficient (D), kinetic coefficient (β), and distribution coefficient (k) for both protein macromolecules and impurities is a prerequisite. The diffusion flux J ($mol/m^2 s$) is

$$\vec{J} = -D\vec{\nabla}C \tag{1.3}$$

where C is the concentration (mol/m^3). D depends on viscosity and temperature and it is around $10^{-11} - 10^{-10}$ m^2/s for proteins. β is the constant of proportionality between the normal crystal growth rate V and the supersaturation, assuming linear kinetics.

$$V = \beta\sigma \tag{1.4}$$

For impurities (i), β_i defines the trapping or the uptake of impurities into the growing crystal surface and its value is roughly inversely related to the molecular size of species and directly with its concentration. The tendency of an impurity to be incorporated during the crystallisation of specific macromolecules depends on the ability of this impurity to be adsorped on kinks, ledges and terraces on the surface of the growing crystal. In its simplest form, the impurity uptake, J_i is directly related to its concentration, C_i, at the direct vicinity of the crystal surface, such that:

$$J_i = \beta_i C_i \tag{1.5}$$

If we want to quantitatively describe the selective segregation (incorporation) of impurities of (in) a crystal, the volumetric distribution coefficient (k) must be determined. k is defined as the ratio of the impurity concentration in the crystal to that in the mother liquor immediately at the interface.

$$k = \frac{C_{i\ crystal}}{C_{i\ solution}} \tag{1.6}$$

Multiplying k by the ratio of the target protein concentration (p) in solution relative to that in the crystal, one obtains the surface distribution coefficient (K) [15].

$$K = k\frac{C_{p\ solution}}{C_{p\ crystal}} = \frac{C_{i\ crystal}/C_{p\ crystal}}{C_{i\ solution}/C_{p\ solution}} \tag{1.7}$$

Both k and K describe the relationship between the protein molecules and the accompanied impurities,[15]. K defines the actual purification upon crystal growth: if $K < 1$, purification occurs upon crystallisation; if $K > 1$, the crystal traps more impurities in the early beginning. k determines the impurity related process during crystal growth. For an impurity i, β_i and k are related through the crystal growth rate,

$$\beta_i = (k-1)V. \tag{1.8}$$

Therefore, if $k < 1$, β_i and thus the net impurity flux, J_i is negative. This implies that impurities are *repelled* during crystal growth, leading to their accumulation in the liquid adjacent to the advancing growth front. On the other hand, if $k > 1$, (as the case for most of structurally related and micro-heterogeneous impurities) β_i and thus J_i are positive and the growing crystal preferentially sequesters the impurity from the solution, which results in a depletion of impurities in the liquid ahead of the growth front. Impurity incorporation and defect formation can be much reduced if convection currents are suppressed [16].

1.5 Importance of Eliminating Convection

Crystal growth takes place by two consecutive steps: the transport of growth units towards the crystal, followed by their incorporation at the crystal surface. If the mass transport of the growth units toward the crystal surface is slow, the transported units are easily incorporated into a crystal surface position of high bond strength and vice versa. This

incorporation proceeds via the Terrace-Ledge-Kink model [17] as displayed in Fig.1.6. Slow mass transport is most likely the case when solution movements are suppressed, while the molecules are individually transported due to their concentration gradient from areas of high to low concentration. This is the so-called diffusive mass transport. If there is a sufficient time for all surface processes, the crystalline surface can easily discern foreign particles (impurities) and detach them by desorption.

However, in a fluid medium which encounters local changes in its concentration, like what a solution encounters at the interface of a growing crystal, convection currents can develop such that areas with lower concentration, and thus density, experience an up-thrust force due to gravity. This is known as natural or buoyancy-driven convection. In addition, the development of a surface tension gradient along the interface between vapour and solution, which in turn is induced by the development of solute concentration gradients, results in another type of convection, called Marangoni convection, even in the absence of gravitational forces. This occurs during the application of the vapour diffusion method.

In the presence of these convection currents, the two step process of crystal growth is easily disturbed and results in fast growth of less ordered crystals which comprise higher fractions of impurities. This is because the rapid convective mass transport continuously refreshes the crystal surface with bulk solution, which contains a relatively high concentration of target macromolecules, but also impurities and microcrystals. This produces instabilities in the crystal growth rate and induces local supersaturation fluctuations in the interfacial layer at the crystal surface. As a result, the target molecules may get randomly incorporated into the crystal surface. In addition, the solution flow enhances the interfacial supply of impurities that are incorporated into the crystal. This induces step bunching even in high purity solutions (99.9%) if the characteristic adsorption times of these impurities are comparable to the exposure times of the terraces between steps [18]. Even worse, at low growth rates, convection enhanced impurity transport can result in complete growth cessation.

In the absence of convection, the mass transport only occurs by diffusive flow. Then the supply of macromolecules is very slow compared to the incorporation /adsorption /desorption process at the crystal surface. In convection-free crystal growth, after nucleation, significant concentration gradients of all the mother liquor constituents develop around the growing crystal without leaving room for fluctuations. Thus, a macromolecule depletion zone develops, but also an impurity depletion zone if $k > 1$.

Regarding impurity incorporation, an impurity with $k > 1$ accumulates in the crystal core, but this in combination with diffusive mass transport enhances the development of an impurity depletion zone in the neighbourhood of the crystal. In this case, the incorporation

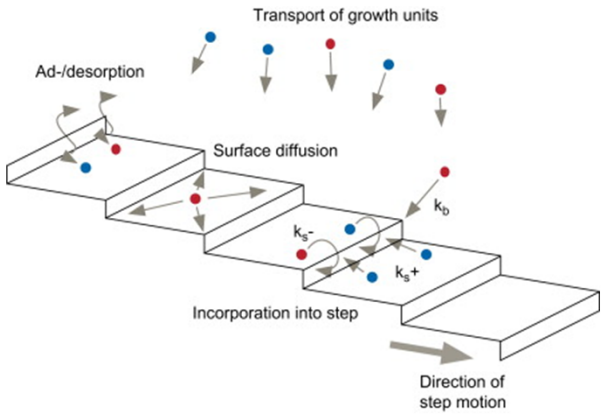

Figure 1.6: A schematic depiction of the mechanisms responsible for the growth of a crystalline surface from a solution. Growth units in the supersaturated liquid are transported to the crystal surface, where they adsorb at a terrace or incorporate directly into a step. Adsorbed growth units may desorb from or diffuse across terraces; they may also incorporate into a step entering its front or back side of the step. Symbols k_b, k_s+, and k_s- denote step kinetic coefficients for the incorporation of growth units from the bulk phase, the lower and the upper terraces, respectively [19]

of impurities is suppressed because of the effective decrease in their flux towards the crystal (Fig. 1.7). Consequently, the crystal can grow further more perfectly and diffracts X-rays to high resolution, unless harmful mosaicity is induced at the very beginning of nucleation [20].

On the other hand, an impurity with $k < 1$ allows crystals to grow with pure cores, because it is excluded from the crystal surface (Fig. 1.7). However, while the crystal grows, the target protein-depleted solution nearby the crystal becomes relatively impurity-rich and, therefore, impurities are more easily trapped into the growing lattice and distort it [21]. In this case, the early harvest of the protein crystal is advantageous. Beside the ability of diffusive mass transport conditions to reduce impurity incorporation, they also prevent sedimentation of microcrystals and polycrystalline growth.

In the presence of natural or Marangoni convection, the crystallisation solution is continuously mixed and no depletion zones develop. The consequent growth rate fluctuations and surface processes lead to less crystalline perfection as they are in the absence of convection. This fact led scientists to look for alternatives in order to eliminate convective mass transport and thereby reduce defect formation.

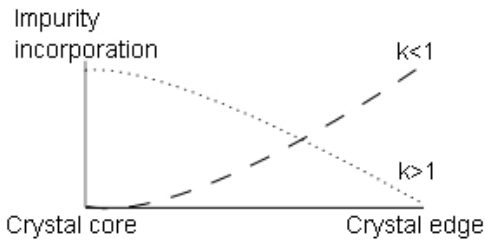

Figure 1.7: Schematic diagram for the relation between segregation coefficient and impurity distribution in the crystal during diffusion-limited growth.

1.6 Attempts to Eliminate Convection

Pointing out gravitational force as a main cause of poor crystal quality, scientists attempted to eliminate its effect in several ways as summarised in Table 1.2. In 1984, Littke and John conducted the first space microgravity experiment [22]. This was considered a great breakthrough, which was quickly published in "Science" as a paper displaying two optical microscope photos. Spacelab I experiments, conducted by the same group until 1988, involved the growth of two macromolecules: Lysozyme and beta-galactosidase [23]. Their report was positive since they observed the growth of larger single crystals. Following Littke's experiments, a number of investigations have been carried out which often resulted in high quality crystals.

Prior to space experiments, other attempts were conducted using capillary tubes and gels. In a capillary, liquid flow against gravity can be realised and thus protein crystals grow in microgravity resembling conditions. This is particularly useful if the macromolecule is too fragile to be transported from the growth cell to the X-ray capillaries or mounting loops [24]. Crystallisation in gels is another alternative in which a highly dense gel matrix counteracts the convection [25]. A series of low and high molecular weight proteins were investigated in gellified media [26] and the results were promising. Yet, the resolution of gel-grown crystals, on average, lies in between those of earth-grown and space-grown crystals [27, 28]. Nowadays, the implementation of gel growth is also investigated under microgravity.

Because of the restricted opportunities and access, space experiments still face a number of unsolved technical and conceptual problems. This explains the continued reliance of the crystallographers on earth-based growth techniques.

Table 1.2: Various methods to suppress convection

Method	Principle	Advantages	Disadvantages
Capillaries	In very narrow vials, the gravitational forces are low compared to solution-surface interaction forces	Requires a small volume of crystallisation solution	Difficulty of retrieving grown crystals, unless measured *in situ*
Crystallisation in gels	Prevents the onset of convection by soaking the crystallisation solution in a polymeric network	Diffusion coefficients of macromolecules are not significantly changed with respect to diffusion in gel-free media	Possible chemical interaction of the gel with solutes, including the target protein itself
Microgravity	Perform the experiment on board a spacecraft	Sedimentations are avoided; major reduction of buoyancy-driven convection	Very expensive; Marangoni convection is not abolished; limited opportunities
Hypergravity	Drastic change in convection and sedimentation, leading to local supersaturated zones of homogeneous entities	Crystallisation can occur in initially undersaturated solution	Due to increased shear stresses, resultant crystals suffer from plastic deformation
Magnetic field	Magnetic force neutralises gravitational field	Suppresses sedimentation and buoyancy-driven convection	Expensive; limited time span

One of these techniques that is capable of dampening the natural convection due to gravity is the use of magnetic fields. Wakayama reviewed the studies conducted on the effects of magnetic fields on protein crystal growth, and she claimed that magnetic fields could improve the quality of protein crystals through four mechanisms [29]. They can (i) magnetically align protein nuclei in the mother liquor and (ii) induce increase in solution viscosity. In addition, magnetic fields can (iii) dampen natural convection by the Lorentz force as well as (iv) by applying an upward magnetic force, to counteract the gravitational force, resulting in a lower gravity growth environment. Later, it was shown theoretically [30] and experimentally [31] that the levitation of the growth solution is not the correct condition to suppress convection. By exploiting gradient magnetic fields, it was shown that completely convection-free crystal growth can be accomplished, not only for inorganic compounds [32], but also for proteins [33]. Nevertheless, the high field strengths required for these diamagnetic protein molecules present an obstacle to generalise this technique. Moreover, the crystal and mother liquor respond differently to the magnetic field; Convection, a property of the fluid, and sedimentation, a property of the crystals, are not eliminated simultaneously, allowing, in principle, the evaluation of their individual importance in protein crystal growth [31].

1.7 Towards an Applicable & *Terrestrial* Microgravity

Despite the awareness of crystallographers of the consequences of working in gravity, they continue to hold on using the vapour diffusion [34] and micro-batch methods [35]. Not only do these methods effectuate buoyancy-driven convection, but the presence of a solution-vapour interface also induces Marangoni convection. Yet, the fact that they are accessible, not expensive and induce crystallisation explains their popularity among structural biologists (Fig. 1.8).

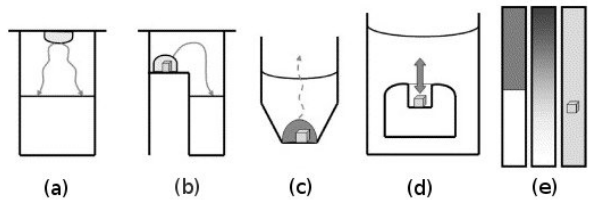

Figure 1.8: A schematic diagram of different commercially available crystallisation techniques: hanging drop (a) and sitting drop (b) vapour diffusion, microbatch (c), micro-dialysis (d), and counter-diffusion in a capillary tube (e) [36]

It was shown earlier through numerical simulations that Marangoni or surface tension driven convection is comparable if not more important in impact than natural or buoyancy driven convection [37]. Even by considering zero gravity, it was shown that the presence of Marangoni convection resulted in a disturbance in the isoconcentration lines in a manner similar to that observed at 1 $\times$ g without Marangoni effects. The ideal situation is if both buoyancy and surface tension driven convections are suppressed. Microgravity and related methodologies are not capable of suppressing the surface tension-induced convection introduced by concentration gradients at the liquid-vapour interface. This partly explains the frustrating results of microgravity experiments which yielded high resolution crystals in only 50 % of the conducted trials [38]. Compared to vapour diffusion, the micro-batch method has the advantage that Marangoni convection is much lower if conducted under oil. In a comparative study, out of 58 crystallisation conditions, 17 hits would have been missed if micro-batch had not been used at all [39]. However, micro-batch conducted under oil (silicon/paraffin) is not always a good choice for all macromolecules. For instance, membrane proteins require the addition of some detergents into the crystallisation solution. This will certainly interfere with the intended function of these oils. To conclude, an accessible, economical, applicable and non-demanding method which permits both nucleation and crystal growth under diffusion-limited solute transport, not disturbed by buoyancy or surface tension driven convections. is required.

1.8 Ceiling Crystallisation

In 2008, Poodt and his co-workers proposed a new upside-down setup to achieve the beneficial effects of microgravity crystal growth by exploiting buoyant forces instead of overcoming them. Sodium chlorate and Hen Egg-White Lysozyme (HEWL) were used as model systems [40]. They concluded that crystal growth in this configuration leads to the formation of a buoyancy-assisted depletion zone where unwanted convection is suppressed. This was indicated by the decreased growth rate and elongated morphology of tetragonal HEWL crystals. These observations confirmed the diffusion limited growth, just as would happen in the absence of gravity (Fig. 1.9).

It is worthy to note that in this configuration a solution-vapour interface is not present and thus Marangoni convection is avoided as well.

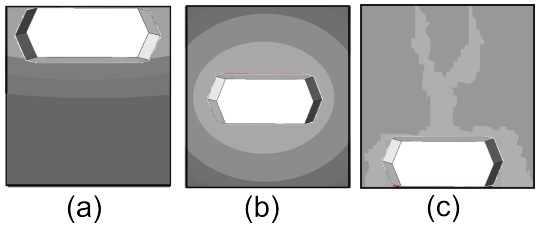

Figure 1.9: The development of the depletion zone around a ceiling crystal (a) is accomplished in a manner very similar to that for a crystal grown in microgravity conditions (b). However, the depleted solution is up-thrust in any other terrestrial crystallisation conditions (c)

1.9 This Thesis

In this thesis, I present a detailed characterisation and validation of the upside-down approach, which is dubbed later the *Ceiling Crystallisation Method*. The figure of merit in protein crystallography is the resolution from X-ray diffraction. Test model proteins are used to examine the diffraction quality of the ceiling crystals and whether they show an improvement compared to batch grown crystals. As elaborated in chapter two, the results are based on characterisation using both laboratory X-ray sources and synchrotron radiation. Numerical simulations combined with Mach-Zhender based Phase Shifting Interferometry (PSI) are presented in chapter three. PSI is a very precise technique able to quantitatively monitor solute concentration profiles during crystal growth. The method is applied to monitor the real time solution processes during ceiling and batch crystal growth and dissolution. The purification effect of the ceiling method is explored using impurities with different segregation coefficients and is characterised by qualitative and quantitative techniques. This is presented in chapter four. Relying on fluorescently labelled protein monomers, a study on the growth history of protein crystals is performed. Characterisations are done using confocal fluorescence microscopy. This is discussed in chapter five. As a technical development, chapter six describes our home-made ceiling kit for an easy optimisation of protein crystal growth using the ceiling method.

Chapter 2

High Resolution Protein Crystals Using an Efficient Convection-Free Geometry[1]

Abstract

Macromolecular crystallography is the most direct and accurate approach to determine the three-dimensional structure of biological macromolecules. The growth of high quality single crystals, yielding diffraction to the highest X-ray resolution, remains a bottleneck in this methodology. Here we show that through a modification of the batch crystallisation method, an entirely convection-free crystallisation environment is achieved, which enhances the purity and crystallinity of protein crystals. This is accomplished by using an upside-down geometry, where crystals grow at the "ceiling" of a growth-cell completely filled with the crystallisation solution. The "ceiling crystals" experience the same diffusion-limited conditions as in space microgravity experiments. The new method was tested on bovine insulin and two hen egg-white lysozyme polymorphs. In all cases, ceiling crystals diffracted X-rays to resolution limits beyond that for other methods using similar crystallisation conditions without further optimisation. In addition, we demonstrate that the ceiling crystallisation method leads to crystals with much lower impurity incorporation.

[1]The content of this chapter has been published as: Alaa Adawy, Etienne Rebuffet, Susanna Törnroth-Horsefield, Willem J. de Grip, Willem J. P. van Enckevort & Elias Vlieg (2013). Crystal Growth & Design 13, 775-781

2.1 Introduction

During biosynthesis, proteins fold into their specific three-dimensional structure, which determines their physico-chemical and biological properties, such as biostability, functionality and interaction pattern. Therefore, knowledge of the three-dimensional structure of proteins has become a crucial tool in bioinformatics, medicinal chemistry and pharmacology, in order to understand and manipulate the structure-function relationships of a protein, both for fundamental (structure and function prediction, synthetic biology) and applied (structure-based drug design) purposes. The most popular and successful methodology to determine the three-dimensional structure of proteins at sufficient resolution (preferably $<$2 Å) is the analysis of their crystals by means of X-ray diffraction [6, 10]. Under the appropriate conditions, proteins can be induced to form crystals, where individual protein molecules align themselves in a repeating series of unit cells by adopting a consistent orientation. However, compared to most other molecules, crystallisation of proteins remains a laborious and complex process. This is mainly due to the difficulty of purifying these macromolecules to an optimal level. While crystallisation itself is one of the most efficient methods to purify proteins, the large number of solution parameters that must be taken into account, such as pH, temperature, as well as buffer and precipitant additives, greatly affect the purity of the grown crystals. While protein purity is a major factor in the success and reproducibility of crystal growth experiments for structure determination, impurities like salts, other protein species, and micro-heterogeneity of the protein itself may affect the size and perfection of the crystals, with concomitant loss of their diffraction resolution[41, 42]. Another difficulty arises because protein crystals are typically grown at a high supersaturation. This is required to form the initial nuclei, but also stimulates defect formation during subsequent growth. From a physico-chemical viewpoint, mass transport is an essential parameter in crystal growth from aqueous solutions. Gravity-driven convection is one of the principal problems that affects protein crystal quality in most terrestrial crystallisation methods[43, 6, 10]. Natural convection causes a random mixing of the solution constituents. This, in turn, induces fluctuation of the supersaturation at the crystal-solution interface, which subsequently causes unfavourable growth rate fluctuations. In addition, convection currents increase the probability of impurity adsorption by transporting them to the vicinity of the growing crystal, with an increasing chance of incorporation at higher crystal growth rates. These scenarios will result in poorly diffracting crystals possessing higher density of impurities and lattice defects. Therefore, in order to regulate the kinetics of the crystal growth, it is important to eliminate the contribution of the convective mass transport and achieve diffusion-limited conditions. Gravity-induced convection inspired researchers to test microgravity for their crystallisation experiments in

parabolic flights and space shuttles [44]. Nevertheless, the efficacy of these space microgravity experiments remains unsettled to date due to the paucity of flight opportunities and the considerable expenses involved [45, 46]. Other attempts to suppress the convection currents on earth, such as crystallisation in capillaries [47], gels [48], hypergravity and magnetic fields [49] have shown to be only partially successful or methodologically demanding. Therefore, protein crystallographers largely hold on to the classical vapour-diffusion method in view of its versatility, low expense, simple set-up and easy conversion to robotic high-throughput assays [34]. Better results are often reported using the batch method, which – although being disturbed by convection – provides relatively constant predefined crystallisation conditions [50]. Here, we present an efficient modification of the batch method, which provides convection-free growth conditions in a laboratory-based set-up, resembling those in a microgravity environment, essentially by exploiting gravity, and yields crystals of improved quality compared to the traditional set-ups.

2.1.1 Ceiling Crystallisation

Recently, we proposed a new method, which mimics the beneficial effects of microgravity by exploiting buoyant forces instead of overcoming them. Our preliminary conclusions were based on the morphology and the optical quality of the tetragonal Hen Egg-White Lysozyme (HEWL) crystals, but no full X-ray diffraction assessment using synchrotron radiation was performed. The principle of the approach is shown in Fig. 2.1. A growth cell is completely filled with a supersaturated protein solution. This cell is sealed with a cover slip, at which nucleation and crystal growth occur. The cover slip can be of any material that favours heterogeneous nucleation. Crystals which nucleate and grow at the "ceiling" of the growth cell gradually deplete the surrounding solution from protein and, thereby, a depletion zone with lower density develops. Owing to buoyancy, this lower-density solution remains at the topmost part of the growth cell, that is, no convection occurs. This depletion zone expands slowly downwards, leading to a vertical concentration gradient. In a vibration-free environment, mass transport of macromolecules through this gradient towards the ceiling will only occur by diffusion, hence crystal growth becomes diffusion-limited. We will refer to crystals growing in this geometry as "ceiling crystals", and to this crystallisation method as "ceiling crystallisation method". Not only does this ceiling method offer diffusion-limited growth, it also improves crystal homogeneity due to the reduced growth rate at the lower supersaturation, and therefore, crystal growth becomes controlled mainly by surface kinetics. Moreover, due to the cessation of convection, the rates of impurity incorporation are greatly reduced and, for obvious reasons, sedimenting microcrystals will not be incorporated. To investigate whether the benefits of the ceiling

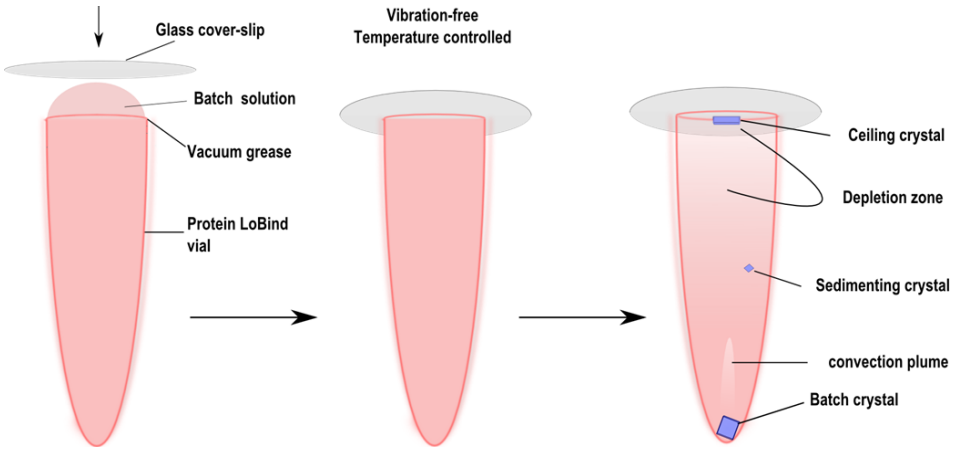

Figure 2.1: The ceiling crystallisation method: The growth vial is completely filled with batch solution. On the cover slip, (heterogeneous) nucleation and subsequent growth of ceiling crystals starts to gradually deplete the nearby solution, resulting in the formation of a depletion zone. Owing to gravity, a vertical concentration gradient is formed in which mass transport occurs only through diffusion. Regular batch crystals, growing at the bottom, will be affected by convection currents and sedimentation.

method lead to the growth of protein crystals which possess higher perfection and diffract X-rays to higher resolution, we applied this method to produce protein crystals which have been extensively studied and we tested their extent of diffraction by using synchrotron radiation. We used T6 bovine insulin, and tetragonal and monoclinic HEWL. We stress that we applied the crystallisation conditions reported in literature without further optimisation and in all cases find significantly improved resolution limits, even while using growth solutions of lower purity.

2.2 Materials and Methods

2.2.1 Crystallisation Conditions

Bovine insulin (powder) was purchased from Sigma (lot number 069k09822) and used without further purification. The stock solutions of the protein as well as the crystallisation solution were prepared using the protocol described in [51], except that the final concentration of insulin was 0.75 mg/ml, and no acetone was used. The ceiling T6 bovine insulin crystals grew as rhomboids up to 75 μm in length after two weeks of incubation at 20°C. HEWL was purchased from Sigma (Cat. No. L6876) and used without further purification. According to the product information the material was about 90% pure monomer,

the remainder consisting of salt and some dimeric HEWL. All other chemicals were of reagent grade. Tetragonal and monoclinic crystals were grown from solutions containing 4% w/v NaCl and 2% w/v $NaNO_3$, respectively, as precipitants in 0.1 M sodium acetate buffer (pH 4.5) at 20^oC. Ceiling tetragonal and monoclinic crystals grew to around 0.5 and 1 mm, respectively, along their c-axis, after 14 days of incubation. Using the fluorescent dye DY-632-01 (MW=950.03 g/mol, Dyomics), HEWL monomers were labeled at a molar ratio of 1:1 and purified by gel permeation (F-Lyz). Bovine Serum Albumin (BSA), purchased from Sigma-Aldrich (Cat. No. 85040C), was used without further purification. Both impurities were used individually as contaminants in tetragonal HEWL crystallisation trials. Control experiments were performed in parallel without addition of these compounds. From every growth cell, crystals were then collected separately from the cover slip (ceiling crystals) and the bottom of the growth cell (batch crystals).

2.2.2 Crystallisation Setups

Protein Lo-bind, PCR clean vials (Eppendorf) were used to prepare the crystallisation setups. Microtubes (volume capacity 800 μl), microplates (384/V-PP; volume capacity 150 μl/well) and nanoplates (1536/V-PP; volume capacity 10 μl/well) were used as growth cells to allow both large and small scale crystallisation trials. A thin bead of a cover slip sealant (vacuum grease) was applied to the upper edge of the vial, which was then completely filled with the batch crystallisation solution to avoid solution or air leakages out of or into the growth vials. The vials were then kept in a thermostated chamber, which was placed on a vibration-free table (TMC sys 366-501) with temperature control ($\pm$ 0.1^oC) by means of a Julabo F-25 circulator.

2.2.3 Characterisation of Crystals

A polarisation microscope (Leica DM-RX) was used in transmission mode, for in situ preliminary observations of the crystal morphology. Images were collected using a video camera (Evolution VF) and processed using Image Pro plus 2 software. A confocal fluorescence microscope (Leica DM IRE2) was used for the in situ characterisation of F-Lyz incorporation into tetragonal HEWL crystals. In order to observe the crystals under the microscope, the glass cover slip with the attached crystals (ceiling crystals) was moved to cover an observation cell, which consists of a rubber ring and a bottom glass slide. This observation setup was completely filled with the mother liquor taken from the growth cell. Batch crystals were collected from the bottom of the vial and were placed in another observation cell, which was also completely filled with the remaining mother liquor.

Fluorophore detection was achieved by excitation using a HeNe laser (632.8 nm). The observation (fluorescence) wavelength range was 645 - 750 nm, using an excitation intensity of 17%, a PMT gain of 422V and a pinhole diaphragm diameter of 72.54 μm. For all diffraction studies, HEWL and insulin ceiling crystals were collected from the glass cover slips. Cryoprotection was rather easy, because the crystals are left with a very small volume of the crystallisation solution and the cryoprotectant is added onto the same cover slip. The crystals are easily dislodged from the glass surface and fishing using a cryoloop is straightforward. The crystals selected for synchrotron diffraction analysis were soaked in more viscous mother liquors containing 25% polyethylene glycol 400 (HEWL polymorphs) and 20% glycerol (bovine insulin), flash-frozen in liquid nitrogen and cooled in a 100 K nitrogen stream during the measurements. These cryoprotection conditions are not optimal, but were not further optimised. Synchrotron data collection was carried out at the microfocus beamline ID23-2 of the European Synchrotron Radiation Facility (ESRF) in Grenoble, with a maximal observable resolution at the edge of the detector around 0.9 Å. This beam line ($\lambda = 0.873$ Å) is optimised for data collection from very small crystals, which is advantageous for the insulin crystals (edge length 25-75 μm) but not necessarily for the larger tetragonal and monoclinic HEWL crystals (length along c-axis 0.35-1.00 and 0.9-2.5 mm, respectively). It is notoriously difficult to define and compare the X-ray resolution of a protein crystal produced by different research groups, because different definitions are used. Here we use for bovine insulin the resolution obtained from the structure determination as discussed in the following section. When a complete data set is not available, we use the highest shell of clearly observable X-ray reflections ($I_{spot}/I_{background} = 1.25$, $\sigma = 0.1$). In order to check the reproducibility and statistical relevance of the results, tetragonal and monoclinic HEWL crystals grown in microplates were subjected to diffraction at 100 K using a laboratory X-ray diffractometer (XCalibur PX, Cu-anode $\lambda = 1.5418$ Å, Agilent Technologies). A ceiling crystal from every growth cell was compared to a batch crystal of comparable size from the same vial, with or without prior cryoprotection.

2.2.4 Structure determination and refinement

For the bovine insulin crystals, the diffraction data were processed using iMOSFLM and scaled with SCALA [52]. The program PHASER [53] was used for the molecular replacement and a dimer of T6 bovine insulin was our search model (pdb code 2ZP6), excluding water and ligands. The crystal packing was checked in Coot and after one round of initial structural refinement using REFMAC a 2Fo-Fc electron density map was calculated.

2.3 Results

2.3.1 Crystallisation of T6 Bovine Insulin

T6 bovine insulin hexamer was selected as a test protein because it has been used extensively in microgravity experiments and its resolution did leave room for improvement. Despite being a globular protein, bovine insulin, unlike the easily crystallisable porcine and human orthologs, tends to form irregular rhombohedral-shaped crystals with poorly defined facets and distorted twin crystals [54, 55]. Experiments with bovine insulin in microgravity showed a resolution improvement to 2.3 Åcompared to their terrestrial counterparts with 2.7 Åresolution [46], but did not exceed the best resolution of 2.25 Åreported to date for crystals grown using the batch method [56]. For the vapor-diffusion method a more demanding procedure was recently reported that yielded large single crystals with a resolution of 1.4 Å[57]. Visual inspection indicated that our ceiling T6 bovine insulin crystals grew to geometrically perfect rhombohedra (Fig. 2.2).

Ceiling crystals were fewer in number compared to the conventionally grown batch crystals at the bottom of the same growth cell, but were, on average, larger, with an edge length of 40-55 μm, compared to the batch crystals with 12-28 μm, after one week of incubation. Large crystals were selected and cryoprotected, before being flash-frozen in liquid nitrogen for synchrotron X-ray diffraction experiments. The ceiling T6 bovine insulin crystals showed diffraction spots to 1.5Åresolution (Fig. 2.3 (a)), which is a significant improvement over the best value of 2.25 Åfor these growth conditions. Notably, this improvement was reached while using starting material of lower purity (Table 2.2).

2.3.2 Crystallographic Analysis of T6 Bovine Insulin Data

To verify that the T6 bovine insulin crystals obtained through the ceiling method are of suitable quality for structure determination, we collected a complete data set to 1.5Åresolution (Table 2.1). The crystals belong to space group R3 with cell dimensions of a = 81.16Å, c = 33.34Åand two molecules in the asymmetric unit. A molecular replacement study was performed in which a well-defined solution was identified with a log likelihood gain (LLG) which is almost twice that of the second best solution. After refinement, the obtained solution showed a LLG of 734.9 and an R-merge of only 4.9% to 1.5 Åand for the outer shell of 40.7%. The crystal packing showed reasonable crystal contacts and no overlap between molecules (Fig. 2.3 (b)). After one round of initial refinement, the resulting 2Fo-Fc electron density map clearly shows features not included in the search model, such as two zinc ions ligated by three His residues, each one from three different symmetry-related insulin molecules (Fig. 2.3 (c)). The resultant initial model has R-factor

and free R-factor of 26.0% and 32.0% respectively.

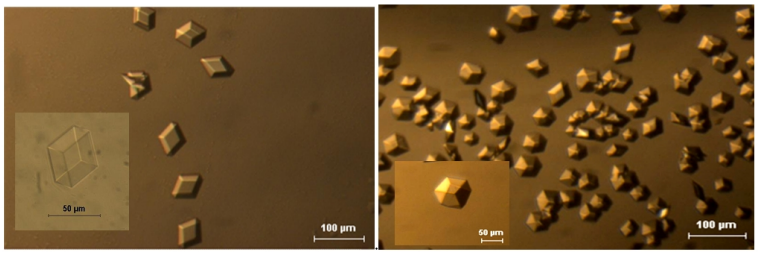

Figure 2.2: Representative images of ceiling (left panel) and batch (right panel) T6 bovine insulin crystals.

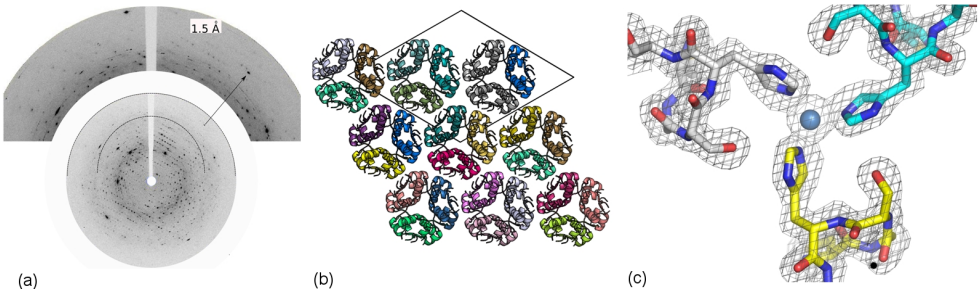

Figure 2.3: (a) X-ray diffraction pattern of a ceiling T6 bovine insulin crystal; (b) Crystal packing for bovine insulin in space group R3. The unit cell is indicated by the diamond; (c) The 2Fo-Fc electron density map contoured at 1.0 σ showing Zn^{2+} ligated by three histidine residues.

2.3.3 Micro-focus X-ray Diffraction of Two HEWL Polymorphs

We next tested the standard model protein in crystal growth, HEWL, from which we grew both the tetragonal and the monoclinic polymorphs while using a commercial preparation of only 90% purity. To date, the crystal structure of tetragonal HEWL crystals has been solved down to 0.94 Å. This was obtained using 99.9% pure HEWL in a counter-diffusion set-up in space microgravity with synchrotron radiation for characterisation [58]. Our tetragonal HEWL ceiling crystals diffracted beyond the limit of the instrumental resolution to around 0.86 Å(Fig. 2.4(a)). The ceiling method promoted the growth of elongated crystals (Fig. 2.5, row 1, left panel), with a final length along the c-axis exceeding 1 mm. This elongation results from the relatively low supersaturation near the crystal surface at the top of the depletion zone in the growth cell, where the interfacial concentration drops significantly, reducing the growth rate of the 110 facets with respect to the 101 facet [59]. This

Table 2.1: Statistics of data collection from a frozen T6 bovine insulin crystal taken at Beamline ID23-2 of ESRF. The values of the outer shell are specified in parentheses

Wavelength (Å)	0.8726	Space group	R3
Resolution range (Å)	30.11-1.50 (1.58-1.50)	No. of observations	30226 (2813)
Unique reflections	12445 (1367)	Rmerge (%)	4.9 (40.7)
Completeness (%)	95.0 (72.3)	Mean I/σ(I)	7.1 (1.9)
Redundancy	2.4 (2.1)		

elongation did not occur in the batch crystals grown through convective mass transport at the bottom of the same growth cell, where the axial ratios (a or b to c) are around one (Fig. 2.5, row 1, right panel). This demonstrates the theoretically predicted lower growth rate of the ceiling crystals compared to the batch crystals.

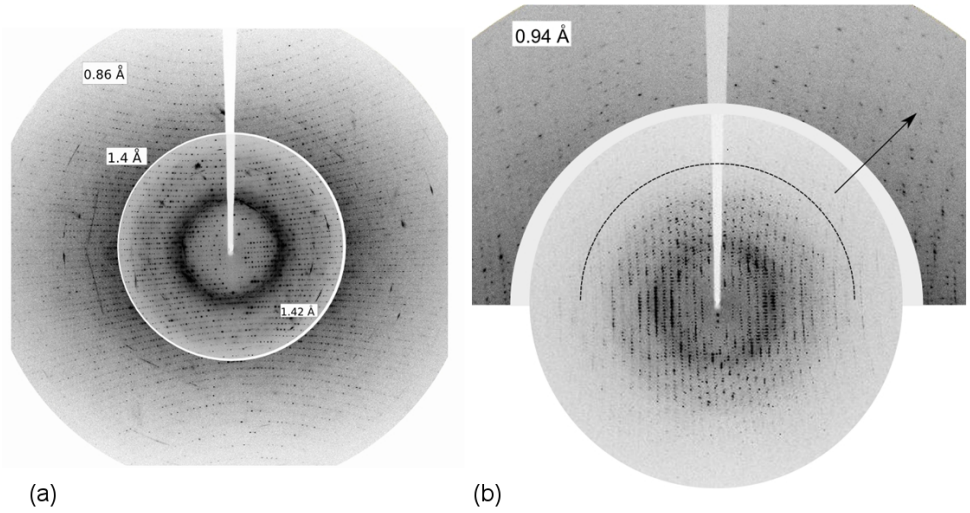

Figure 2.4: X-ray diffraction image of ceiling tetragonal (a) and monoclinic (b) HEWL crystals. The patterns are recorded from a cryo-cooled crystal at beamline ID 23-2 of ESRF (European Synchrotron Radiation Facility), using X-rays of 0.873Åwavelength. Diffraction spots extend to a resolution around 0.86 Å(a) and 0.94 Å(b).

For monoclinic HEWL crystals, the reported best diffraction limit stands currently at 1.13 Å, measured on cryoprotected crystals by using Cu-Kα radiation at 273 K [60]. These crystals were grown from 99.9% pure HEWL in D_2O-based mother liquor instead of H_2O.[61] The use of a quite viscous crystallisation solution precluded problems in the

cryoprotection step. Our monoclinic ceiling crystals, grown from much lower purity HEWL and plain H2O-based mother liquor, diffracted to a resolution of 0.94 Å, Fig 2.4(b). This can be further improved, since the obtained diffraction spots represent a multiple-lattices pattern, which results from split crystals or low-angle grain boundaries.[62] In our case, crystal splitting was not a consequence of perturbed crystallisation, since the crystals were visually perfect in their mother liquor, but started to deteriorate upon incubation in the cryoprotectant. Cryoprotection is therefore another important issue for these crystals, but this is beyond the scope of this paper. Thus, for both HEWL polymorphs, the ceiling method resulted in crystals diffracting to better resolution, despite the fact that a less pure protein preparation and regular aqueous solutions were used, Table 2.2.

2.3.4 Batch *versus* Ceiling Crystals

As we mentioned before, it is not straightforward to compare the X-ray resolution of crystals that have been analysed using different X-ray sources and analysis software, and executed by different groups. It is sometimes claimed that only a double-blind comparison can establish the difference between different growth methods, but even a properly operated laboratory source can already demonstrate the differences between crystals. In order to obtain more unambiguous results, we have compared ceiling and batch crystals that grew simultaneously in the same vial, thus under otherwise identical starting conditions. Table 2.3 shows the results, using the highest observable shell as resolution criterion for the cryoprotected crystals and $I/\sigma = 2$ for the non-protected crystals.

As usual, there is a considerable spread between crystallisation runs, but our statistical analysis shows that the ceiling crystals always outperformed their batch counterparts of comparable size from the same vial at confidence level of 99%, 95% and 75% for monoclinic and tetragonal HEWL and bovine insulin, respectively. Note that also for the batch crystal of bovine insulin we obtained a higher resolution than that reported in 2005 [56]. This may be the result of the different crystallisation recipe (zinc chloride instead of zinc acetate). Therefore, we expect that combining the ceiling method with the use of the chelation step adopted by [57] will result in further resolution improvement.

Table 2.2: Summary of our best results (obtained at beamline ID23-2) compared to the current best values recorded using equivalent crystallisation conditions: resolution *versus* purity.

Protein	Bovine insulin		HEWL			
Lattice	Rhombohedral		Tetragonal		Monoclinic	
Method	Ceiling	Batch [56]	Ceiling	Counter diffusion in space [58]	Ceiling in H_2O	Batch in D_2O [60]
Purity	95% Sigma	99% Lilly	90% Sigma	99.9%Seikagakuo	90% Sigma	99.9%Seikagakuo
Resolution	1.5Å	2.25Å	0.86Å	0.94Å	0.94Å	1.13Å
Space group	R3	R3	$P4_32_12$	$P4_32_12$	$P2_1$	$P2_1$
Unit cell parameters	a=81.37Å, c=33.40Å	a=81.64Å, c=33.62Å	a=79.01Å, c=36.98Å	a=77.06Å, c=37.22Å	a=28.15Å, b=62.86 Å, c=59.41Å, β=93.64^o	a=28.01Å, b=62.92Å, c=60.49Å, β=90.6^o

Table 2.3: Comparative analysis of ceiling and batch crystals using a laboratory X-ray diffractometer (X Calibur PX, 100K, $\lambda = 1.5418$ Å). The highest resolution values were used, corresponding to the highest scattering angles with clearly observable X-ray reflections ($I_{spot}/I_{background} = 1.25$, $\sigma = 0.1$ for cryoprotected crystals and $I/\sigma = 2$ for uncryoprotected crystals). The mean value, standard deviation (σ) and number of samples (N) are also listed.

Crystal	Origin	Cryo?	Best value	mean	σ	N
T6 bovine insulin	Ceiling	Yes	1.53 Å	1.64 Å	0.16	2
	Batch	Yes	1.94 Å	1.94 Å	0	2
Tetragonal HEWL	Ceiling	Yes	0.85 Å	1.07 Å	0.23	4
	Batch	Yes	1.33 Å	1.91 Å	0.75	4
	Ceiling	No	1.90Å	2.13 Å	0.23	5
	Batch	No	2.50 Å	3.02 Å	0.59	5
Monoclinic HEWL	Ceiling	No	1.59 Å	2.19 Å	0.40	8
	Batch	No	2.33 Å	3.19 Å	0.62	8

2.3.5 Intrinsic Purification Effect of the Ceiling Crystallisation Method

In order to examine more precisely the favourable effect of the ceiling method on the incorporation of impurities, we added known contaminants to the HEWL crystallisation solution, and grew both ceiling and batch crystals in the same vial. The obtained tetragonal crystals were characterised using polarisation microscopy. Bovine Serum Albumin (BSA), as a heterogeneous impurity for HEWL, is known to enhance nucleation and crystal twinning of HEWL crystals. The batch crystals exhibit an increase in defect formation and a strong size reduction in the presence of up to 5 mg/ml BSA in the crystallisation solution (Fig 2.5, row 2, right panel). In contrast, the ceiling crystals did not show visible defects and maintained their elongated morphology, but with a reduction in size and axial ratio (Fig 2.5, row 2, left panel). We also observed pyramidal-prismatic sector boundaries, resulting from differences in impurity content between adjacent growth sectors [63]. This distortion in lattice parameters due to the segregation of impurities was much more severe in batch crystals, which also developed cracks as well as complete misorientation that could eventually lead to prominent pseudo-twinning. Secondly, we tested a micro-heterogeneous

impurity, viz. HEWL derivatised with one fluorescent label (F-Lyz), which incorporates easily into the crystal lattice. In this case, incorporation and distribution of the impurity were monitored in situ by using confocal fluorescence microscopy. Despite the high segregation of F-Lyz [20], its incorporation in ceiling tetragonal HEWL crystals was significantly lower than in the corresponding batch crystals. Even at high F-Lyz levels, incorporation in ceiling crystals was lower by at least 40% (Fig 2.5, row 3). In this case, the surface kinetics, which become more important at decreased growth rate will play a major role in preferentially incorporating unmodified HEWL.

2.4 Discussion

As shown above, the vital element of the ceiling crystallisation method is the elimination of gravity-driven convection, which perturbs the classical terrestrial vapor-diffusion and batch crystallisation set-ups, as well as Marangoni convection, which can still perturb space microgravity experiments [64]. Moreover, the ceiling method shares simplicity, accessibility and affordability with the traditional vapor-diffusion and other laboratory-based methods. In addition, the diffusion-limited growth enhances the intrinsic purification effect of crystal growth. The subsequent reduced transport of macromolecules and impurities towards the crystal surface allows the crystals to undergo an enhanced self-purification process. Under these conditions, the molecules have enough time to be adsorbed on the crystal surface in the appropriate orientation and conformation, whereas trapping of impurities will largely depend on their distribution coefficient. The decrease of the crystal growth rate has a favourable effect, because at high growth rates, the adsorbed impurity molecules are easily buried by other growth steps covering the interstep terraces on which the impurity molecules are mainly adsorbed. At a low growth rate, in contrast, desorption of these impurities is facilitated, allowing self-purification of the crystal. For the proteins we tested here, just the glass cover slip is sufficient to obtain nucleation at the ceiling. If heterogeneous nucleation needs to be promoted, bio-glass or other nucleation agents can be applied. We developed the ceiling method using microvials with a volume of 800 μl. With typical protein concentrations of several mgs/ml, the quantities required for systematic screening of crystallisation conditions cannot be easily obtained for most native as well as recombinant proteins. Hence, we set out to reduce the crystallisation volume. Meanwhile, we have extensively tested microplates (150 μl/well) and obtained reproducible results identical to those in microvials. Also, we tested nanoplates (10 μl/well) and, again, results so far are completely in line with those obtained in the larger-volume set-ups. These accumulated results indicate that the ceiling method works well over a large volume

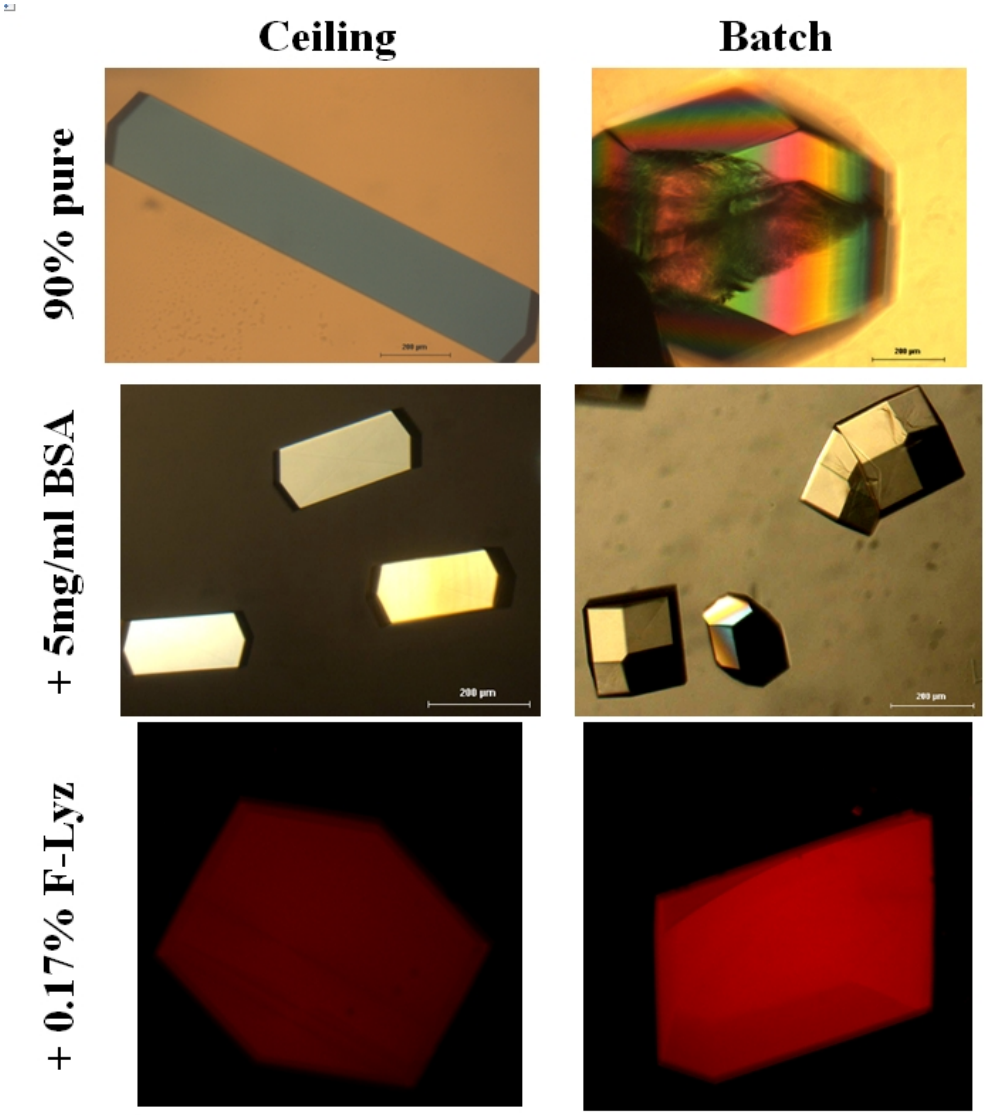

Figure 2.5: The effect of impurities on the growth of tetragonal ceiling and batch HEWL crystals. Rows 1 and 2 show optical polarisation micrographs of crystals grown under the same conditions (10 mg/ml HEWL, 40 mg/ml NaCl in 0.1 M sodium acetate buffer pH 4.5 at 20°C), without (row 1) or with (row 2) 5 mg/ml BSA. The bar represents 200 μm. The effects of the ceiling method (row 1) and its much lower susceptibility to impurities (row 2) are obvious. Row 3 displays the strongly reduced incorporation of F-Lyz under ceiling conditions; images were taken at the same settings of the confocal fluorescence microscope.

range, as long as a dimensional ratio of height to diameter ≥ 2 is preserved. However, we do not recommend to use capillaries with a diameter $<$0.5 mm for the ceiling method, since the capillary forces will then perturb the proper formation of a depletion zone at the top of the capillary. The use of micro/nano-plates puts the ceiling method in principle up for robotic automation. A crystallisation volume of 10 μl usually requires less than 50 μg of protein per well, which for a large range of recombinant proteins will allow extensive screening. On the other hand, it may in general be more practical to screen for optimal crystallisation conditions using conventional methods like hanging drop vapour-diffusion or a micro-bath method, which can go down to a volume of 10 nl. Once proper growth conditions have been established, the ceiling method can be tested to achieve a higher crystal quality and resolution.

Currently, we are investigating the applicability of the ceiling method to other globular as well as membrane proteins. This requires primarily a compromise between the leakage-free set-up and the detergent-based mother liquors or even exploiting detergent-free nanodiscs for membrane protein solubilisation and crystallisation. In view of the paucity of membrane protein crystal structures and the suboptimal resolution for most of them ($>$2 Å) [65], we consider this a top priority in the further improvement of the ceiling crystallisation approach.

In conclusion, our results demonstrate that through a simple but effective adaptation of the batch method, we can exploit the gravitational force to our advantage. The resulting ceiling crystallisation method yields a significant improvement in crystal quality and reduced impurity incorporation. This can ultimately lead to a substantial refinement of our insight in the 3-dimensional build-up of macromolecules, with far-reaching impact on proteomics and genomics.

Chapter 3

The Development of the Depletion Zone during Ceiling Crystallisation: Phase Shifting Interferometry and Simulation Results [1]

Abstract

The growth of high quality protein crystals is essential for the determination of their structure. This process is governed by many physical factors such as mass transport and solution flow. The quality of the crystals is usually better under diffusion-limited growth conditions, where a depleted zone of the solution encapsulates the crystal. We developed a MachZehnder-based phase shifting interferometer coupled to image processing software to study the concentration gradients which develop around a crystal during its growth or dissolution. The depletion zones and the diffusion boundary layers around growing and dissolving KH_2PO_4 crystals are monitored and processed by a MATLAB based algorithm. Our main emphasis was to analyse the ceiling crystallisation conditions in which the crystal is placed at the very top of the growth cell and therefore the solute transport is largely diffusion-limited. The experimental results are compared with simulations using finite element-based numerical calculations. The combined results clearly demonstrate the positive effect of the ceiling crystallisation approach on crystal growth.

[1] The content of this chapter has been published as: Alaa Adawy, Kess Marks, Willem de Grip, Willem van Enckevort & Elias Vlieg (2013). CrystEngComm 15, 2275-2286.

3.1 Introduction

Crystal growth takes place at the crystal–solution interface, involving both solute mass transport and growth kinetics. As a consequence, the solution in the direct vicinity of the crystal generally undergoes a decrease in density [66]. This is due to the incorporation of solutes into the crystal from the surrounding solution and, to a lesser extent, the release of thermal energy. This low density portion of the solution can either settle around the growing crystal (diffusion–limited growth), or it can undergo a rapid exchange with its surroundings by gravity–induced natural convection.

From the two regimes, diffusion–limited crystal growth is an amenity in obtaining high quality protein crystals [10]. Many methods were developed in order to provide convection–free growth conditions such as the counter diffusion method [48], exploiting magnetic fields to counter the gravitational field [32], or space microgravity experiments [43]. In these methods and after nucleation, crystal growth induces the development of a depletion zone, which is not disturbed by natural convection. The developing concentration gradient limits the mass transport of growth units towards the growing crystal to be solely diffusive. This has a positive impact on the crystal quality because the growth rate slows down, allowing the crystal to embed growth units at the right orientation on the crystal surface. In addition, sedimentation of small crystals and incorporation of impurities are reduced [67].

In a previous paper it was shown that diffusive crystal growth can also be accomplished in a simple terrestrial setup by using an upside–down geometry which exploits gravity [68]. In this setup, the crystals at the top (ceiling) of a growth cell grow in a diffusion–limited crystallisation environment. Ceiling crystals grow slowly and because of the "upside–down" geometry, the growing crystals are not affected by sedimentation. This eventually results in better diffracting crystals with lower impurity content when compared with those grown at the bottom of the same setup [69]. This was clearly demonstrated by statistical analysis, which showed that the resolution limit of ceiling crystals (diffusive growth) is significantly improved over that of the batch crystals (convective growth) at a high confidence level. Quantitative experimental data are beyond the scope of the present paper and are presented elsewhere [69].

To examine the different hydrodynamics during ceiling and batch crystallisation, we used tetragonal crystals of potassium dihydrogen phosphate (KDP) as a model compound. [70] We used aqueous KDP solutions of either 10% and 20% supersaturation or 10% and 20% undersaturation level to study both the growth and the dissolution processes. Emphasis is laid on monitoring the development of the depletion zone during ceiling growth.

To visualise the buoyancy–driven convection plumes (batch growth) or the development

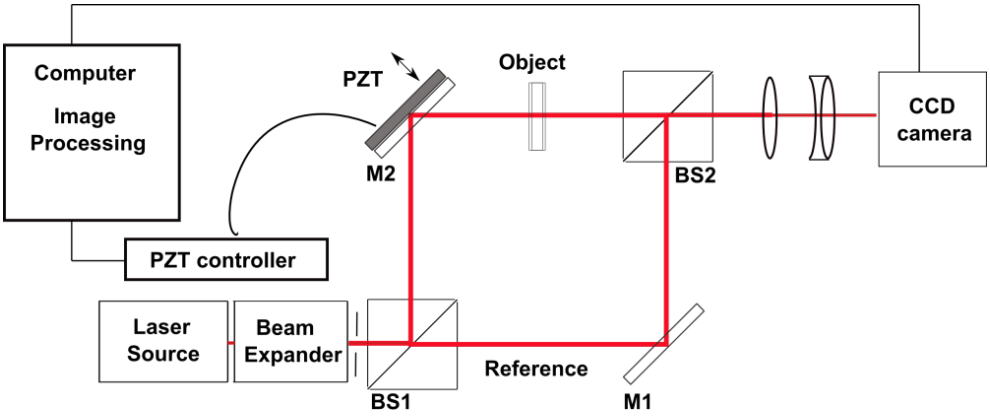

Figure 3.1: Schematic diagram of Mach-Zehnder phase shift interferometer. A piezo electric transducer (PZT) accomplishes the phase shifts, while the beam splitters (BS1 & BS2) and the mirrors (M1 & M2) are arranged in a two beam interferometer configuration.

of the depletion zone (ceiling growth), we relied on optical interferometry to map the solute concentration profile in the solution [71]. The concentration profile around the growing crystal can be monitored as a local change in the refractive index of the crystallisation solution, which is a function of solute concentration. Interferometric techniques provide a route to map these differences in the refractive index in terms of changes in the optical path length [72]. We designed a Mach-Zehnder-based phase shifting interferometer and used a five frame algorithm in order to study the changes in the spatial distribution of solute concentration, which take place during the growth or dissolution of KDP. These observations are supplemented by finite element-based numerical simulations for the same dissolution or growth conditions. Some conclusions from this study are validated by comparing the morphological quality of ceiling and batch grown Hen Egg-White Lysozyme (HEWL) crystals grown in cells of different sizes.

3.2 Concentration profile measurements

3.2.1 Mach-Zehnder Phase Shifting Interferometer (PSI)

To map the concentration profiles, we used a Mach-Zehnder phase shifting interferometer (Fig. 3.1). This two-beam interferometer for transmitted light favours high accuracy and easy quantitative interpretation. The incident monochromatic laser beam is split into two

coherent beams, one of which passes the transparent specimen, i.e. the growth cell which contains the crystal and the solution, and the other acts as a reference beam. The two beams superimpose after travelling approximately the same geometrical distance resulting in an interference pattern *I(x,y)*, which embeds the information of the amplitude and phase [73], such that :

$$I\ (x,\ y) = I_o + \ I_r\,(x,\ y) + \sqrt{I_o I_r}\,(x,\ y)\cos\varphi\,(x,\ y) \tag{3.1}$$

where I, I_r and I_o are the intensities of the resultant, reference and object beam, respectively and ϕ (x, y) is the position dependent phase difference of both beams.

In order to retrieve the object phase information, physical shifts are introduced between the two beams. This is accomplished by recording a sequence of interferograms, each with the object beam displaced by a phase shift of $\pi/2(\propto \lambda/4)$. In this way, the phase information can be retrieved by using the appropriate algorithm to process the consecutively recorded interferograms. Here, we adopted the 5B-frame algorithm introduced by Schmidt and Creath [74], because it is the most efficient in obtaining a high accuracy. In this case, the total phase shift after the acquisition of the five interferograms is 2π, and the algorithm yields

$$\varphi\,(x,y) = -\ tan^{-1}\left[\frac{3I_2 - 3I_3 - I_4 + I_5}{I_1 - I_2 - 3I_3 + 3I_4}\right] \tag{3.2}$$

with $I_j = 1-5$ the intensity of the five interferograms at point *(x,y)*. The phase information reveals the spatial changes in the refractive index and thus, the concentration profile. Based on this algorithm, a MATLAB script was written, which combines the five $\pi/2$-phase shifted interferograms and a mask frame (representing the crystal body) to give a discontinuous phase profile disregarding the body of the crystal. The discontinuities in the calculated phase profile, owing to the nature of the arctangent function, introduce errors in the calculated phase. In order to remove these errors, we developed a correction script, which compares the phase value at each pixel with that of the previous neighbouring vertical or horizontal pixel. If the difference is $< -3\pi/4$, π is added to the pixel and if this difference is $> 3\pi/4$, π is subtracted from this pixel, otherwise the phase value is not changed. Finally, the corrected phase profile is used to compute the concentration profile. This is done by exploiting the relation between the refractive index and the resultant phase difference;

$$\varphi\,(x,y) = \frac{2\pi}{\lambda}\ \int_0^d n\,(x,y,z)\,dz + C \tag{3.3}$$

where $n(x,y,z)$ is the position dependent refractive index of the solution in the growth cell, d is the thickness of the cell and λ is the wavelength of the laser light used. The

constant C comprises the resultant phase difference of the object and reference beam excluding the solution in the cell. Using the relation between the refractive index and the difference $\delta c(x, y, z)$ in solute concentration with respect to the equilibrium concentration, which corresponds to a refractive index n_o,

$$n(x, y, z) = n_o + n_1 \Delta c(x, y, z) \tag{3.4}$$

an expression for the average solute concentration difference as a function of the phase difference is obtained

$$\frac{1}{d} \int_0^d \Delta c(x, y, z)\ dz = \frac{\lambda}{2\pi n_1} \varphi(x, y) + D \tag{3.5}$$

where D is a constant, which can be set to zero.

A schematic diagram of the PSI is shown in Fig. 3.1. The whole optical setup is based upon the one that was introduced earlier by Duan and Shu, [75], and is mounted on a vibration-free table. A HeNe laser source of wavelength 632 nm is passed through a beam expander and the resultant beam diameter is controlled by a diaphragm. The beam is incident on a beam splitter (BS1) and divided into two equal beams: one functions as the reference beam and the other as the object beam. Both are then reflected by the mirrors (M1 & M2). In order to apply the consecutive phase shifts, we used an ultra-precise piezo electric transducer (S-303, Physik Instrumente (PI), Germany) (PZT) connected with a digital piezo transducer controller (E-750, PI Germany). The PZT was mounted vertically at the back of M2. The controller in the "servo mode" was used such that a series of interferograms is collected by successively displacing M2 over 112 nm (corresponding to a phase shift of $112\sqrt{2}nm = \lambda/4$ or $\pi/2$). The reference and the object beams are then superimposed by the second beam splitter (BS2) and directed through two consecutive achromatic lenses (L1 & L2) to the CCD camera (PS 4 - 205 GigE, Kappa). The images are recorded, digitised and processed using the MATLAB script.

3.2.2 Experimental Procedure

The concentration profile development during ceiling and batch growth/dissolution was investigated by experiments using a Mach-Zehnder phase shifting interferometer. KDP (KH_2PO_4, Merck) was used as a model compound in this study. Quartz cells of high optical quality, $1 \times 1 \times 4cm^3$ and $0.1 \times 1 \times 4cm^3$ in size (Hellma Analytics, Germany) were used as growth cells in the PSI experiments. KDP seed crystals were mounted with Vaseline (Sigma-Aldrich) in the cell with their long c-axis either parallel or perpendicular

to the plane of the cell top or bottom. Four KDP solutions were prepared to achieve concentration levels of 20% and 10% below saturation and levels of 10% and 20% above saturation, respectively. The cells were completely filled with the appropriate solution and sealed using a small film of Vaseline and glass cover slip. After preparation, the growth cell was placed in the object beam optical path of the interferometer. HEWL (lot# L6876), bovine insulin (lot# 069k09822) and BSA (lot# 85040C) were purchased from Sigma-Aldrich and used without further purification. Other inorganic salts were also purchased from Sigma-Aldrich at the best grade available. The tetragonal HEWL crystals were grown from 20 mg/ml HEWL and 35 mg/ml NaCl as a precipitant in 0.1M sodium acetate buffer adjusted to pH 4.5 using acetic acid. The effect of different impurities on the protein crystal growth of HEWL was investigated by adding either bovine insulin or bovine serum albumin (BSA), to final concentrations of 0.2 mg/ml and 6 mg/ml, respectively. All experiments were conducted in a temperature-controlled room set at 20^oC.

3.2.3 Results and Analysis

Dissolution of batch crystals

To validate the PSI approach, we started with dissolution experiments. A KDP seed crystal with dimensions of $0.1 \times 0.1 \times 0.7 cm^3$ was placed with its c-axis parallel to the bottom of a $0.1 \times 1 \times 4 cm^3$ growth cell filled with 10% or 20% undersaturated solution. A time series of concentration profiles around a KDP crystal dissolving in 20% undersaturated solution measured by PSI is shown in Fig. 3.2. As follows from this figure, the concentration of the solution near the dissolving crystal is higher than that of the undersaturated bulk solution far from the crystal surface. Because of its higher density, this enriched part of the solution remains at the bottom of the growth cell due to gravity and the solute transport to the rest of the solution (upwards) is governed by diffusion rather than natural convection. It can be shown that if the dissolution of a planar crystal surface is completely determined by volume diffusion, the dissolution rate, R_d, decreases with time, t, according to

$$R_d(t) = \frac{D\Omega(c_s - c_b)}{\sqrt{\pi D t}} \propto \frac{1}{\sqrt{t}} \tag{3.6}$$

where, D is the diffusion coefficient and Ω is the molecular volume of the dissolving units; $c_s (\simeq c_{eq})$ and c_b are the solute concentrations at the crystal surface and the bulk solution, respectively. The dissolution rate of the crystal is equal to the flux of the dissolving units away from its surface. This implies that the dissolution rate can be derived from the solute concentration gradient near the crystal surface, using

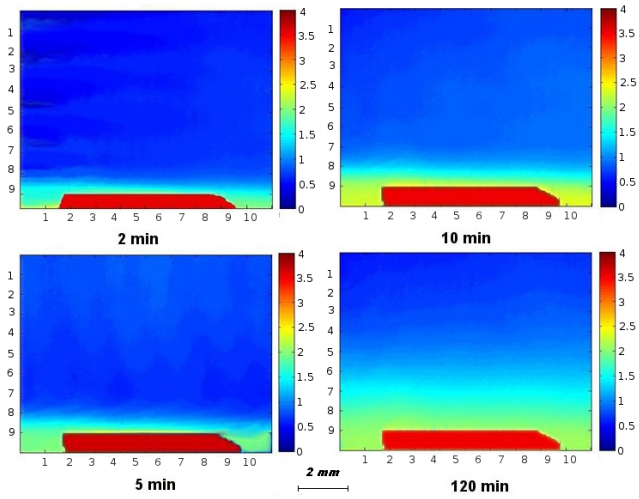

Figure 3.2: The change of the concentration as a function of time for a KDP crystal in a 20% undersaturated solution. The concentration differences are expressed in mass fractions.

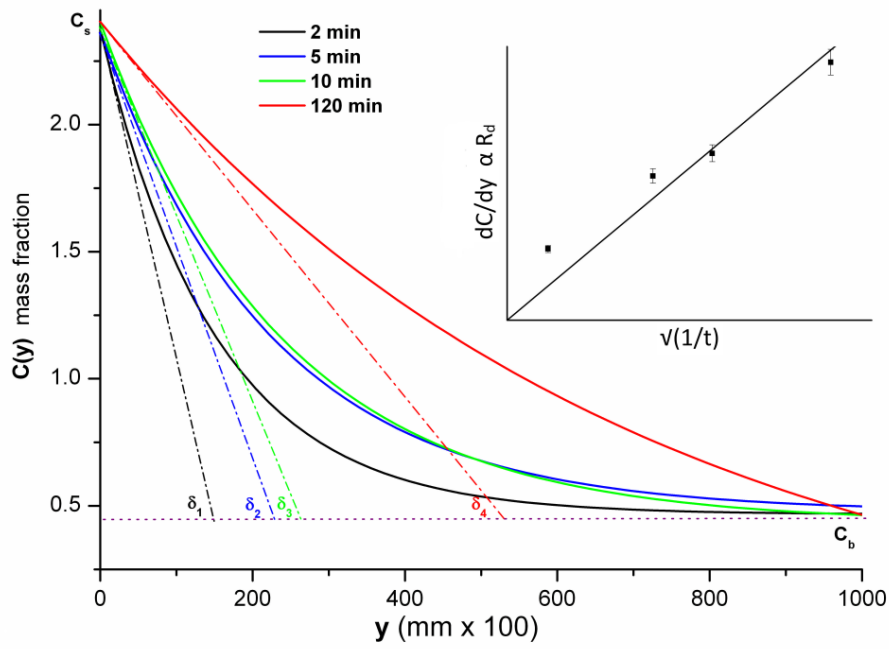

Figure 3.3: The spatial distribution of concentration during the dissolution of a KDP crystal in a 20% undersaturated solution, The upper frame shows the linear relation between the dissolution rate and the inverse of the square root of time.

$$R_d = \Omega D \left. \frac{dc}{dy} \right|_{crystal\ surface} \tag{3.7}$$

where y is the vertical coordinate of the growth cell.

Fig. 3.3 shows the solute concentration profiles perpendicular to the crystal surface as a function of time, derived from PSI measurements shown in Fig. 3.2. Taking the derivatives dc/dy at the crystal surface for different times indeed shows linear dependence on the inverse of the square root of time (Fig. 3.3, insert). This demonstrates that the mass transport in this case is controlled primarily by diffusion. Hence, these phenomena can be successfully monitored using PSI.

Growth of batch crystals

Similar to the dissolution experiments, a tetragonal KDP crystal of dimensions $0.09 \times 0.15 \times 0.7 cm^3$ was placed at the bottom of a $0.1 \times 1 \times 4 cm^3$ growth cell, filled with 10% or 20% supersaturated aqueous KDP solution. Due to the growing crystal, the solution becomes depleted of solute at the crystal-solution interface and by the action of gravity this lower density solution is forced upwards in the form of convection plumes (Fig.3.4). Here, the mass transport growth is effectuated by natural convection and the diffusion boundary layer is thus very thin $< 30 \mu m$, and hardly changes in time. The convection plumes can extend up to 1 cm above the crystal and their reduction in supersaturation lies in the order of 2.5% of that in the bulk solution for the case of 10% supersaturation (Fig.3.4, left column). The 20% supersaturated solution showed the nucleation of many crystals, which due to gravity deposited on the crystal surface (Fig.3.4, right column).

Ceiling crystal growth

Fig. 3.5 shows the changes of the solute concentration profile around a ceiling KDP crystal growing in 10% and 20% supersaturated solution. The dimensions of the crystal and the growth cell are the same as for the batch experiments mentioned above. In the ceiling configuration with the crystal at the top of the growth cell, the solution at the direct vicinity of the crystal again experiences a decrease in its molar concentration due to solute uptake by the growing crystal. But now, the depleted solution stays stagnant around the growing crystal by the action of gravity and the solute transport towards this ceiling crystal becomes essentially diffusion-controlled. The time dependent spatial distribution of the solute concentration perpendicular to the crystal surface is derived from the associated PSI maps. The width of the depletion zone clearly increases in time (Fig. 3.5,3.6).

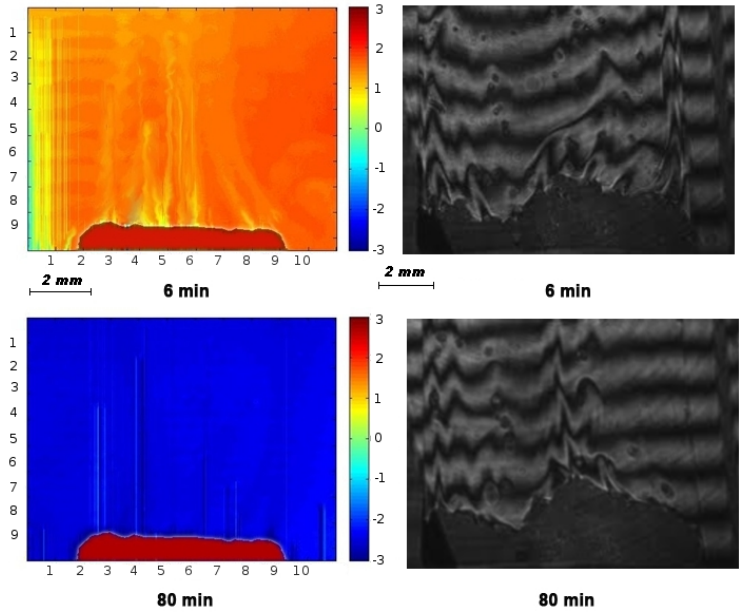

Figure 3.4: Left column shows the change of the concentration profile around a batch KDP crystal growing in a 10% supersaturated solution. The interferograms of a KDP crystal growing at 20% supersaturation are shown in the right column. Sedimentations on the crystal completely covered its surface.

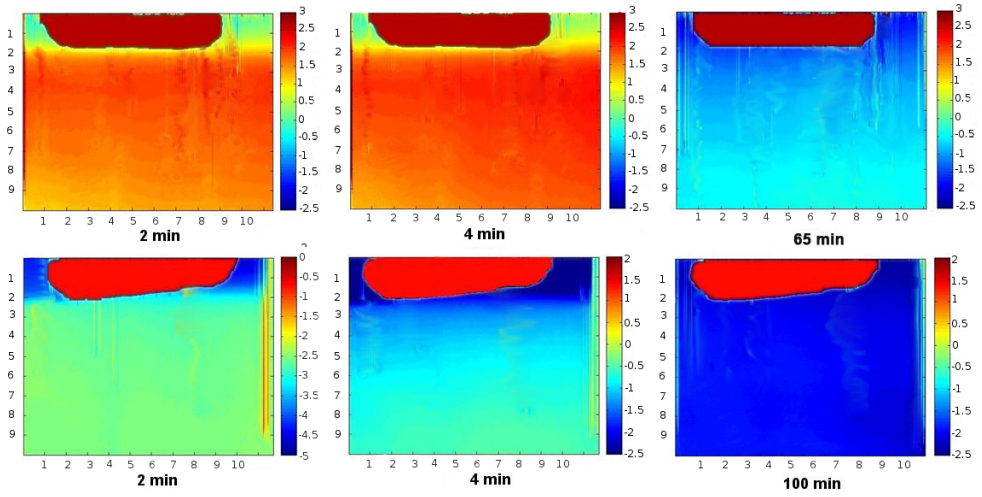

Figure 3.5: The change of the concentration profile as a function of time around a ceiling KDP crystal growing in 10% (upper row) and 20% (lower row) supersaturated solutions.

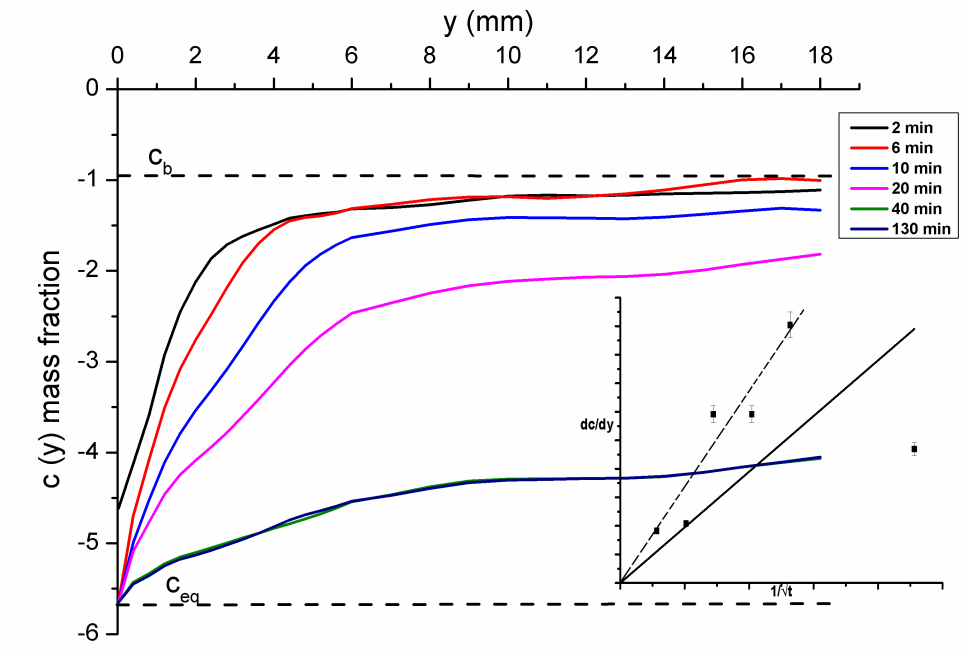

Figure 3.6: The spatial distribution of the solute concentration during the ceiling growth of a KDP crystal in a 20% supersaturated solution, The insert shows the relation between the crystal growth rate and the inverse of the square root of time. The dashed line provides a good fitting disregarding the initial convection mediated stage.

The width and flow of the depletion zone (δ), as shown in the interferograms, varies directly with the concentration difference, between the bulk solution and that at the crystal interface ($c_b - c_s$), and inversely with the flux (J_D) such that:

$$\delta = \frac{-D}{J_D}(C_b - C_s) \tag{3.8}$$

This can be explained as a decrease of the flux occurring in a stagnant solution (Fig. 3.6, insert) with the consequence that δ extends setting mass transport to the crystal in the diffusive mode. When the oblong crystal was mounted with its c-axis parallel to the ceiling, the space around the crystal was filled with depleted solution within two minutes by natural convection (Fig. 3.5). After this stage, the diffusion layer starts to develop. This early phenomenon may account for the different spatial concentration profile of the solution near the crystal surface after two minutes (Fig. 3.5). This phenomenon is even more obvious if the oblong crystal is mounted to the ceiling with its long axis

(the c-axis) perpendicular to the plane of the ceiling plate (Fig. 3.7). Due to the natural convection, the depleted solution flows upwards towards the ceiling and the development of the depletion zone to enclose the whole crystal took close to one hour (Fig. 3.7). Only then, the solute transport to the entire crystal is mediated by diffusion.

Interestingly, when we use the ceiling method to induce nucleation and crystal growth of KDP as well as a variety of proteins we always observe that the crystals nucleate and grow such that their longest axis is parallel to the plane of the ceiling plate of the growth cell. Under these conditions, when starting from small nuclei, this initial convection hardly occurs, in particular when several ceiling crystals grow simultaneously.

In the case of 20% supersaturation many crystallites nucleated at the bottom and on the side walls of the growth cell. Fortunately, the convection plumes of these crystals did not disrupt the depletion zone around the ceiling crystal. Due to convective mixing of the bulk solution, its concentration dropped significantly during the progress of the experiment (Fig. 3.5,3.7).

Deriving crystal growth rates from the time dependent concentration profiles in figure 6, using equation 3.7, gives a somewhat irregular dependence as a function of $1/\sqrt{t}$ (Fig. 3.6, insert). This indicates that, in contrast to dissolution, equation 3.6 is less applicable. This may be accounted for by the initial convective stage of growth, the nucleation and growth of crystallites at the bottom and the walls of the growth cell and by the influence of surface kinetics. It is well known that surface kinetics often plays a far more important role in the growth of crystals than in their dissolution.

3.3 Numerical Simulation

3.3.1 Method

As shown in the previous section, the growth or dissolution of crystals is largely controlled by the concentration dependent solute flux at the crystal surface . This process of unit migration towards (growth) or away (dissolution) from the crystal, is described by fluid mechanics involving the concepts of continuity, flow motion and solute diffusion [76].

The continuity describes the transport of a conserved quantity of fluid and can be expressed as:

$$\frac{\partial^2 \psi}{\partial y^2} + \frac{\partial^2 \psi}{\partial x^2} + \omega = 0 \tag{3.9}$$

where ω is the vorticity and Ψ is the potential stream function.

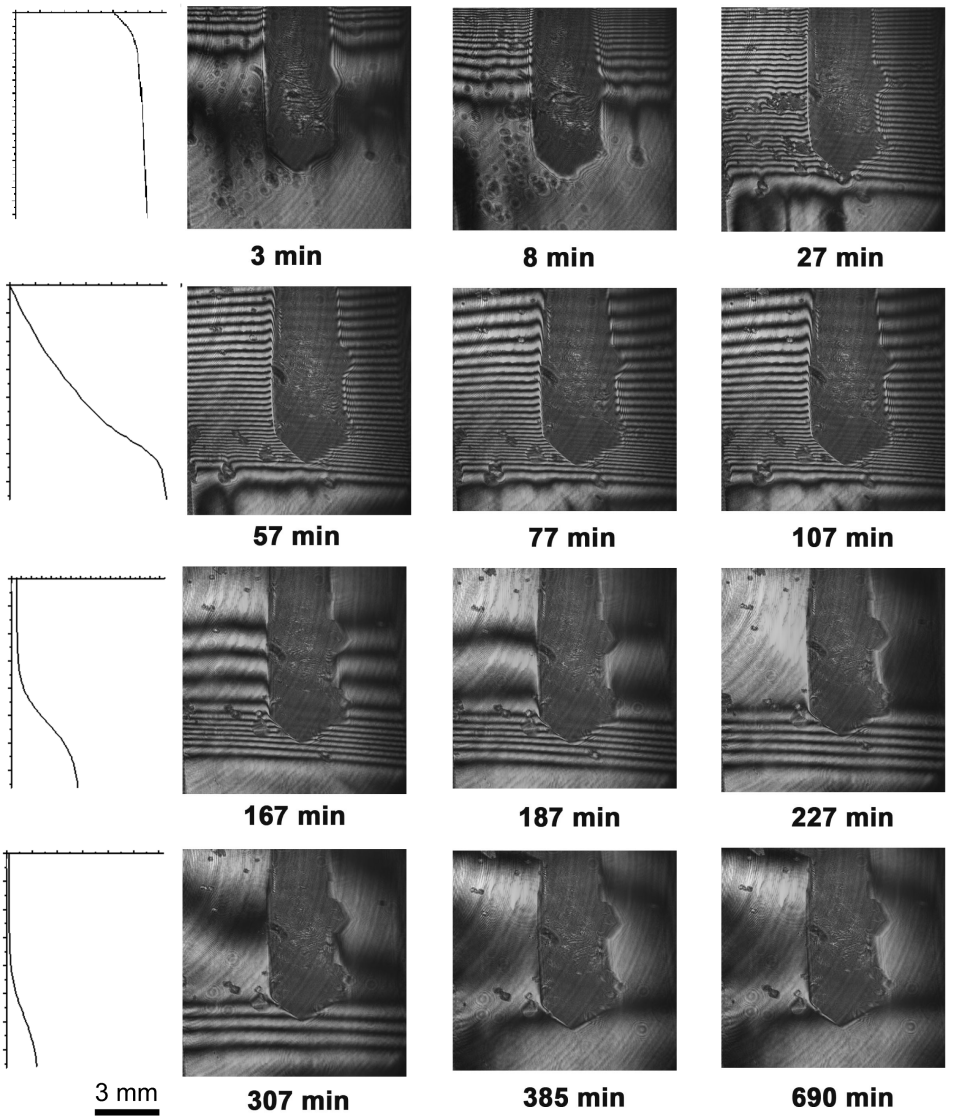

Figure 3.7: Timelines of the interferograms of ceiling KDP crystals which extends deeply in the growth solution and grows in 20% supersaturated solutions. The concentration profiles at the centre of the figure are deduced from the left column of the interferograms. The profiles are calculated by using equation 3.5 and the fact that the distance between two interference lines corresponds to a phase difference of $\phi = 2\lambda$.

Because our quantitative experiments were done in a thin growth cell (1 mm), we chose a 2D model and performed the calculations by using Cartesian (x, y) coordinates. Combining Euler's and Navier-Stokes' equations of motion and taking their curl, the motion of the fluid can be described by the Navier-Stokes stream function vorticity equation:

$$\frac{\partial \omega}{\partial t} - \frac{\partial \psi}{\partial x}\frac{\partial \omega}{\partial y} + \frac{\partial \psi}{\partial y}\frac{\partial \omega}{\partial x} = \mu \nabla^2 \omega + g\frac{\partial(\rho - \rho_o)}{\partial x} \tag{3.10}$$

In this partial differential equation, $\mu\nabla^2\omega$ is the viscosity component with Îij the kinematic viscosity; $g\partial(\rho-\rho_o)/\partial x$ is defined as the force vector with g the acceleration due to gravity and ρ and ρ_o are the actual and the offset value of the fluid density, respectively.

Because in our case the fluid is a solution containing the growth units, diffusive solute mass transport is a function of concentration (c) and local flow position such that;

$$D\nabla^2 c = \frac{\partial c}{\partial t} - \frac{\partial \psi}{\partial x}\frac{\partial c}{\partial y} + \frac{\partial \psi}{\partial y}\frac{\partial c}{\partial x} \tag{3.11}$$

where D is the solute diffusion coefficient.

Equations 3.9, 3.10 and 3.11 are partial differential equations, which can be solved by finite element analysis. Our aim here was to develop a numerical simulation in order to determine the stream function, vorticity and concentration for growth or dissolution processes, by providing known values for the kinematic viscosity, off-set density, gravitational acceleration, and the diffusion coefficient of the compound under study. For this, we used FlexPDE software, version 6.20, which is a multi-purpose finite element analysis package capable of simulating complex physical processes [77]. We applied a non-slip condition at the crystal interface and the cell walls by using a penalty method [78]. The crystal was assumed to be either situated at the ceiling, the bottom or at both locations simultaneously in the growth cell. We assumed that the crystal does not show an apparent change in size during growth. The boundary conditions were defined with respect to the crystal surface and the growth cell walls such that:

$$\frac{\partial c}{\partial n} = \begin{cases} 0, & \textit{at the growth cell walls} \\ -k\left(c - c_{eq}\right), & \textit{at the crystal edges} \end{cases} \tag{3.12}$$

where, k is the kinetic coefficient and c and c_{eq} are the concentrations at the crystal surface and at equilibrium, respectively. The physical constants for the compounds used in this study are given in Table 3.1.

Table 3.1: The physical constants used in the numerical simulations.

Parameter	Value		
	HEWL	KDP	$NaClO_3$
c_b	3×10^{-2} g/cm^3	21.25 g%	0.714 g/cm^3
c_e	3×10^{-3} g/cm^3	17.709 g%	0.70 g/cm^3
ν	0.01 cm^2/s	1.125×10^{-2} cm^2/s	1.3×10^{-2} cm^2/s
D	1×10^{-6} cm^2/s	6.738×10^{-6} cm^2/s	1.5×10^{-5} cm^2/s
g		981 cm/s^2	
α	0.3032	0.1196	0.55
ρ_o	1.0049 g/cm^3	1.1316 g/cm^3	1.043 g/cm^3

3.3.2 Results and Analyses

Fig. 3.8 shows the simulations for the ceiling growth of a downwards pointing oblong KDP crystal from a 20% supersaturated solution. There is an obvious clear agreement with the experimental data in Fig. 3.7. The simulated time series clearly shows the two stages in the development of the depletion layer. After 100 seconds, a thin concentration gradient normal to the crystal surface is formed by solute uptake at the crystal surface. The width of the boundary layer ($45\mu m$) is quite similar to that observed experimentally. As can be seen in the subsequent images, the depleted solution is pushed upwards by buoyant forces until the flow is prohibited any further at the "ceiling" of the growth cell. After about 5000 seconds the depleted solution encloses the whole crystal and the second stage sets in, expansion downwards by diffusion-limited mass transport.

The simulations show that the second stage of the depletion zone development, apart from a scaling factor ($c_b - c_{eq}$), is independent of supersaturation (Fig. 3.9: upper row, right). This readily follows from the equation of the development of the solute concentration profile, $c(x, y, t)$, during growth in a one dimensional system limited by mass transport:

$$c(x, y, t) = -(c_b - c_{eq}) erfc \ \frac{y}{2\sqrt{Dt}} + c_b \tag{3.13}$$

where *erfc* is the complementary error function.

In contrast, the dissolution of a ceiling crystal is governed by natural convection, leading to a thin boundary layer around the crystal and a downward directed convection plume. As seen in Fig. 3.9, upper row, left, the diffusion boundary layer gets thinner for increasing undersaturation.

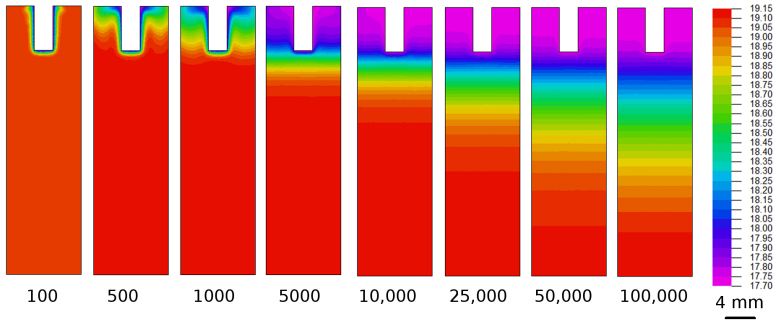

Figure 3.8: Time series of the development of the vertical solute concentration gradient in the case of ceiling KDP crystal growth in a 20% supersaturated solution. The calibration bar accounts to the concentration profile (in gm%) and the time is counted in seconds after the initiation of growth.

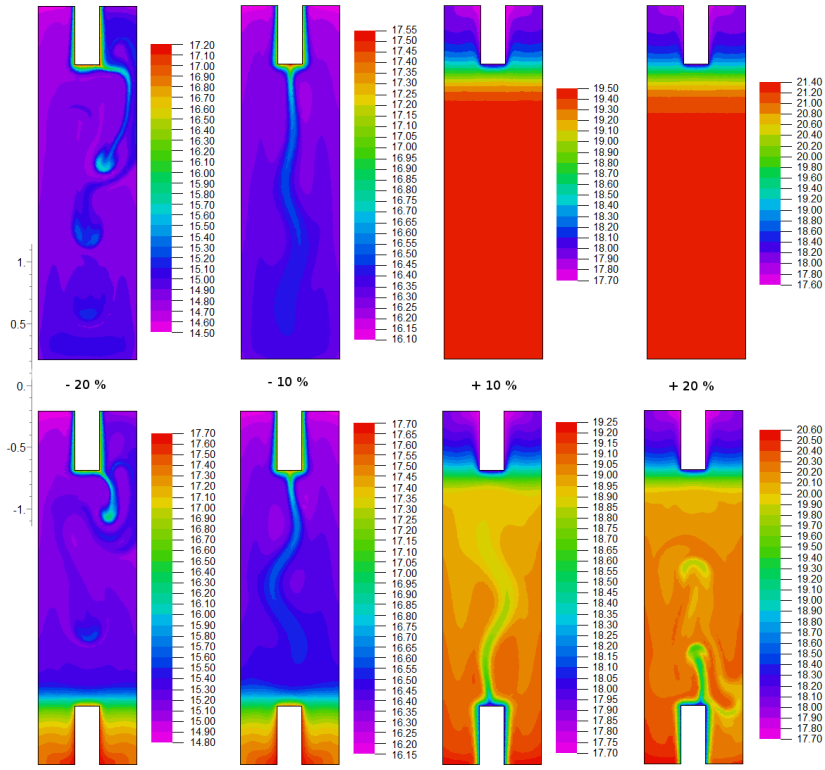

Figure 3.9: Simulations of the development of concentration gradients and/or convection plumes as a function of supersaturation and crystal growth geometry. For each separate simulation, the resultant concentration profile after one hour of growth or dissolution is presented along with its associated legend (KDP in g%).

Because in practice it is very difficult to avoid nucleation at the bottom of the growth cell, in particular at high supersaturation, which is the optimal condition for most protein crystallisation protocols, we also simulated the condition where two crystals grow or dissolve at both locations simultaneously (Fig. 3.9, lower row). At higher supersaturation, the developed convection plumes are able to reach the depletion zone around the ceiling crystal, still the latter is hardly distorted. In the presence of more batch and ceiling crystals the solution depletes faster, but the overall mechanism remains the same. Another effect that can be easily spotted is that the concentration of the bulk solution decreases rapidly, due to the faster growth of the batch crystals and the continuous mixing of the solution by the action of natural convection. As a consequence, the depletion zone of the ceiling crystals, despite being intact, fades away in the course of time. This was also observed in our KDP growth experiments (Fig. 3.7). The simulation of two crystals simultaneously dissolving at the top and bottom of the cell yielded the same results, but in opposite directions (Fig. 3.9, lower row, left).

Among the factors which affect the growth process, are the intrinsic properties of the solutes (molecule to be crystallised, buffer, salts, precipitant) and the solvent used to prepare the crystallisation solution. One of these properties, the diffusion coefficient of the molecule to be crystallised has the highest influence on the shape, progression and extension of the concentration profiles. Fig. 3.10 displays simulations of the concentration profiles for three different compounds; sodium chlorate (NaClO3), KDP and HEWL. The diffusion coefficients D of these compounds are 1.5×10^{-5} , 6.7×10^{-6}, and $1.0 \times 10^{-6} cm^2/s$, respectively. [79]

The decrease of these values for the three compounds is directly related to the decrease of the progression of the depleted zone and therefore, the growth rate of the three types of crystals as follows from equations 3.5 and 3.11. Experimentally, at the same starting supersaturation under diffusion-limited crystal growth conditions, the final crystal size of an average HEWL crystal is about five times smaller than that of KDP, which again is smaller than $NaClO_3$. In our simulations, starting from the same size of seeding crystals, the development of the depletion zone is the slowest for HEWL and the fastest for $NaClO_3$, in accordance with their crystal growth rate and diffusion coefficient. This rate of development can be enhanced by the nucleation of several crystals at the ceiling of the growth cell as discussed below, which generally is the case for ceiling growth. In comparison with other proteins, HEWL has one of the highest values for its diffusion coefficient (e.g. BSA $= 6.09 \times 10^{-7} cm^2/s$, bovine insulin $= 7.3 \times 10^{-7} cm^2/s$). This makes the method broadly applicable as long as certain dimensional ratios are preserved, as discussed below. In such a case, the size of the growth cells can be much reduced and still the buoyancy-assisted diffusion and the depleted zone of the ceiling crystals will not

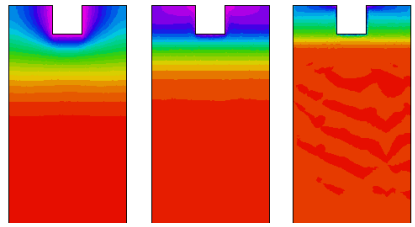

Figure 3.10: Simulated concentration profiles of (from left) $NaClO_3$, KDP and HEWL ceiling crystals one hour after the initiation of growth. The figure displays only a magnified view for the upper part of the growth cell (which is $1 \times 4cm^2$).

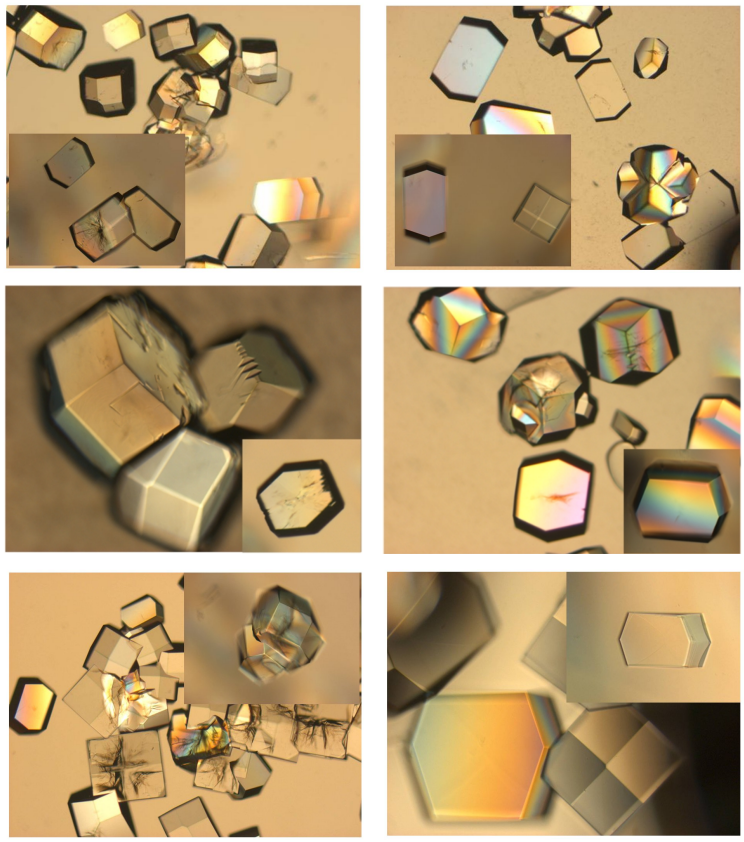

Figure 3.11: Ceiling (inserts) and batch HEWL crystals grown in wide (left column, top) and narrow (right column, top) growth cells. The second and third rows display HEWL crystals grown in the presence of bovine insulin and BSA as an impurity, respectively. Often ceiling crystals were fewer. All images are displayed at the same scale. Pictures are representative for the entire population.

be disturbed by the convection plumes rising from any batch crystals which happen to grow at the bottom.

3.4 Dimensions of the Growth Cell

As follows from the experimental and simulation results, successful ceiling crystallisation depends on many factors. One of the most important points for protein crystallographers is the achievable sample volume per trial. Nowadays, many commercially available crystallisation set-ups adopt vapour diffusion and micro-batch platforms in the nano- to microliter range for both globular and membrane proteins. The ceiling method is not suitable for broad initial screening of crystallisation conditions, because of the minimal volume requirement of about $10\mu l$ per trial, but rather for improving crystal quality under preselected conditions. In this context it is important to consider the dimensions of the growth cells, in order to achieve diffusion-limited mass transport.

Experimentally, we examined this by performing two sets of trials using differently sized growth cells of 7 mm radius and 2 mm height (group 1) and 3.5mm radius and 2mm height (group 2) in which tetragonal HEWL crystals were grown. The effect of adding impurities with different segregation coefficients *(k)* [80] to the mother liquor, i.e. bovine insulin and bovine serum albumin (BSA), was also studied. As shown in Fig. 3.11, the ceiling crystals grown in the narrower vials (right column) in all cases are morphologically defect-free when compared to their counterparts in the wider vials (left column) and also are hardly affected by any impurities present ($k< 1$). Similar results were reported earlier in a space microgravity experiment. [15] In addition, preliminary SDS PAGE analysis indeed confirmed the optical data, indicating lower incorporation of BSA in ceiling crystals grown in the narrower cells (not shown).This demonstrates that the ceiling method succeeds to accomplish a similar diffusion-limited growth condition.

In order to understand this effect of the vessel width, we simulated the growth cells by considering crystals on the ceiling and at the bottom simultaneously (Fig. 3.12). Obviously, the depth of the depletion zone varies inversely with the width of the growth cell at constant height of the growth cell. This probably is because it takes longer time in the wider cell to fill the horizontal layers with depleted solution and hence to start diffusion limited growth. At the early convection mediated stage, the probability of impurity incorporation is relatively high. Therefore, regardless of the value of the segregation coefficient, the impurities will find their way to the tetragonal HEWL crystal nuclei (in case of BSA), inducing more nucleation and twinning, or during crystal growth (in case of bovine insulin) leading to crystals possessing rougher surfaces. Thus, we surmise that rapid enclosure

of growing ceiling crystals by the depletion zone will result in better quality crystals. Further, we anticipate that this will be enhanced by simultaneous growth of a relatively large number of ceiling crystals and by a not too small ratio of the height of the growth cell relative to its width (e.g. in the order of 3 to 4, as used routinely and also accords with the 10 μl. nanoplate wells). This was indeed borne out by further simulations, showing that the presence of many nucleation sites improves the solute depletion pattern of every individual ceiling crystal (not shown).

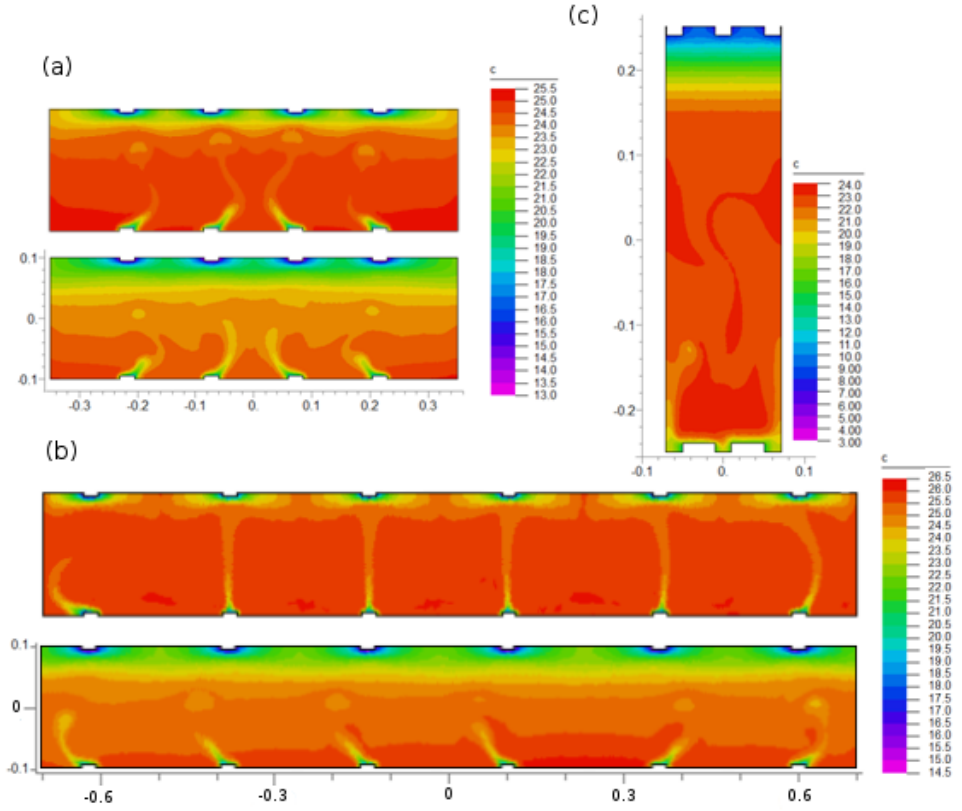

Figure 3.12: Numerical simulations of HEWL crystal growth in cells with dimensions mimicking those in Fig. 3.11 and of a 10μl well in a nanoplate. After 10 minutes, the depletion zone is more developed in the narrow vial (a) compared to the wider vial (b). After one hour, the depletion zone at the top extends deeper in the narrow vial than in the wide vial. In addition, the convection plumes from the bottom crystals reach the depletion zone faster in the wide vial. The nanoplate well shows the best development of the depletion zone (c). (scale in cm, concentrations in mg/ml)

We also simulated a nanoplate well, and although it provides limited space for nucleation, it does show rapid development and extension of the depletion zone downwards (Fig. 3.12), confirming that the ceiling method is also applicable to this very small volume scale.

3.5 Conclusions

We studied the solute concentration profiles developing during growth as well as dissolution of crystals mounted at the top (ceiling method) and/or at the bottom of the growth cell (batch method). Through a Mach-Zehnder phase shifting interferometer (PSI) and a five-frame algorithm, we successfully monitored these profiles which develop during dissolution and growth of KDP crystals. The PSI data are substantiated by finite element based numerical simulation.

The profiles resulting from dissolving batch crystals showed a morphological resemblance to that from growing ceiling crystals. In both cases, after an initial period of formation of an expanding enrichment/depletion zone (governed by natural convection), the process becomes largely controlled by diffusion-limited solute transport. Yet, the observed differences between dissolution and growth provide evidence that in the latter case the surface kinetics and, at higher supersaturation, the nucleation of crystallites play a non negligible role.

In addition, the growth of ceiling HEWL crystals and the simulation of this process reveal that the cell dimensions are critical for effective ceiling crystallisation. At a low height to width ratio, diffusion controlled mass transport develops slower, giving more chances for the rising convection plumes to perturb the growth of ceiling crystals and thus making the merits of the method less favourable. The simulations also showed that the ceiling method can be effective at a very small scale, given that the cell aspect ratios are such that the initial convection stage is as short as possible.

In short, our investigations generally confirm that the ceiling approach affords a simple and economical set-up to realise fully convection-free mass transport and therefore diffusion-limited crystal growth.

Chapter 4

A Comparative Study of Impurity Effects on Protein Crystallisation: Diffusive *versus* Convective Crystal Growth[1]

Abstract

The incorporation of impurities during protein crystallisation is one of the main obstacles that prevents the growth of high quality crystals. Mass transport has been shown to affect the incorporation of impurities. Here we used a special growth configuration which enables the simultaneous investigation of the two main means of mass transport: diffusion and convection, under otherwise identical conditions. Two polymorphic forms of hen egg-white lysozyme were crystallised using this configuration in the presence of structurally related or unrelated impurities at various degrees of contamination. In contrast to the common opinion, the diffraction quality of crystals grown under diffusion-limited conditions is better than that of those grown in the presence of natural convection, even in the presence of impurities which are not easily segregated. The results also reveal a significant difference in impurity uptake for the different polymorphic forms of the same protein. The combined results show that, also in the presence of large fractions of impurities, the most perfect crystals grow when the rate of accretion of molecules is slow and orderly, as realised under diffusion-limited conditions.

[1]Content of this chapter is to be submitted as Alaa Adawy, Esther van der Heijden, Johan Hekelaar, Willem J. De Grip, Willem van Enckevort & Elias Vlieg

4.1 Introduction

The most serious obstacle in the route of macromolecular structure determination is the growth of high-quality crystals that diffract X-rays to high resolution limits.

The final crystal shape and perfection are determined by the interplay between the transport of growth units towards the crystal and their subsequent integration into the crystal surface. The balance between these two steps determines the solute concentration profile around a growing crystal. While the transport of the target macromolecules and other constituents in the solution is isotropic, the interfacial processes are anisotropic owing to the anisotropic distribution of bonds in the crystal structure. As a consequence, at the same supersaturation crystal surfaces with different orientations have different growth rates and slightly different composition. These effects together with defect formation during growth limit crystal perfection upon growth from solution. The presence of macromolecular impurities in the crystallisation solution, which is almost always the case, may deteriorate the structural resolution upon incorporation, by inducing internal stress (mosaicity) and enhancing the rotational disorder in the crystals [81, 82].

According to their structural relation to the target macromolecule [42], impurities are either structurally-related, micro-heterogeneous: preferentially incorporated into target protein crystals at an early stage of growth typically resulting in imperfections in the crystal core, or structurally-unrelated, heterogeneous: largely repelled at the beginning, but often later adsorbed on the crystal surface, inducing reduction of the average step velocity and blockage of the advancing steps [83, 84].

Beside the impurity type, the supersaturation (σ) can directly affect the level of impurity incorporation [85]. The presence of convectional currents disturbs the interface incorporation processes by inhibiting the development of a depletion zone at the crystal-solution interface, thereby maintaining a high local supersaturation and a corresponding high growth rate with a constant incorporation of impurities. This is the common situation in most terrestrial crystallisation techniques in which natural convection is imposed by the action of gravity.

In diffusion-controlled crystal growth conditions, significant concentration gradients of all the mother liquor constituents develop around the growing crystal. Not only does a stagnant solution reduce the transport of impurities towards the crystal primarily by *diffusional purification* and possibly by *diffusional filtration* , but also allows the crystal surface sufficient time for *self purification* in which it desorbs infiltrating impurities to the surrounding solution.

Eventually, crystallographers are mainly interested in the diffraction quality of the crystals and for that, several methods have been established to grow high quality crystals.

Optimisation can be accomplished by reducing gravity-induced convection currents [25].

Earlier studies have compared the crystallographic quality of protein crystals grown in microgravity to that of crystals grown in parallel in terrestrial setups under roughly the same conditions [86]. The statistical analysis revealed that in about half the cases, the suppression of convection leads to better crystals. These results suggest that diffusion-controlled growth cannot always be the magic wand.

Recently, we described the ceiling crystallisation method in which diffusion-limited growth is realised by allowing crystals to grow downwards from the lid of a growth cell overfilled with crystallisation solution [40, 69, 87]. If we allow the simultaneous growth of crystals at the bottom of this cell, where gravity-driven convection currents occur, we can precisely compare the effect of diffusive and convective mass transport on the incorporation of impurities during protein crystallisation in the same growth cell and thus under otherwise identical conditions. In this report, we use two polymorphic forms of Hen Egg-White Lysozyme (HEWL), tetragonal and monoclinic, as our model crystals. HEWL crystals were grown in the presence of a broad range of molar fractions of different impurities. We investigated and compared nucleation, crystal morphology, impurity segregation and X-ray diffraction quality of convectively and diffusively grown crystals. The aim was to monitor the strength of self-purification in the presence of different impurities and to study whether crystals can grow from highly contaminated or mixed solutions. Notwithstanding all the parameters which co-affect crystal quality, we have found that steady slow growth mediated by diffusion-controlled conditions leads to the growth of crystals with higher ordering.

4.2 Theory

We briefly describe the theory of impurity incorporation during crystal growth, because this is needed to interpret the experimental results. Most of this description can also be found in the literature [88, 89, 90, 66, 91, 15]

The concentration C_i^c of the impurity (i) in the crystal (c) with respect to its concentration C_i^s in the solution (s) can be characterised by various segregation coefficients (also called partition or distribution coefficients). If we use the concentrations relative to the target protein (p) concentration C_p we obtain the fractional segregation coefficient:

$$K = \frac{(C_i^c/C_p^c)}{(C_i^s/C_p^s)} \tag{4.1}$$

It is important to realise that the concentrations are the values at the growth interface,

which may differ from the values in the bulk. K describes whether crystallisation leads to purification ($K < 1$) or not ($K > 1$). Micro-heterogeneous impurities are normally difficult to remove and have $K > 1$, while heterogeneous impurities typically have $K < 1$.

In order to describe the purification of the target protein with respect to the solution, the volume segregation coefficient is used:

$$k = \frac{C_i^c}{C_i^s} = \frac{C_p^c}{C_p^s} * K \tag{4.2}$$

k is related to the flux Ji of impurities at the interface by:

$$J_i = R(k-1)C_i^s \equiv \beta_i C_i^s \tag{4.3}$$

with R the growth rate and β_i the impurity kinetic coefficient. (β_i is mentioned for completeness, but is not be used here). Equation (4.3) shows that for $k > 1$ there is a net flux towards the crystal, while for k < 1 this flux is negative. The ratio C_p^c/C_p^s is typically in the range 10-100 for protein crystallisation and thus in most cases, even when $K < 1$, the value of k is larger than 1, i.e., there is a net flux of impurities towards the crystal.

Experimentally, it is difficult (if not impossible) to determine the protein and impurity concentrations at the growth interface, and thus mass transport is modelled in order to derive the values at the interface from the known bulk concentrations. This leads to an effective value K_{eff} for the segregation coefficient with respect to the bulk concentration [89]. Moreover, the growth conditions may vary as a function of time and as a consequence the impurity concentration in the crystal may not be constant. K_{eff} is also used to denote the value of K averaged over these variations, both theoretically and experimentally [91, 15].

In protein crystallisation it is often assumed that K is constant for a given impurity-protein combination [20], but segregation coefficients can depend on the growth rate and other parameters [88]. At very low growth rates, K will be equal to its thermodynamic equilibrium value K_o, but at high growth rates kinetics may change its value. Reducing the growth rate may thus lead to a smaller value of K and this is called enhanced self-purification.

Using k and K we can roughly predict the impurity concentration profiles under both diffusion-limited and convection-mediated conditions. This is schematically shown in Fig. 4.1 a. During crystal growth, protein and impurity molecules are removed from the solution. When convection is present, the mixing will keep the concentration in the solution approximately constant as indicated by the dashed lines in the solution.

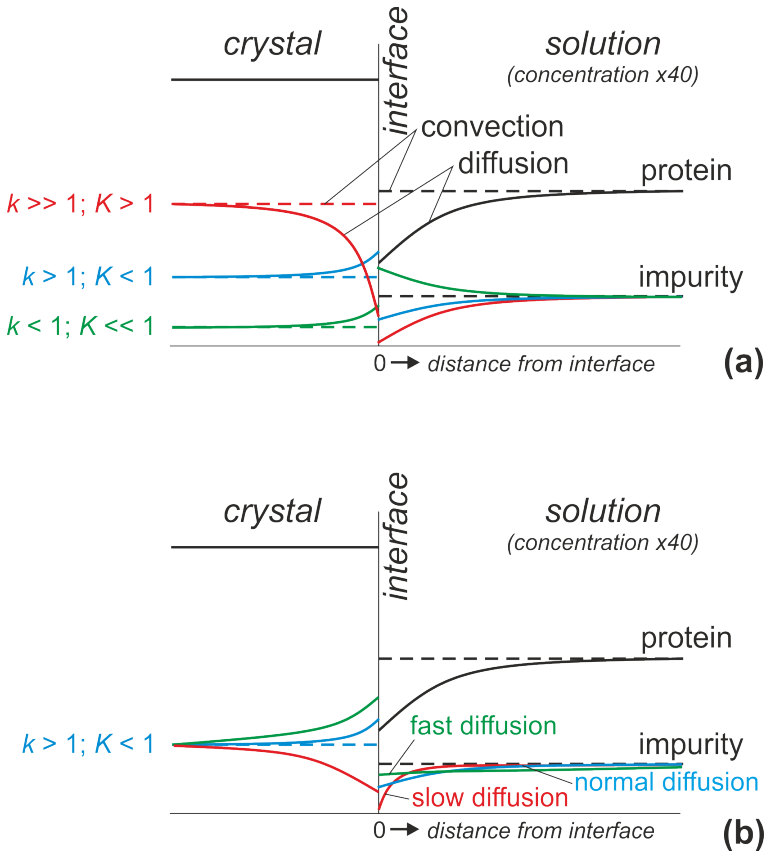

Figure 4.1: Schematic diagram for the impurity concentration profiles at the crystal-solution interface, under convective (dashed lines) and diffusive (solid lines) crystal growth conditions, in the presence of macromolecular impurities bearing (a) different K and k values: the crystallising protein and impurities are assumed in this diagram to have the same D; (b) same K, but different D. Under diffusion controlled conditions, if the flux of an impurity is slow enough, it may help in developing an impurity depletion zone at the crystal interface. The initial concentrations for crystallising protein and impurity are shown in dashed black lines. The concentration of protein in the crystal (solid black line) is assumed to be constant and much higher than that of the impurity.

The impurity concentration in the crystal will therefore also be constant, with a value determined by K. This is indicated by the three dashed lines drawn in the crystal, for three different values of K. Because of the constant concentration and the slow growth of proteins, the K_{eff} value is very close to the actual K value for convective growth.

Now consider diffusion-limited growth. A protein depletion zone will develop around the crystal and the growth rate will decrease. The concentration of the protein in the crystal will of course be constant. The evolution of the impurity concentration depends on the values of K and k. For $K > 1$ (and thus k $\gg$ 1), impurities will be preferentially incorporated, leading to a stronger depletion of the impurities than of the protein in the solution. As a consequence, the impurity concentration in the crystal will decrease as growth continues (red curves in Fig. 4.1 a). This is called diffusional purification. Such crystals will exhibit a core with an enhanced impurity concentration. For $K < 1$ and $k > 1$ there is still depletion of the impurity in the solution, but less than of the protein and thus the concentration in the crystal will increase (blue curves). For $K \ll 1$ and $k <$1, finally, there is an accumulation of impurities in the liquid ahead of the growth front while, just as for the previous case, the impurity concentration in the crystal will increase over time (green curves).

For the conditions assumed here, we thus find that for $K > 1$, diffusion-limited growth is beneficial as compared with convection-mediate growth in terms of impurity incorporation. For $K < 1$ the reverse is true [92]. The above discussion assumes that the diffusion coefficients of the impurity and protein are approximately the same. This does not have to be the case and Fig. 4.1 b schematically shows the expected behaviour for $k > 1$ and $K < 1$. For heterogeneous impurities larger than the target protein, the case of slower diffusion may frequently occur. This slow diffusion leads to a more rapid depletion adjacent to the interface such that the concentration in the crystal may decrease as well (red curve). This therefore identifies a regime where diffusion-limited growth can be beneficial, even for $K < 1$. This is called diffusional filtration.

4.3 Materials and Methods

4.3.1 Materials

Hen egg-white lysozyme (HEWL)(Cat. No. L6876), albumin from bovine serum (BSA, fraction V, fatty acid-free; Cat. No. 85040C) and from egg white (ovalbumin; lot # 066K7020V), and avidin from hen egg-white (lot # 031M7025V) were purchased from Sigma-Aldrich and used without further purification. Some relevant properties of these macromolecules are listed in Table 4.1. The activated fluorescent dye, DY-632-01 NHS

ester, ($C_{14}H_{49}N_3O_{14}S_3Na_2$, MW = 950.03 g/mol) was obtained from Dyomics. All other chemicals were of reagent grade.

Table 4.1: Summary of relevant physico-chemical properties of the proteins used in this study. MW: molecular weight, IEP: isoelectric point, D: diffusion coefficient

Protein	MW (KDa)	IEP	D (m^2/s)
HEWL	14.307	10.5-11	1×10^{-10}
Avidin	16.5-17.25	10.5-11	$5.98 - 6.4 \times 10^{-11}$
Ovalbumin	43-45	4.6-4.7	$7.1 - 7.8 \times 10^{-11}$
BSA	66.5	4.7	6.09×10^{-11}

4.3.2 Methods

Protein labelling with fluorophore

DY-632-01 was dissolved at 12mg/ml in DMF and mixed with HEWL monomers dissolved at 5mg/ml in 50 mM $NaHCO_3$ solution (pH 8.3) at 1:1 molar ratio and incubated in the dark for 2 hrs at 20^{o}C. Subsequently, the excess dye was removed by gel filtration on a Sephadex G-25M column (GE-Healthcare) equilibrated in 100mM PBS-buffer (pH 7.4). The spectra of eluted fractions were recorded after suitable dilution (Lambda 35-UV/VIS spectrophotometer, PerkinElmer instruments). HEWL and DY-632-01 have absorbance bands peaking at 281 nm (ε: 2.64 $mg^{-1}.cm^{-1}$) and 631nm (ε: 210.5 $mg^{-1}.cm^{-1}$), respectively. HEWL fractions that showed the highest extent of labelling were combined. MALDI-TOF analyses of the selected fractions showed that >50% of HEWL molecules were labelled, all with one dye molecule. The labelled HEWL will be designated as F-Lyz.

Crystallisation

Tetragonal and monoclinic crystals of HEWL were grown from solutions of NaCl (30-40 mg/ml) and $NaNO_3$ (20 mg/ml), in which HEWL was added to a concentration of 1 and 0.7 mM, respectively, in 50 mM NaOAc buffer, pH 4.5, at 19 $\pm$ 0.5^{o}C in a vibration-free environment. The protein concentrations C_p^s are $6.02 \times 10^{14} mm^{-3}$ and $4.22 \times 10^{14} mm^{-3}$ in the mother liquor of tetragonal and monoclinic crystals, respectively. From the crystallographic structure the protein concentrations in the crystals C_p^c are calculated to be $3.47 \times 10^{16} mm^{-3}$ and $3.94 \times 10^{16} mm^{-3}$ for tetragonal and monoclinic

crystals, respectively. We therefore use conditions in which the ratio C_p^c/C_p^s is 58 and 93 for the growth of tetragonal and monoclinic crystals, respectively.

The resultant supersaturation in both solutions is below the supersaturation at which homogeneous nucleation occurs [93], but optimal for crystal growth [94]. The crystallisation behaviour of monoclinic HEWL is very sensitive to the presence of certain impurities, which may result in the growth of spherulites.

To study the effect of protein contamination on crystal characteristics, we added F-Lyz and avidin, which have a similar structure and/or size as that of HEWL, and ovalbumin and BSA, which differ strongly in size and structure. In the cases of F-Lyz and BSA, a number of crystallisation experiments were prepared with a range of impurity concentrations to systematically investigate their effect on crystal growth: From 0.01 up to 3% of the molar ratio in case of F-Lyz and from 2 up to 50% molar ratio in case of BSA. Avidin and ovalbumin were added to accomplish molar ratios of 10 and 20% with respect to the initial concentration of HEWL. Routinely, we prepared two parallel setups, one to monitor crystal growth and the other for *in situ* analysis by confocal microscopy. For the first set, microtubes (800 μl) or microplates (150 or 350 μl) were used and the wells were overfilled with the mother liquor and covered by a thin glass slip [40, 69]. Crystallisation in these oblong cells is very suited to compare ceiling (diffusive growth) and batch (convective growth) crystal growth [87]. For confocal laser scanning microscopy, 0.1 ml of the mother liquor was sandwiched between two glass cover slips separated by a rubber ring 0.6 cm in inner diameter and 0.25 cm thick.

Crystal characterisation

1. *In situ* measurements: Crystals were monitored under a polarisation microscope in transmission mode (Leica DM-RX), for *in situ* observation of crystal morphology. Micrographs were collected using a video camera (Evolution VF) and processed using *Image Pro plus 2*. For the *in situ* monitoring of the incorporation of F-Lyz into single HEWL crystals, a confocal laser scanning microscope (CLSM) (Leica DM IRE2) was used. Excitation was performed with a HeNe laser (632.8 nm). The observation (fluorescence) wavelength range was 645-750 nm, using an excitation intensity of 17%, a PMT gain of 422 V and a pinhole diaphragm diameter of 72.54 μm.

2. Analysis of crystal composition: Quantitative analyses were performed to allow the estimation of K_{eff} of macromolecular impurities incorporated into the ceiling and batch crystals.

Impurity incorporation in the HEWL crystals was analysed by size exclusion chro-

matography (gel filtration). Crystals from every single vial were carefully rinsed by buffer to remove the adhering mother liquor solution before being dissolved in water. Their contents were separated on a Discovery Bio Gel Filtration Column (MW range 500–150,000), in the HPLC mode (Aligent Technologies 1260 infinity) using 150 mM phosphate buffer as a mobile phase with detection at 214 nm. A standard curve was run for every constituent and used for quantification of HEWL and the contaminating proteins. The HPLC analysis showed that the BSA sample largely consisted of monomers (82.9%), but also contained trimers (13.8%) and tetramers (3.3%)

3. X-ray diffraction: The effect of increasing the levels of BSA contamination on the diffraction quality of ceiling and batch tetragonal HEWL crystals was examined by using a Cu-Kα rotating anode X-ray source (FR591, Bruker Nonius). For each contamination level, tetragonal batch and ceiling crystals of comparable sizes were fished and immersed in freshly prepared mother liquor containing 30% PEG400 before being exposed for 30 seconds to X-rays. Resolution limits realised at $I/\sigma = 3$ were determined using iMOSFLM [95].

4.4 Results

4.4.1 F-Lyz as an impurity

We observed nucleation after two days of incubation for tetragonal HEWL ceiling and batch crystals in the presence of F-Lyz. This did not occur until one week later in the reference experiments (0% F-Lyz). The number of nuclei increased and the average crystal size decreased with increasing F-Lyz content (Table 4.2).

Table 4.2: Effect of F-Lyz contamination (% w/w) on the average size and total number of tetragonal ceiling crystals and the segregation coefficients of ceiling and batch crystals one week after starting the crystallisation experiments

F-Lyz %	Size (mm^3)	Number	K_{eff} (ceiling)	K_{eff} (batch)
0	0.125	15	–	
1	0.064	40	1.50	2.30
2	0.027	50	4.37	6.44
3	0.008	60	6.21	10.46

As shown in Fig. 4.2 panels a and b, F-Lyz was not homogeneously distributed over the tetragonal crystals. The highest level was detected in the crystal core with much reduced levels of F-Lyz at the crystal edges, where it was preferentially incorporated into

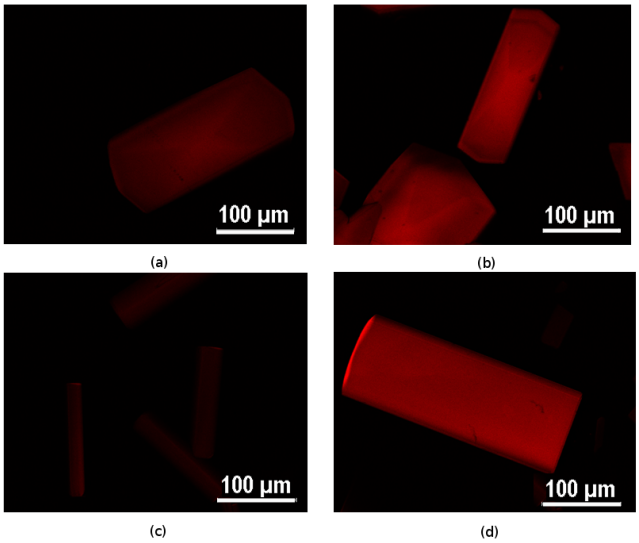

Figure 4.2: Confocal fluorescence micrographs of ceiling (left column) and batch (right column) tetragonal (a,b) and monoclinic (c,d) HEWL crystals. The plane of observation corresponds to the center of each crystal, where F-Lyz is relatively highly incorporated. All images were acquired under the same excitation and detection settings.

the {110} sectors. The ceiling crystals were less fluorescent than their batch counterparts. This is confirmed by the quantitative analysis using UV-Vis spectroscopy (Table 4.2).

For monoclinic HEWL crystals, F-Lyz did not show an apparent effect on the size or nucleation and confocal microscopy showed that F-Lyz was homogeneously distributed through the crystals, except for a preference to the easily poisoned $(0\bar{1}0)$ faces (Fig. 4.2 panels c and d). Also, the fluorescence micrographs showed that the ceiling crystals exhibited significantly lower contamination than their batch counterparts (Fig. 4.2).

4.4.2 Avidin as an impurity

Avidin did not show a clear effect on the nucleation or the size of tetragonal HEWL crystals (Fig. 4.3). Microscopic inspection showed that the crystals have smooth and sharp edges with cracked cores. For the monoclinic polymorph, regular, but smaller ceiling crystals grew at 10% and 20% avidin molar fractions, respectively (Fig. 4.4). Batch crystals were obtained as spherulites. For both polymorphs, the ceiling crystals showed a smaller K_{eff} compared to their batch counterparts and the values mostly varied inversely with the initial contamination level (Table 4.3).

Table 4.3: K_{eff} at 10 and 20% molar ratios of different impurities (X) for their incorporation into tetragonal and monoclinic HEWL ceiling and batch crystals

	Tetragonal				Monoclinic			
X:HEWL(M)	0.1		0.2		0.1		0.2	
Growth	Ceiling	Batch	Ceiling	Batch	Ceiling	Batch	Ceiling	Batch
Avidin	1.65	2.27	1.14	1.61	1.41	1.62	0.93	1.87
	(0.52)	(0.26)	(0.26)	(0.27)				(0.27)
Ovalbumin	0.28	0.02	1.06	0.03	0.09	0.02	0.05	0.02
			(0.04)		(0.19)		(0.03)	
Total BSA	0.27	0.06	0.04	0.03	0.03	0.02	0.02	0.02
BSA 1ers (82.9%)	0.33	0.03 (0.02)	0.05	0.02	0.03	0.01	0.02	0.01
BSA 3ers (13.8%)	–	0.13	–	0.05	–	0.10	–	0.03
BSA 4ers (3.3%)	–	0.55 (0.01)	–	0.28	–	5.3E-06	–	0.07

Data are the medians of triplicate experiments of every condition, each analysed independently twice. The results which were below the detection limit are indicated by a dash. The standard error is only indicated if it is >0.01 (numbers in parentheses below the data).

4.4.3 Ovalbumin as an impurity

In contrast to F-Lyz, ovalbumin reduced nucleation for both polymorphs, except for the batch crystals grown at the 20% level of contamination. Tetragonal crystals showed some sawtooth edges, and the crystals were slightly smaller than those grown in the presence of avidin and there was no effect on the crystal morphology. The monoclinic ceiling crystals grew as large as they did in the presence of avidin (Fig. 4.4). Only among batch crystals spherulites were observed.

K_{eff} values for the ceiling crystals were greater than that for batch ones and in all cases they were <1 (Table 4.3). In addition, K_{eff} values for ceiling monoclinic crystals were much smaller than for their tetragonal counterparts. For the ceiling tetragonal crystals, K_{eff} increased with the initial impurity concentration. In batch growth, both polymorphs reacted on the excessive impurity content of ovalbumin by enhanced nucleation, resulting in the growth of many small crystals, probably since the crystals stopped growing at a very early stage. This explains the big difference in K_{eff} values determined between the tetragonal ceiling crystals and their batch counterparts (Table 4.3).

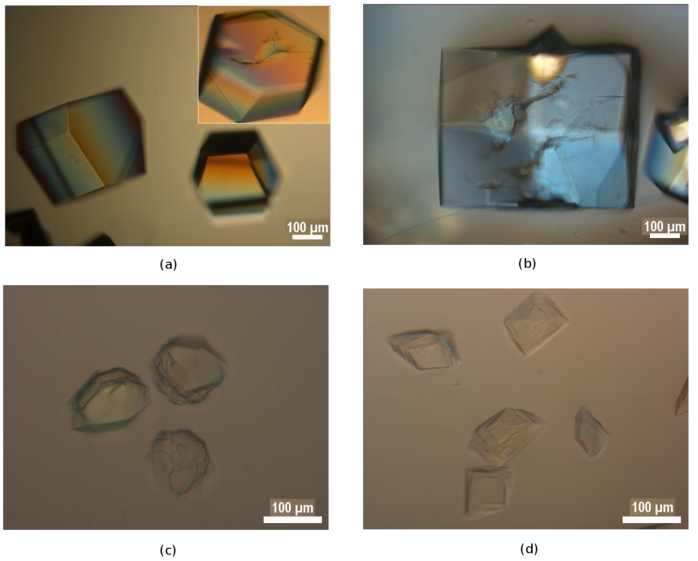

Figure 4.3: Tetragonal ceiling HEWL crystals grown in the presence of avidin at molar ratio of (a) 10% and (b) 20% and in the presence of BSA at molar ratio of (c) 10% and (d) 20% of the HEWL in their mother liquor. Calibration bar represents 100μm.

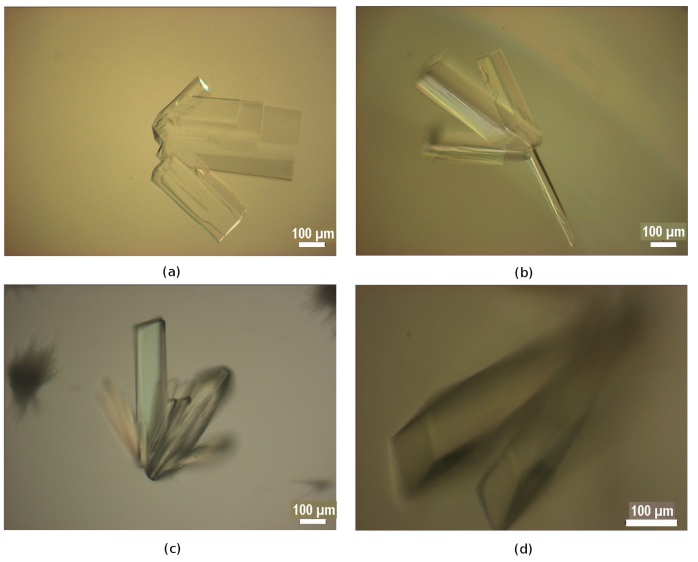

Figure 4.4: Monoclinic ceiling HEWL crystals grown in the presence of avidin at molar ratio of (a) 10% and (b) 20% and in the presence of ovalbumin at molar ratio of (c) 10% and (d) 20% of the HEWL in their mother liquor. Calibration bar represents 100μm.

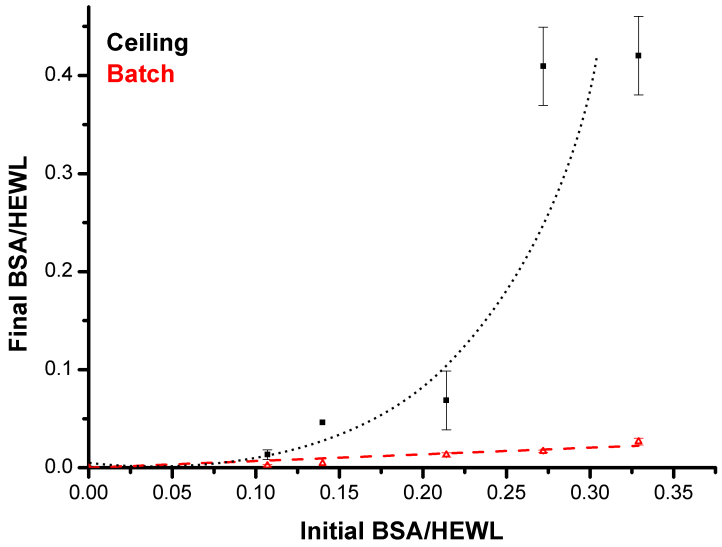

Figure 4.5: The variation of the final BSA monomers to HEWL molar ratio of tetragonal HEWL ceiling and batch crystals as a function of the initial BSA to HEWL molar ratio in the mother liquor. The slope of this function is the K_{eff}, which is constant for batch crystals (linearly fitted) and increasing for the ceiling crystals (The curve is a guide to the eye). (1.4 mM HEWL, 35 mg/ml NaCl in 100 mM NaOAc pH 4.5, $20^{o}C$).

4.4.4 BSA as an impurity

K_{eff} for incorporation of BSA monomers were always <1, albeit ceiling crystals were more contaminated than batch ones (Table 4.3). The quantitative analyses also revealed that the incorporation of BSA into tetragonal batch crystals increased with the initial concentration of BSA in the solution in a way that led to an almost constant K_{eff} regardless of the BSA concentration (Fig. 4.5). For the tetragonal ceiling crystals the incorporation showed a weak trend for both increased incorporation and increased K_{eff} at high contamination levels (Fig. 4.5). Remarkably, the HPLC data showed that BSA trimers and tetramers, which represent 13.8 and 3.3 %, respectively, of the used BSA sample, were only present in the batch crystals. These impurities are thus the exception to the common notion that convection-free grown crystals have a smaller K_{eff} for micro-heterogeneous impurities and a larger K_{eff} for heterogeneous impurities.

BSA showed an inhibitory effect on the nucleation of ceiling tetragonal crystals.

Nucleation was delayed and resulted in fewer crystals at higher BSA concentrations (Fig. 4.6). This effect may be due to the larger crystal-glass slip interfacial energy induced by the prescence of of BSA, which is known for its strong adherence to glass [96]. Microscopic inspection showed that the tetragonal ceiling crystals had highly ordered cores, highly defined sector boundaries and rough edges with a gradual decrease in their aspect ratios (c-axis/a or b-axis) with increasing BSA contamination. In contrast, batch crystals encountered enhanced nucleation with increasing BSA contamination and at higher concentrations, twinned crystals and poly-crystallisation sites were observed (Fig. 4.6). The resulting batch crystals were in most cases smaller than their ceiling counterparts.

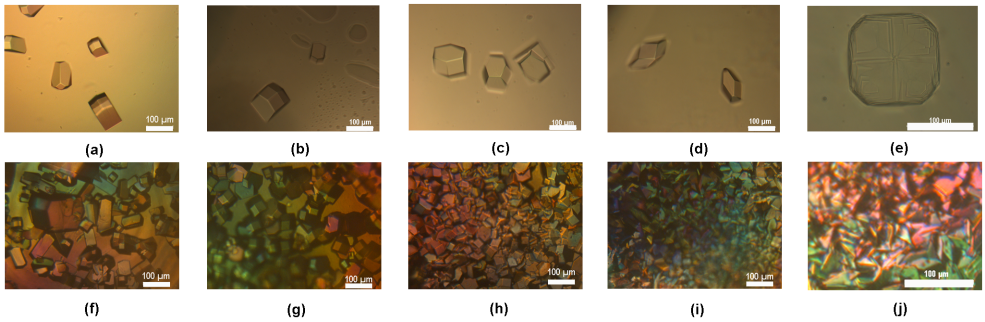

Figure 4.6: Micrographs of the ceiling (upper row) and batch (bottom row) tetragonal HEWL crystals (1.05 mM HEWL, 30 mg/ml NaCl in 100 mM NaOAC pH 4.5, $20^{o}C$) grown in the presence of 0 (a,f), 19 (b,g), 37 (c,h), 75 (d,i) and 150 (e,j) μM BSA in the mother liquor. Calibration bar represents 100 μm

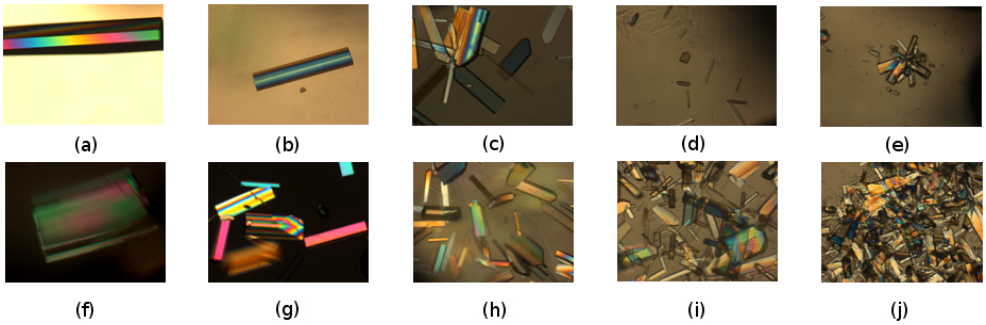

Figure 4.7: Overview of the ceiling (upper row) and batch (lower row) monoclinic HEWL crystals (1.05 mM HEWL, 20 mg/ml $NaNO_3$in 100 mM NaOAC pH 4.5, $20^{o}C$) grown in the presence of 0 (a,f), 19 (b,g), 37 (c,h), 75 (d,i) and 150 (e,j) μM BSA in the mother liquor. All the micrographs are displayed at the same magnification.

For monoclinic HEWL crystallisation, the nucleation was enhanced with increasing BSA concentration both for the ceiling and batch crystals and the final size of the crystals was again decreasing (Fig. 4.7). Monoclinic HEWL crystals showed a decrease in the growth of their (010) faces as a direct effect of BSA contamination. In addition, the crystals showed an increased tendency to share the poisoned ($0\bar{1}0$) faces and to grow in columnar groups. These groups turned into spherulites in case of the ceiling crystals and into completely disordered globular structures for batch crystals at high molar fractions of BSA (10 and 20%). These morphological changes are not a consequence of an effective increase in the initial supersaturation of HEWL because HPLC analyses of the drained solution after the crystallisation experiments did not show a significant change in the concentration of HEWL for all levels of BSA contamination.

X-ray Resolution For tetragonal HEWL crystals grown in the presence of BSA, we determined very small K_{eff}'s for the batch crystals and significantly higher values for their ceiling counterparts. We expected that this would decrease the diffraction quality of the ceiling crystals. Hence, we decided to compare the X-ray resolution for the two growth modes in this protein-impurity combination. Table 4.4 shows the X-ray diffraction data for tetragonal ceiling and batch HEWL crystals grown in the presence of different levels of BSA contamination. Surprisingly, the difference in diffraction quality shows that the ceiling crystals, grown under diffusion-limited conditions, have better diffraction quality than their batch counterparts especially at the higher contamination levels. The estimated mosaicity was lower in the ceiling crystals than in their batch counterparts and the deviation in lattice parameters was very limited.

4.5 Discussion

The results revealed that the behaviour of the different impurities during HEWL crystallisation depends on impurity type, mass transport and polymorphic form.

4.5.1 Impurity incorporation under diffusive *versus* convective growth

The main results with respect to impurity incorporation are summarised in Tables 4.2 & 4.3. From the K_{eff} values obtained for the batch crystals that, owing to the solution mixing, are closest to the real K values, the involved macromolecular impurities used in this study are distinguished into three main groups:

Table 4.4: Laboratory X-ray diffraction data for the structural resolution of ceiling and batch tetragonal HEWL crystals grown in the presence of different molar ratio's of BSA

Impurity	Growth regime	Best value	Crystal size	mean	n	S.D.
1.25%	ceiling	1.63 Å	400 μm	1.75 Å	5	0.10
	batch	2.00 Å	400 μm	2.04 Å	5	0.04
2.5%	ceiling	1.70 Å	300 μm	2.39 Å	4	0.92
	batch	1.61 Å	300 μm	3.29 Å	5	1.69
5%	ceiling	1.73 Å	200 μm	2.73 Å	5	1.19
	batch	1.70 Å	200 μm	3.38 Å	4	1.93
10%	ceiling	1.56 Å	160 μm	1.87 Å	4	0.41
	batch	2.20 Å	160 μm	2.22 Å	3	0.07
20%	ceiling	1.92 Å	160 μm	2.57 Å	5	0.68
	batch	4.65 Å	160 μm	5.29 Å	3	1.22

We used the closest crystal-detector distance (9 mm) in order to realise a resolution of 1.44Å at the edge of the detector. Resolution limits were determined at $I/\sigma = 3$. Crystal size is given by their length along their c-axis. N.B. The ceiling crystals are always thinner along their {110} compared to their batch crystals, which are more symmetric in shape.

a) Micro-heterogeneous impurities: F-Lyz and avidin (K_{eff} >1)

The crystals incorporate a relatively high concentration of the micro-heterogeneous impurities F-Lyz and avidin with respect to the instantaneous concentration in the solution at the interface. As shown in Fig. 4.1 a, for this case the ceiling crystals are expected to have a lower average impurity uptake due to the rapid impurity depletion in the solution. This fully agrees with our observations: for all concentrations of both impurities and for both polymorphs, K_{eff} for the ceiling crystals is less than for the corresponding batch ones. Fig 4.2 shows the corresponding impurity-rich cores that are formed in the tetragonal crystals under these conditions. These are clear cases of diffusional purification in the regime K >1 where diffusion-limited growth is known to be beneficial.

The only unexpected observation is the increase of K_{eff} with increasing F-Lyz concentration (Table 4.2). This seems to contradict the common observation that K is constant [20], as was the case with avidin (Table 4.3). However, this case can be explained by the strong effect that F-Lyz has on the nucleation: the more F-Lyz the more crystals.

Table 4.2 lists the number of crystals for the ceiling configuration; the batch crystals were countless and also increased in abundance with F-Lyz concentration. This means that for a higher F-Lyz concentration, more but smaller crystals are formed. Each crystal has an impurity-rich core and a small rim with a lower impurity and thus high average impurity concentration. This explains the increase in K_{eff} for both ceiling and batch crystals.

b) Heterogeneous impurities: ovalbumin and BSA monomers ($K_{eff} \ll 1$)

As heterogeneous impurities ovalbumin and BSA monomer clearly fall in the regime $K \ll 1$ (Fig. 4.1 a, Table 4.3). Since C_p^c/C_p^s is 58 and 93 for tetragonal and monoclinic HEWL, respectively, these impurities have k values around 1. Whether k is less or greater than 1 determines if the impurity concentration profile in the liquid for ceiling growth is enhanced or depleted, respectively. Nevertheless, in both cases the impurity concentration in the crystal is expected to be higher for ceiling crystals, since this is determined by the value of K. This is exactly what is observed: in all cases K_{eff} is higher for ceiling than for batch crystals.

Here, the batch crystals have benefited from the continual solution mixing resulting from natural convection, which helped in maintaining a reasonably low impurity to HEWL ratio at the crystal vicinity, reducing impurity incorporation. A subsequent result of continual solution mixing is the enhanced nucleation in convective growth (Fig. 4.6, Fig. 4.7). This is because the effective supersaturation stays high enough to induce nucleation of new crystals after the *rapid* surface blockage of the other growing batch crystals. This is not the case in diffusion-controlled crystallisation conditions, where a HEWL-depletion zone develops around the crystal.

For the BSA monomers the final ratio between BSA and lysozyme in the crystal has also been determined for a wider range of initial ratios in the solution (Fig. 4.5). The slopes of these data corresponds to K_{eff}. We see that K_{eff} is much smaller for the batch crystals, in agreement with the more limited data from Table 4.3. For the batch crystals K_{eff} appears to be constant, for the ceiling crystals the K_{eff} seems to increase for increasing impurity concentrations, but the spread in the data makes it difficult to draw firm conclusions.

c) High molecular weight heterogeneous impurities (K_{eff} <1)

Next we consider the oligomers of BSA, where K_{eff} of the crystals is also less than 1. In most cases the values for K_{eff} for the batch crystals are larger than 0.03 and thus k $>$ 1. Following the explanation used for ovalbumin and the BSA monomer, one would

expect the ceiling crystals to have a higher impurity content than the batch crystals. Surprisingly, this is not the case, the concentration of the BSA oligomers in the ceiling crystals is below the detection limit, and thus about a factor 100 lower than expected at first glance. This large difference cannot be explained by the lower diffusion coefficient of the oligomers. The BSA oligomer molecules are significantly larger and thus will have a significantly slower diffusion than the lysozyme molecules. Fig. 4.1b sketches the role of reduced diffusion for the regime $k > 1$, $K < 1$, i.e. the regime of these oligomers. Based on this, the observed K_{eff} values for the ceiling crystals are expected to be a factor 2-4 lower than for the batch crystals. We find a much stronger effect, and thus diffusional filtration does not play a role here. On the contrary, since the oligomers are found to have $K \approx 0$, the impurities are completely expelled and will accumulate at the interface. This is an extreme case of the situation $K \ll 1$ in K_{eff}a (green curve). The low diffusion coefficient of the impurities is now a disadvantage, because the impurities will only be slowly removed from the interfacial region. The data show, however, that even under these circumstances no impurities are incorporated. As an explanation for the observed behaviour we propose that the K value depends strongly on the growth rate. The BSA oligomers are heterogeneous impurities that do not fit easily in the crystal lattice of lysozyme ($K < 1$). At the high growth rates during batch crystallisation these oligomers are likely embedded in the crystals by being captured by the steps that rapidly flow across the surface. For ceiling growth the step rate is much reduced and there is more opportunity for the BSA oligomers to be released from the surface. We thus propose that K depends on the growth rate and is much smaller for ceiling than for batch growth. Even in the regime $K < 1$ diffusion-limited growth can therefore be beneficial owing to the enhanced self-purification.

4.5.2 Impurity effects on structural resolution

As mentioned, we tested the diffraction quality of ceiling and batch tetragonal crystals grown in the presence of BSA, because the ceiling crystals show higher K_{eff} values for BSA monomers than the batch crystals, while only the latter incorporated BSA trimers and tetramers. The diffraction results show that there are no big differences in the diffraction quality between the ceiling and batch crystals at low contamination levels (Table 4). Possibly, this is because the ceiling tetragonal HEWL crystals tend to grow as thin elongated crystals, while the batch crystals grow as symmetric ones [59, 69]. It was also shown before that the realised structural resolution limit is directly related to the crystal volume [40]. Based on the latter, ceiling crystals are therefore expected to possess worse resolution than their batch counterparts, which was not the case. At

higher contaminations, it becomes clear that ceiling crystals significantly beat their batch counterparts in structural resolution (Table 4.4). From the experimental results, we can identify three main factors that potentially explain the better structural resolution of ceiling crystals than batch ones:

a) growth rate

By growing crystals more slowly, HEWL molecules have more time to order and are expected to yield better crystals. Indeed, despite being thinner, the ceiling crystals have a resolution that is at least the same as the batch crystals. However, the fact that at low impurity levels the batch crystals have nearly the same resolution while having very different growth rate, shows that the growth rate itself is not the main explanation in this case. As discussed below, the effect of the growth rate on the impurity uptake *is* important.

b) BSA monomers concentration

The BSA monomer concentration is higher in ceiling than in batch crystals, and thus this anti-correlates with the resolution. Apparently the BSA monomers fit quite well in the tetragonal crystal lattice and thus they do relatively little harm. It is possible that, even when the concentration of the BSA monomers in the ceiling crystals is higher, the slower growth rate leads to a more ordered incorporation and thus less disturbance of the crystal lattice.

b) BSA oligomers concentration

The BSA oligomers are not detectable in ceiling crystals, but are present in relatively large concentrations in the batch crystals. These oligomers do not fit in the crystal lattice and the resulting lattice distortions are therefore most probably responsible for deteriorating the diffraction quality of the batch crystals.

4.5.3 Effect of impurities on crystal morphology

Changes in the morphology of crystals have only been observed in the presence of heterogeneous impurities (BSA and ovalbumin). Our residue HPLC analyses indicate that even at high levels of contamination none of the impurities affect the supersaturation, as was also shown before [97]. This demonstrates that the triggered nucleation and morphological changes are not side effects of a net increase in supersaturation [59].

BSA retard the growth of {101} facets, while having little effect on the {110} facets (Fig. 4.6). We argued in the previous section that BSA monomers easily fit in the crystalline lattice of tetragonal HEWL, but this is clearly not the case for the {101} facets. The reason for this is the step height (34Å)and shape (jagged) of the {101} facets [98]. The BSA monomers, with a size of 45Å, do not fit on the {101} facets and thus they are easily poisoned giving rise to macro-steps consisting of multiple growth layers as we detected at the 14% molar BSA contamination (Fig. 4.6 (e)), or completely leaf-like polycrystals at higher contamination (Fig. 4.3), and consequently early cessation of growth for the {101} faces, resulting in thicker and shorter tetragonal crystals (Fig. 4.6). On the other hand, the relative smoothness of the {110} faces allows for the addition of growth units if only these units conform to the {110} bimolecular growth step height (54Å). This facilitates the incorporation of BSA monomers.

While tetragonal crystals showed only changes in their aspect ratios, monoclinic crystals show substantial morphological changes from very large crystals in the reference condition, to clusters of small columnar crystals, subsequently spherulites and finally amorphous globules at increasing levels of contamination Figs. 4.4,4.7). This can be a result of the adsorption of impurity molecules on the growing {010} faces in a way that triggers their tip splitting [99]. The crystal morphology shows also that this tip splitting of {010} faces is accompanied by a blockage of the {001} faces.

4.5.4 Impurity incorporation in different polymorphs

Compared to the tetragonal polymorph, the monoclinic crystals showed on average lower impurity incorporation in nearly all cases (Table 4.2). The difference in impurity distribution between both polymorphs may be a consequence of the difference in the facets that grow and the corresponding sites in which an impurity is incorporated with respect to the intermolecular contact areas of the adjacent HEWL building blocks [92]. More importantly, monoclinic crystals maintain their growth by the incorporation of growth units comprising two HEWL molecules [100], whereas tetragonal crystals maintain their growth by 4_3 tetrameric helices [98]. Because of this size difference, single molecules of ovalbumin or BSA can easier substitute growth units of tetragonal crystals than those of monoclinic ones. These reasons together explain the relatively lower K_{eff} values for monoclinic HEWL crystals in the presence of all kinds of impurities, compared to those for tetragonal HEWL crystals. This shows that growing different polymorphs of the same protein can lead to significantly different crystals qualities under otherwise the same conditions.

4.6 Conclusions

The ceiling crystallisation method, while designed to grow crystals under diffusion-limited conditions, allows the direct comparison of protein crystals that are grown under conditions of diffusional as well as convective mass transport within the same vial, thus with all other parameters being equal. The comparison using two polymorphs of HEWL and several impurities shows that in most cases the impurity incorporation follows the expected behaviour: for micro-heterogeneous impurities ($K > 1$) diffusion-limited growth leads to less impurities, while for heterogeneous impurities ($K < 1$) diffusion-limited growth leads to a higher impurity concentration as compared to batch growth.

We found, however, that even in the regime of $K < 1$, diffusion-limited growth can be highly beneficial because, in contrast to most reports in the literature, the value of the segregation coefficient can depend strongly on the growth rate and thus enhanced self-purification can occur. For the case of BSA oligomer impurities we found that the slow growth rate during ceiling crystallisation leads to a complete absence of these impurities in the crystals.

We also found, unlike the common knowledge on impurity segregation, that impurity incorporation of a certain impurity-protein combination is constant only if the impurity is not functioning as a co-nucleant.

We further found that the monoclinic polymorph incorporated less impurities than the tetragonal one for HEWL. This suggests that if the target protein is crystallizable in two or more polymorphic forms, it could be advantageous to choose the polymorph with the lowest impurity distribution, because this would result in crystals bearing lower mosaicity and thus higher crystallinity.

In all investigated cases, the tetragonal ceiling HEWL crystals grown in the presence of the heterogeneous impurity BSA had an equal or better X-ray resolution than the batch-grown crystals. This is likely caused by an improved crystal packing of the BSA monomers and the almost complete self-purification from BSA oligomers at the slow growth rate during diffusion-limited growth.

There are many ways in which impurities can affect crystal growth, crystal purity and perfection, but our results show that diffusion-limited growth, for example using the ceiling crystallisation method, often gives higher-quality crystals with lower impurity content for both micro-heterogeneous and heterogeneous impurities.

Chapter 5

Illuminating Protein Crystal Growth using Fluorescent-Labelled Proteins[1]

Abstract

By using trace amounts of fluorescent labelled protein monomers, we studied several optical properties and the growth history of protein crystals. This was facilitated by using confocal laser scanning microscopy and polarisation microscopy. The distribution profile of these labelled monomers showed that during crystal growth they do not always act as micro-heterogeneous impurities for the crystals of their native monomers. Their orientation, distribution and incorporation efficiency into the host crystals showed a wide variation which depends on the crystal symmetry and other biophysical structural properties.

[1]The content of this chapter is to be submitted as: Alaa Adawy, Willem van Enckevort, Willem J. de Grip, Elias Vlieg

5.1 Introduction

Fluorescence is one of the most powerful phenomena used for studying macromolecules and their interactions in solution. Most proteins contain intrinsic fluorescent amino acids, but at the high concentrations in a crystal this intrinsic fluorescence suffers from the quenching effect and is therefore difficult to use [101]. Instead, small fluorophores can be covalently bonded to a small fraction of the macromolecules [102].

With respect to protein crystallisation, fluorophores are used for two purposes. The first one is identifying protein crystals, as a step for high output for structural genomics projects [103]. For this, labelling is not required and fluorphores can be directly added to the crystallisation solution. This is perfect for initially scanning to differentiate protein from salt crystals, because salt cannot bind to a dye. Second, fluorophores are used to study the impurity effect of structurally related impurities on the crystallisation of macromolecules [81, 102, 103, 104, 105, 106]. For these studies, fluorphores are used as labels on the impurity molecule. In this approach, the derivatised molecules should not markedly affect the crystal packing and easily replace the original macromolecules during crystallisation. Therefore, the molecules should be labelled at sites that do not block vital intermolecular contacts which markedly affect crystal packing or cause early cessation of crystal growth [107].

Labelling proteins is essentially a modification process in which the native macromolecule encounters a slight change in its molecular weight, molecular charge and contact points on the monomer surface. However, it was also proven that modifications induced by binding or substituting amino acids on a macromolecule surface could lead to the formation of a low-entropy surface patch and thus enhance its crystallisability [108]. Nevertheless, in most cases, these derivatised macromolecules act as micro-heterogeneous impurities, which are preferentially incorporated at the early stages of nucleation and protein crystal growth. Matsui and co-workers modified the ε-amino group of the N-terminal lysine of hen egg white lysozyme (HEWL) with a fluorescent reagent, forming F-lysozyme, which is 455 daltons heavier than HEWL (14.307 KD) [105]. They showed that even at low concentration, F-lysozyme suppressed the nucleation and growth rate of the tetragonal polymorph of HEWL, while it did not cause any change for the monoclinic form. This can be directly explained by the location of the modified tail with respect to the intermolecular contact areas, being inside for tetragonal crystals and outside for monoclinic ones. Their results agreed with the argument of Thomas and co-workers that inhibiting the formation of specific intermolecular contacts plays a crucial role in the crystallisation processes [20]. Later, Van Driessche and co-workers studied the effect of the same modified monomer on the elementary growth steps on {110} faces of tetragonal HEWL crystals [109]. They

found that F-lysozyme molecules preferentially adsorb on steps, just like the native HEWL molecules, and are then incorporated into the crystal via the kinks on steps. In addition, they did not find any experimental evidence for pinning of step advancement by F-lysozyme adsorbed at kinks. They explained this observation by the very similar molecular surface and molecular weight of F-lysozyme compared to that of native lysozyme.

Here, we use fluorescently labelled proteins (F-proteins) as tracers of protein crystal growth history. This is possible, because derivatised monomers are incorporated non-uniformly during protein crystal growth. Their different interactions with the growing crystal lead to different incorporation efficiencies ranging from preferred incorporation to complete rejection. This also affects the optical properties of the crystals. If the segregation of an F-protein differs for different growth sectors in a crystal, the visible sector boundaries provide information on the different growth rates of adjacent faces in time.

In order to *in situ* monitor the crystal growth history, the observations are performed by using a confocal fluorescence microscope [110]. This microscope gives the ability to view the crystal as a finite number of transverse sections at different heights, which are afterwards reconstructed to give a 3D image. The optical properties are determined by the assembly of the molecules within the crystals and the symmetry elements governing their spatial relations to one another. The preferential orientation of F-proteins within the crystals is monitored by polarisation microscopy, which can reveal crystallographic symmetry elements. Taking into account that many protein crystals do not exhibit the appropriate external features of regular crystals, these microscopic characterisations can be used as a tool for protein crystallographers in order to improve their inspections.

In this study we focus our attention on the role of F-proteins of HEWL (F-Lyz), bovine insulin (F-ins) and bovine serum albumin (F-BSA) on the growth and properties of HEWL, insulin and bovine serum albumin (BSA) crystals. We qualitatively focus on the incorporation, distribution and orientation of the F-proteins in the different protein host crystals by using confocal fluorescence microscopy and polarisation microscopy. A quantitative study on impurity segregation is given in chapter four of this thesis.

5.2 Materials and Methods

Hen egg-white lysozyme (Cat. No. L6876), fatty acid free BSA (Fraction V, Cat. No. 85040C) and bovine insulin (lot # 069k09822) were purchased from Sigma-Aldrich and used without further purification. All other chemicals were of reagent grade. 1 mg of the fluorescent dye DY-632-01 NHS ester ($C_{14}H_{49}N_3O_{14}S_3Na_2$) (MW = 950.03 g/mol,

Dyomics) was dissolved in 80 μl DMF, giving a dense solution of 10.5 mM, before being mixed with the different protein solutions. For HEWL there are seven possible sites for labelling with the activated DY-632-01: one α-amino group of the N-terminus and the ε-amino groups of the six lysine residues. HEWL was dissolved in 50 mM $NaHCO_3$ solution (pH 8.3 at 5 mg/ml concentration) before being mixed with fluorophores at a molar ratio of 1:1 and incubated in dark for 2 hrs at 20^oC. After labelling, the excess reagents were removed by gel filtration on a Sephadex G-25M column (GE-Healthcare) equilibrated in 100mM PBS-buffer (pH 7.4). The labelled fractions were afterwards eluted in dark centrifuge microtubes. Using basically the same protocol, one of the 12 free N-termini of both the A- and B-chains of hexamer bovine insulin was labelled, with the molar ratio of the dye to insulin monomer set at 0.3. BSA has three lysine residues (Lys473, Lys349 and Lys116) which participate in binding fatty acids and two other lysine residues (Lys475 and Lys351) located on the molecule surface [111]. It was labelled in the same way with the dye in a molar ratio of one. The absorbance of the eluted fractions was measured using a spectrophotometer (Lambda 35-UV/VIS, PerkinElmer instruments) after suitable dilution. HEWL, bovine insulin, BSA and DY-632-1 showed absorbance bands at 281 nm (ε: 2.64 $mg^{-1}.cm^{-1}$), 276nm (ε: 1.04 $mg^{-1}.cm^{-1}$), 279nm (ε: 0.65 $mg^{-1}.cm^{-1}$) and 631nm(ε :210.5 $mg^{-1}.cm^{-1}$), respectively. The fractions that showed the highest labelling content were mixed together. MALDI-TOF measurements for the selected fractions showed labelling efficiency of $>$50% for F-Lyz, and $>$90% for F-BSA and F-Ins.

Tetragonal and monoclinic HEWL crystals were grown from solutions containing 4% w/v NaCl and 2% w/v $NaNO_3$ as precipitants mixed with 12 mg/ml and 10 mg/ml HEWL , repectively, dissolved in 0.1 M sodium acetate buffer (pH 4.5) at 20^oC [69]. Bovine insulin crystals were grown using the protocol described in [51], except that the final concentration of insulin was 0.75 mg/ml, and no acetone was used (pH 6.1). BSA crystals were grown according to the protocol reported earlier for human serum albumin in which 100 mg/ml of the protein is used with 40% PEG400 in 0.1 M KH_2PO_4 as crystallisation precipitant (pH 7.0 at 4^oC [111]. F-proteins were added into the different crystallisation solutions to a total concentration of 1% w/w of the unlabelled protein. The crystallisation solutions were then sandwiched between two glass cover slips separated by a rubber ring of 3 mm thickness in order to allow for both crystal growth and microscopic inspection. Crystals growing underneath the upper slip experience essentially diffusion-limited conditions, whereas crystals at the lower slip grow in the presence of convection currents [87]. The observations were performed using a polarisation microscope (Leica DM-RX) in the transmission mode. Images were collected with a video camera (Evolution VF) and processed by means of Image Pro plus 2 software. The orientation dependent dichroism of the crystals was examined by the same microscope, using a single polariser. *In situ* observation of the preferential

distribution of F-proteins into the different crystals was done on a Leica Confocal Laser Scanning Microscope (CLSM), using a HeNe laser (632.8 nm) as an excitation source. The observation (fluorescence) wavelength range was 645 - 750 nm, using an excitation intensity of 17 % and a pinhole diaphragm diameter around 80 μm. The photomultiplier tube (PMT) gain was varied from 250V to 570V, while all other settings were kept constant, for different crystallisation groups. In this way optimum image contrast is obtained and saturation of the confocal micrographs is avoided. Higher PMT voltages indicate lower fluorescence intensities (Table 5.1).

Table 5.1: The PMT voltages used for the different crystallisation combinations during CLSM examinations

Combination	**PMT (V)**
Tetragonal HEWL + F-Lyz	278
Tetragonal HEWL + F-Ins	315
Tetragonal HEWL + F-BSA	412
Monoclinic HEWL + F-Lyz	250
Monoclinic HEWL + F-Ins	385
Monoclinic HEWL + F-BSA	424
Rhombohedral insulin + F-Ins	500
Trigonal BSA + F-BSA	570

5.3 Results and Discussion

5.3.1 Tetragonal HEWL

F-Lyz into tetragonal HEWL crystals

In the presence of F-Lyz, the nucleation of the tetragonal HEWL crystals was enhanced and therefore the crystals were not bigger than 100 μm along their c-axis (Fig. 5.1). Under a bright field microscope, the crystals show a bluish colour, which is a consequence of the preferential absorption of the incorporated fluorophore in the red-infrared part (620 - 750 nm) of the light spectrum. Tetragonal HEWL crystals grow through two main crystallographic facets, {110} and {101}. The dependence of the final morphology of the crystals on the level of supersaturation was shown earlier [59, 112]. At low supersaturation, {101} grow faster than {110} and the crystals become oblong along ⟨001⟩. At higher supersaturation, {101} and {110} grow at the same rate and thus the crystals are more

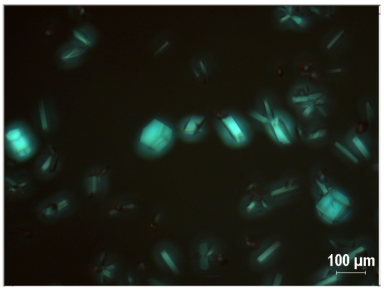

Figure 5.1: Polarisation micrograph of tetragonal HEWL crystals grown in the presence of 0.05% (w/v) F-Lyz in their mother liquor. Here the crystals are imaged between crossed polarisers to eliminate the bluish background colour of the mother liquor.

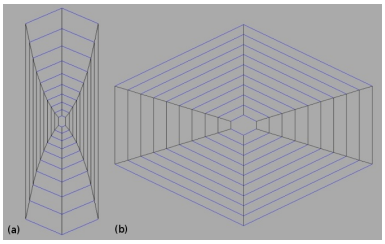

Figure 5.2: Calculated $(1\bar{1}0)$ cross-section profiles for the growth of tetragonal HEWL, showing the {110} and {101} growth sectors. The growth morphology is determined by two crystallographic faces: {101} (blue) and {110} (grey). If the growth rate of {101} prevails, the resultant crystal is oblong along ⟨001⟩ (a). If the growth rate of {110} prevails, the crystals tend to be extended along ⟨110⟩ (b).

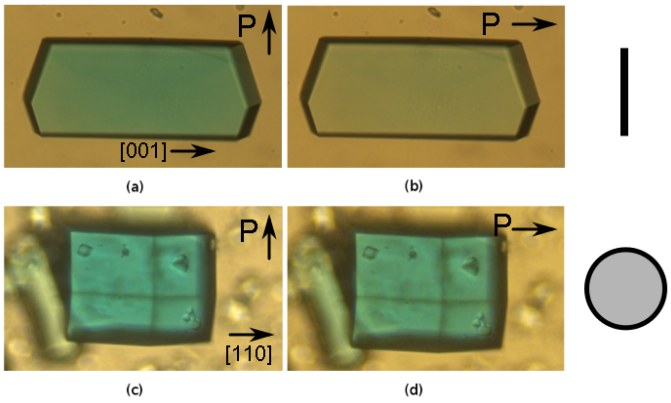

Figure 5.3: Tetragonal HEWL crystal, grown in the presence of 0.05% (w/v) F-Lyz, viewed under the polarisation microscope along [110] (a,b) and along [001] (c,d) using a single polariser. Rotating the polariser 90^o (from a to b, and c to d) shows that the crystal exhibit dichroism only when viewed along [110]. On the right, the plane of conjugated π-bonds in both cases is shown.

block shaped. At extremely high growth rates, {110} grow much more rapidly than {101} and the crystals tend to become flattened bi-pyramids with edges pointing towards ⟨100⟩. This leads to differently shaped {110} and {101} growth sectors in the crystals (Fig. 5.2). The optical transmission micrographs reveal a difference in the colour for the two kinds of growth sectors, {110} being more bluish/greenish than {101}(Fig. 5.3 a). This difference indicates that F-Lyz is preferentially incorporated in the {110} sectors. In addition, when the crystals are monitored along ⟨110⟩ using a single polariser, the fluorescent dye shows dichroism, while they do not show this effect along ⟨001⟩. As can be seen in Fig. 5.3 when viewing along ⟨110⟩ with the polariser parallel to $[1\bar{1}0]$, blue light is visible, i.e. red light is absorbed. This effect is absent if the polariser is parallel to [001]. Both the preferential occurrence in the {110} sectors and the dichroic effect indicate that the fluorophores have a preferential position and orientation in the crystals and, therefore, they cannot be independently distributed, but have to be attached to HEWL molecules. This was further confirmed by photo-bleaching a part of a crystal using a highly intense laser beam and re-examining its fluorescence distribution after 2 hrs. The resulting micrographs revealed that there was no free diffusion of the individual fluorophores within the water channels in the crystal (Fig. 5.4). This is different from the work reported in reference [113] in which the small fluorescein molecules were freely moving within the water channels of the HEWL crystals, while in this study the fluorophores were covalently bonded to protein monomers.

In order to understand this preferential orientation, we have to look into the native HEWL molecule, which is ellipsoidal and has 6 lysine residues on its surface: Lys 1 and Lys 116 along the z-axis, and Lys 33 and Lys 97 along the y-axis so that these four are almost equally distributed on the molecule surface. Lys 96 and Lys 13 are located close to Lys 97 on the same side along the x-axis (Fig. 5.5). Of all lysine residues, Lys 97 and Lys 33 were shown earlier to have the highest reactivity for labelling [114]. Taking into account the initial ratio of the dye to protein during the labelling experiments (1:1) and the labelling efficiency of about 50%, we expect that the labelled residues are those lying along the y-axis and therefore the fluorophore is expected to be covalently bonded to Lys 97 or Lys 33 in such a way that the conjugated π-bonds of the fluorophores (Fig. 5.6) lie in x-z plane of the molecule. The latter plane is almost normal to the crystallographic c-axis of the tetragonal crystal [2].

Returning to the microscopic inspection, the observed dichroism of the F-Lyz doped tetragonal HEWL crystals complies with their 422 point group symmetry. Viewed along the ⟨001⟩ 4-fold axis, no change in colour is observed upon rotation of the polariser over

[2]look at http://www.rcsb.org/pdb/explore/jmol.do?structureId=2YVB& opt=3

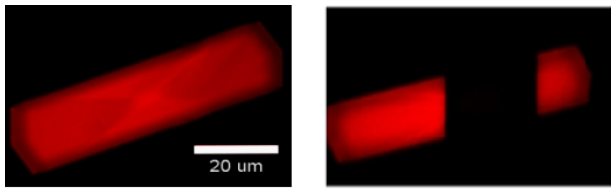

Figure 5.4: CLSM micrographs of the central (110) slice of a tetragonal HEWL crystal (a). The highest fluorescence intensity is located at the central core of the crystal. After 2 hrs from photobleaching a section of this crystal no diffusion of fluorophores was detected (b), confirming that the dye is only bound to protein molecules and not freely moving within the crystal.

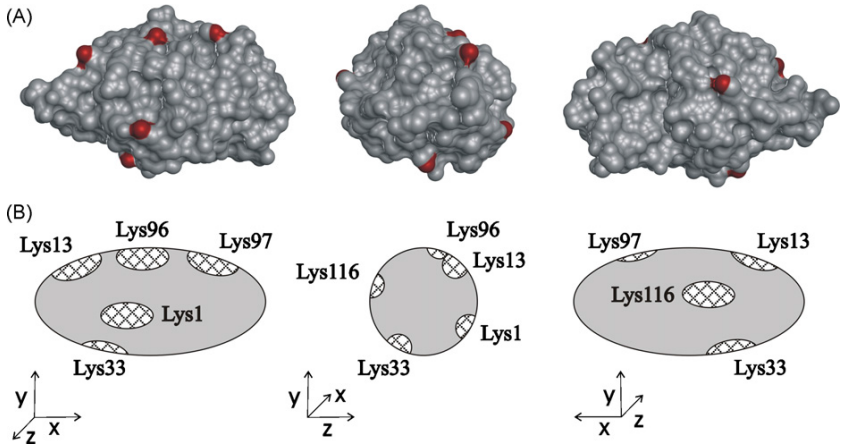

Figure 5.5: The ellipsoidal HEWL molecule with 6 lysine residues (a); A schematic drawing showing the molecules rotated around the y-axis in 90^o steps (b). Adapted from [114] with the kind permission of the authors & publisher (Licence # 3240681117906)

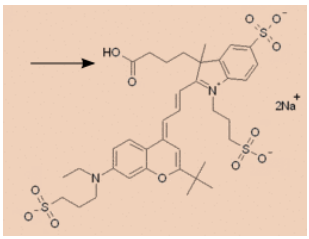

Figure 5.6: The chemical structure of DY-632. The arrow points to the carboxyl group that is activated as the NHS-ester.

90^o. On the other hand, when viewed along a $\langle 110 \rangle$ 2-fold axis a 90^o rotation gives a change in colour, but a rotation over 180^o gives no change. This dichroism also indicates a preferential orientation of the dye attached to the labelled molecules in the HEWL crystal lattice. If the E-vector of the polarised light beam is parallel to the plane of conjugated π-bonds of the fluorophore, the red component of the beam is absorbed, giving a bluish colouration of the crystals (Fig. 5.3). Since this bluish colouring was observed for all polarisation (E-vector) directions when the crystal was viewed along $\langle 001 \rangle$ (Fig. 5.3 c,d), as well as for the polarisation direction parallel to [110] when viewed along $[1\bar{1}0]$ (Fig. 5.3 a), it follows that the conjugated plane is parallel to {001} in the crystal on average. If the E-vector is parallel to [001], i.e. perpendicular to the conjugated π-bond plane, no absorption occurs and the crystal is colourless (Fig. 5.3 b).

CLSM images displayed in Fig. 5.7(a) show that crystals monitored along their c-axis ($\langle 001 \rangle$) yield stronger fluorescence than those monitored along $\langle 110 \rangle$. This is a logical consequence of the fact that these micrographs are obtained by using non-polarised laser light. For the crystals viewed along $\langle 110 \rangle$, only laser polarisation directions near $[1\bar{1}0]$ lead to absorption and thus fluorescence, whereas all polarisation directions contribute to the light absorption and subsequent fluorescence for the crystals viewed along $\langle 001 \rangle$. Viewing the crystals along their $\langle 110 \rangle$ direction shows that the distribution of F-Lyz is not homogeneous throughout the crystals, but differs for the two main crystallographic faces, with a higher incorporation within the {110} growth sectors as compared to the {101} sectors (Fig. 5.7). In addition, the crystal cores have the highest fluorescence intensity which decreases towards their peripheries. This happens because F-Lyz acts as a structurally related, i.e., micro-heterogeneous impurity for HEWL that is preferentially incorporated at the early stages of crystal growth [15]. This leads to a substantial depletion of F-Lyz in the crystallisation solution during continued growth.

The sector boundaries, which are formed between the prismatic {110} and pyramidal {101} faces, are curved in a way revealing that the {101} faces continued to grow for a longer time or at a higher rate than the {110} faces. The slope angle of these boundaries, $\varphi = \mathrm{atan}(dy/dz)$, is related to the relative growth rates of the adjacent {101} and {110} faces according to

$$\frac{R_{101}}{R_{110}} = 0.3056 + \sqrt{\frac{0.8133}{sin^2\varphi} - 0.8133} \tag{5.1}$$

as derived in the appendix and displayed in Fig. 5.8. This allows for mapping the growth history of the crystal. The measurement of the sector boundary slope of the crystal shown

in Fig. 5.8 gives the relative growth rates of the {110} and {101} faces as a function of the position in the crystal, starting from the central nucleus. It can be seen that at the early stage of growth R_{110}/R_{101} is about 0.5, which is characteristic for high supersaturation [59, 112]. Upon further growth the supersaturation decreases by depletion of the solution,

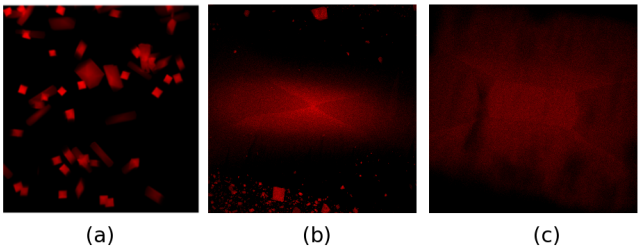

Figure 5.7: CLSM micrograph of HEWL crystals: (a) shows the difference in fluorescence intensity for crystals viewed along ⟨001⟩ (high) and ⟨110⟩ (low); Along ⟨110⟩, the non-uniform distribution of F-Lyz is shown at (b) The central plane of the crystal; (c) A slightly higher plane, showing the central upward {110} growth sector more clearly.

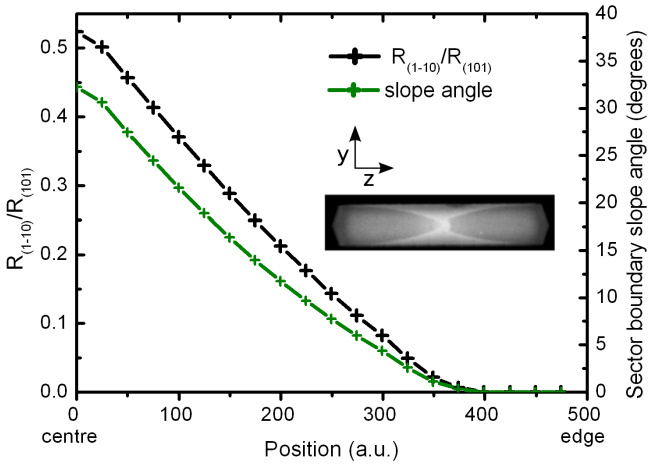

Figure 5.8: Sector boundary slope angle between the growth sectors of the adjacent {101} and {110} as a function of the distance from the crystal core. This is directly related to the relative growth rates of the {101} to {110} faces at different stages, which reflects the history of crystal growth.

leading to a decrease in $R_{(110)}/R_{(101)}$. At the end the {101} still grows, but the {110} face is completely blocked. Probably the 110 face enters the so-called dead zone where growth is inhibited by impurity (F-Lyz) adsorption [84]. Thus, the crystal growth becomes

dominated by one type of growth sector, {101}. This agrees with the lower uptake of F-Lyz into these {101} facets.

Boundaries between the {110} and {101} growth sectors can, with more difficulty, also be determined in crystals that are F-Lyz-free. The curvature of the boundaries depends largely on the initial solution supersaturation, which decreases during growth. As shown in Fig. 5.9, the curvature of the sector boundaries indicates a decrease in the growth rate ratio R_{110}/R_{101} upon continued growth. In addition, the optical image contrast of the sector boundaries points to a slightly different refractive index of the adjacent sectors, which is likely due to a slightly different composition (e.g. water, NaCl, impurity content) of these regions, which may retard the growth of certain faces and change the final shape of the crystal (Fig. 5.9).

In several crystals, CLSM not only reveals the different growth sectors, but also fossil patterns of spiral hillocks or 2D islands in {110} sectors (Fig. 5.10). The patterns exhibit an elongated lens-shaped morphology with tips pointing towards ⟨110⟩. The same patterns, amongst others, have been earlier observed *in situ* by high-resolution phase contrast optical microscopy on the {110} faces of growing HEWL crystals [115]. This observation shows that not only different growth sectors, but also different step orientations on a given protein surface can lead to differences in F-Lyz uptake.

F-Ins and F-BSA into tetragonal HEWL

The presence of F-Ins in the crystallisation solution reduces the nucleation of tetragonal HEWL crystals and the crystals grow only as oblong crystals. In contrast to F-Lyz, F-Ins becomes preferentially distributed into the {101} sectors, especially at the intermediate stage of growth. The cores of the tetragonal crystals as well as the crystal edges show no fluorescence. Unlike F-Lyz, F-ins acts as a heterogeneous impurity for HEWL that is preferentially expelled by the crystal. This explains the uncontaminated cores (Fig. 5.11a).

F-BSA mimics the action of F-ins on the nucleation and the impurity-free core, but oblong as well as symmetric tetragonal crystals are observed. Surprisingly, F-BSA is completely rejected from the {110} faces and is preferentially trapped by the {101} faces (Fig. 5.11b). In addition, its incorporation leads to the development of cracks in some of the symmetric crystals in both crystallographic sectors.

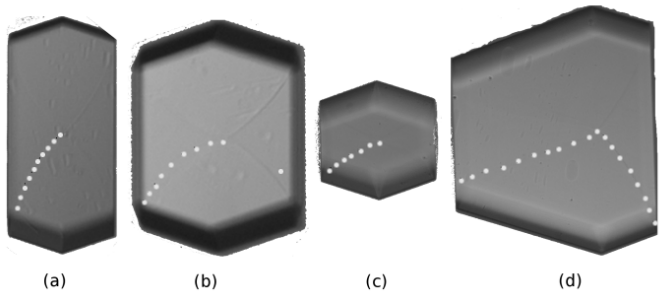

Figure 5.9: Transmission micrographs showing {110}/{101} sector boundaries in tetragonal HEWL crystals grown at low (a), moderate (b), and high (c) initial supersaturation. The presence of impurities can also affect the crystal morphology if symmetric facets do not grow equally fast because of surface blockage or the presence of different densities of screw dislocations (d). All crystals are displayed at the same magnification.

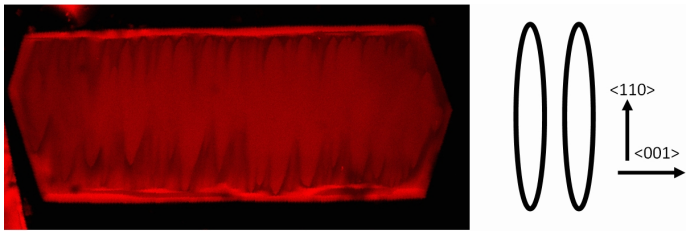

Figure 5.10: (left) Fossil pattern of spiral or 2D island growth in a {110} sector of tetragonal HEWL crystal monitored by CLSM; (right) Shape and orientation of the spiral patterns as reported in the literature [116, 115]

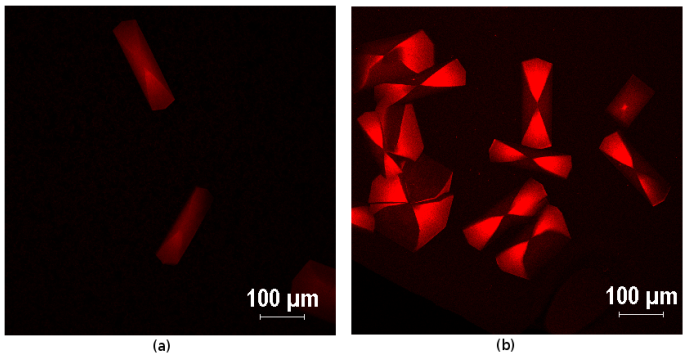

Figure 5.11: CLSM micrographs at the central (110) plane of tetragonal HEWL crystals grown in the presence of 0.05% (w/v) F-ins (a) and F-BSA (b) in their mother liquor.

5.3.2 Monoclinic HEWL

Under the applied crystallisation conditions, the monoclinic HEWL crystals grow as oblong crystals along [010], bounded by the crystallographic habit faces {010}, {10$\bar{1}$}, {101} and {001}. The planar (010) face has the highest growth rate. The opposite face (0$\bar{1}$0) is not related to (010) by symmetry, and is largely blocked. This polar growth of the crystal with point group 2 was reported previously [117, 118]. {001} faces have usually a very high growth rate and are consequently hidden by slowly growing {10$\bar{1}$} and {101} facets, which possess the largest surface area on the crystals (Fig. 5.12).

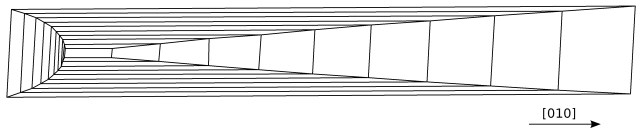

Figure 5.12: Calculated growth profile for a monoclinic crystal, showing polar growth in the [010] direction

The optical transmission micrographs show that F-Lyz is readily incorporated into monoclinic HEWL crystals. Interestingly, the crystals have the same size and shape with or without F-Lyz, which indicates that F-Lyz hardly affects the crystal growth and habit. The solution was colourless afterwards, while the crystals where very bluish/greenish and the intensity of colouration is almost uniform throughout the crystals (Fig. 5.13). This points to a unity segregation coefficient. The solubility of monoclinic solution was about 2 mg/ml and, therefore, virtually all F-Lyz is consumed by the crystals.

Viewing the crystals along their (10$\bar{1}$) plane, they show dichroism upon 90^o rotation with one fixed polariser (Fig. 5.14). The crystal colour vanishes when the crystallographic b-axis is parallel to the polarisation direction. This together with the case of tetragonal HEWL crystals confirms that there is a preferential orientation of the fluorophore conjugated π planes in the crystals.

The confocal micrographs show that the fluorescence intensity is much higher than that for the tetragonal crystals grown using the same molar ratio of native to labelled HEWL monomers. The fluorescence is almost homogeneous over the crystals except for a slightly higher value for the rounded (0$\bar{1}$0) faces (Fig. 5.15a).

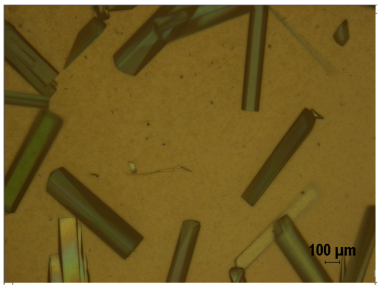

Figure 5.13: Overview of monoclinic HEWL crystals grown in the presence of F-Lyz in their mother liquor. The crystals trapped all the F-lyz, leaving the depleted solution almost colourless.

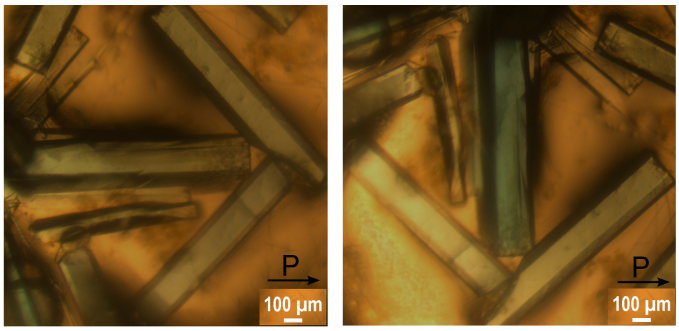

Figure 5.14: Polarisation micrographs of a F-lyz containing monoclinic HEWL crystal which encounters dichroism upon 90^o rotation (a to b). A single polariser is used, its direction is indicated by an arrow.

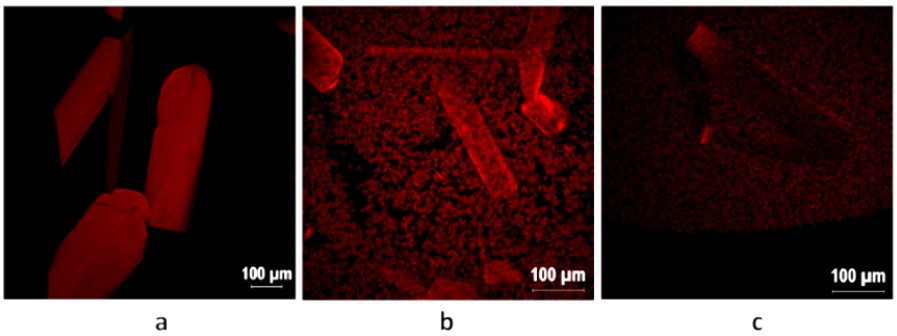

Figure 5.15: CLSM micrographs of the central slices in monoclinic HEWL crystals grown in the presence of F-Lyz (a), F-Ins (b) and F-BSA (c) in their crystallisation solutions.

Although HEWL monoclinic crystals show a high tolerance for F-Lyz incorporation within their sectors, they reject incorporation of F-Ins almost completely (Fig. 5.15b)and of F-BSA completely (Fig. 5.15c). The luminescence intensity of the crystals is equal to or less than the very weak background luminescence induced by labelled molecules in the solution or light scattering, which can only be detected using the highest PMT voltages (Table 5.1). This shows that when macromolecules crystallise in different polymorphic forms, they can display very different impurity incorporation [119].

5.3.3 Rhombohedral Bovine Insulin

The bovine insulin monomer consists of two polypeptide chains (A and B) linked by disulfide bonds, which normally associate with another monomer to form dimers. During crystallisation, three dimers assemble together into a cylindrical hexamer, which acts as the asymmetric unit of the unit cell. The crystals then grow as rhombohedral crystals (Fig. 5.16) with space group R3, in which the asymmetric units are arranged at the corners of the unit cell with a tilt of 258^{o} out of the {100} crystallographic planes. The growth of this crystal occurs through 2D nucleation and spiral growth on {100}, resulting in a rhombohedral morphology bounded by {100} faces [54].

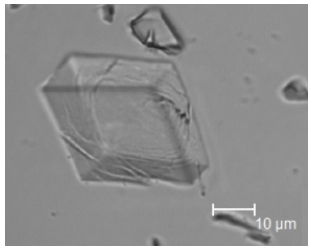

Figure 5.16: Bright field transmission micrograph of rhombohedral bovine insulin crystal bounded by {100} faces.

One would expect that F-ins should behave as a micro-heterogeneous impurity for the crystals of native insulin, which would be incorporated mostly at the early stage of crystal growth. In contrast, CLSM showed that the crystals did not possess fluorescent cores and the incorporation of fluorescently labelled monomers (F-Ins) was only observed toward the peripheries of the crystals (Fig. 5.17). This indicates a preferential incorporation of F-Ins at later stages of crystal growth, i.e., F-ins acts as a heterogeneous impurity. Under diffusion-limited crystallisation accomplished by using the ceiling method [69, 87], fewer crystals were obtained, but their final size was about four times larger than those

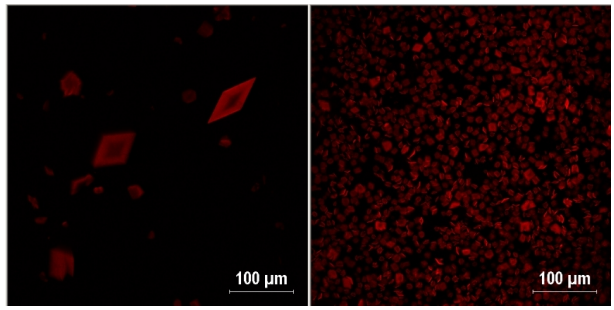

Figure 5.17: CLSM micrographs of rhombohedral bovine insulin crystals grown in the presence of F-Ins in their mother liquor. Diffusion-limited crystallisation conditions led to the growth of crystals (left panel) which are four times larger than those grown in the presence of convection (right panel). The micrographs display the central plane within the crystals.

grown in the presence of convection (Fig. 5.17). This shows the positive effect of diffusive mass transport on the growth, which facilitated the growth of bigger crystals compared to those grown in the prescence of convection, which in turn were poisoned and stopped their growth at a much earlier stage.

Using a single polariser in the polarisation microscope, no dichroism was observed for the insulin crystals. However, under a polarisation microscope with two crossed polarisers, the crystals showed an unusual sort of birefringence. The crystals changed colour from bright bluish to dark upon 60^o rotation and restored their bright colour by a further 30^o rotation in the same direction.

The complete segregation of F-ins except for crystal peripheries can again be explained by looking into the molecular surface and its environment. From the molecular structure, B chains have lysine residues which are involved in the intermolecular contact. In addition, both A and B chains have a free N-terminus, which lies at the surface of the hexamer, and is thus available for labelling. Earlier, Bergeron and co-workers showed that the significant release of water molecules upon the attachment of an insulin molecule to a growth site may account for the hydrophobic nature of the intermolecular bonds in insulin crystals [120]. Hence, labelling one of the potential 12 N-terminal amino groups (as we did by reducing the molar ratio during the labelling process) with a hydrophilic fluorphore is expected to seriously perturb the crystal packing as well as the crystal growth. Therefore, F-ins, despite its very close structural relationship to insulin monomers, acts as an impurity which is rejected by the bovine insulin crystal. This explains its incorporation only at the later stages of crystal growth, which is the usual behaviour of a heterogeneous impurity [15] .

5.3.4 BSA crystals

The BSA crystals are very small and display an elongated lozenge shape (Fig. 5.18). In a number of cases cross twins could be identified. The morphology of most crystals

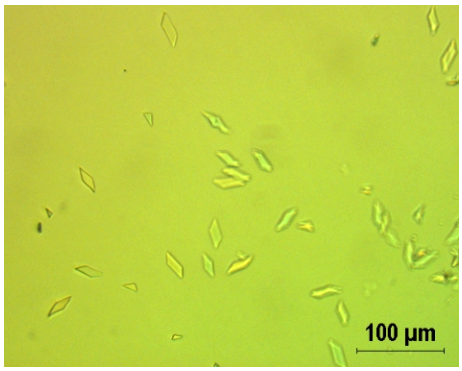

Figure 5.18: Polarisation micrograph of BSA crystals grown in the absence of fluorophores, the crystals had no detectable birefringence.

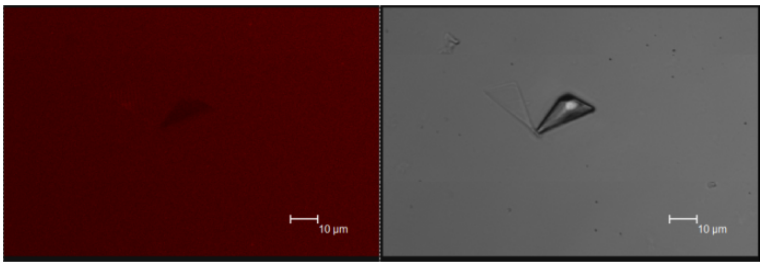

Figure 5.19: CLSM micrograph (left) and its bright field transmission counterpart (right) of BSA crystals grown in the presence of F-BSA in their mother liquor. The very weak background light intensity results from luminescence of F-BSA in the solution and from light scattering.

seems to comply -on average- with point group 2/m (monoclinic), which was also recently reported elsewhere [121, 122], though we used a very different crystallisation protocol.

No birefringence was observed between crossed polarisers, regardless of crystal orientation. Presumably, the crystals were too thin to show this effect. Adding F-BSA did not change the nucleation and growth properties of BSA crystals. Under CLSM, the crystals showed no fluorescence, even at their peripheries. This indicates that F-BSA was completely rejected from the BSA crystal lattice (Fig. 5.19). A hypothesis explaining the rejection of F-BSA from BSA crystals, which still needs further confirmation, is enclosed in the appendix. Here, we can account the complete rejection of F-BSA from BSA crystals

for an abrupt increase of negative charges at a certain site of F-BSA, which increases the repulsive forces at essential intermolecular contact points, but also perturbs the packing within the crystal lattice.

5.4 Conclusions

In this paper, we showed the possibility of studying the growth history of protein crystals by labelling their monomers with a fluorophore. Only trace amounts of F-proteins were added into the mother liquor of the native monomers. The crystals were examined by polarisation as well as confocal fluorescence microscopy. This provides a powerful means to visualise the crystals as if they were monitored over time during their nucleation and subsequent crystal growth, without the need to record the entire experiment.

Our study shows that in many cases the distribution of impurities is not uniform within the crystals and can vary for the different growth sectors, cores and peripheries of the crystals. This implies that likely the diffraction quality of the crystals is position dependent. So, using an X-ray micro beam targeting a specific position in a crystal, known from preliminary inspections for its relatively higher perfection, can lead to an improved diffraction quality in protein crystallography.

We also found that the incorporation and optical properties of the labelled proteins differ to a large extent for the different systems investigated, showing either preferential or partial/complete rejection The interaction between the target protein and its F-protein can be very different from expected as was the case for F-Ins and F-BSA into respective insulin and BSA crystals. This highlights the importance of the surface hydrophobicity, which is sometimes more influential than other parameters regarding the intermolecular interactions between the macromolecules and eventually the crystal growth structure. Therefore, studying the optical properties of protein crystals "illuminated" with F-proteins can provide essential observations on their growth and perfection. This can help to better reveal more about the macromolecular structures of those proteins that are still not solved to high degrees of precision.

Appendix

Derivation of Equation 5.1

Orientation of the ($1\bar{1}0$) and (101) growth sector boundary in tetragonal HEWL viewed in a (110) cross-section plane as a function of the relative growth rates of the adjacent

(1$\bar{1}$0) and (101) growth faces.

We consider a cross-section plane (110) (the plane scanned by the confocal fluorescence microscope, shown in Fig. 5.4) in the tetragonal HEWL crystal. The boundary between the sectors of the two adjacent side faces (1$\bar{1}$0) and (101) is the trajectory of the intersection point of the two intersecting lines of both faces with the basic plane (110) (Fig. A.1). In the following the indices 1 and 2 refer to the (101) and (1$\bar{1}$0) planes respectively.

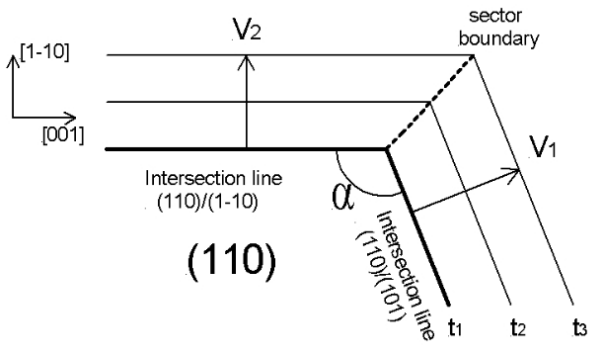

Figure A.1: The trajectory of the sector boundary between the two adjacent faces (1$\bar{1}$0) and (101) imaged on the cross-section plane (110) is given by the intersection point of the two intersection lines of both side faces with the basal plane (110). Top view on (110).

The advancement rate of the two intersection lines (Fig. A.2) is given by:

$$V_i = \frac{R_i}{sin\beta_i} \tag{A.1}$$

with R_i the growth velocity of side face i, V_i the advancement rate of the intersection line and β_i the angle between the basal (110) plane and the side face in question. For the (101) plane $\beta_1 = 72.21^o$; for (1$\bar{1}$0) $\beta_2 = 90^o$.

The trajectory angle, ϕ, of the intersection point of the of the two intersection lines can now be derived by using Fig. A.3 and considering that the trajectory velocity is given by the vector sum $V_t' = V_1' + V_2'$. Here V_i' prime holds for the intersection point velocity 'component' of face i parallel to the intersection line of the other face. From Fig. A.3 it follows that

$$V_1' = \frac{V_1}{\sin} \; and \; V_2' = \frac{V_2}{\sin \alpha} \tag{A.2}$$

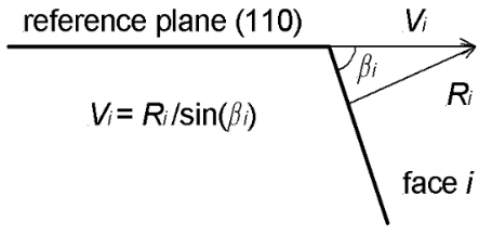

Figure A.2: The advancement velocity of the intersection line between the basal face and a side face as a function of side face growth rate velocity and its angle with the basal face. Side view.

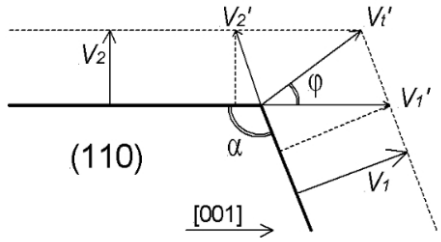

Figure A.3: The trajectory angle, ϕ, is determined by the angle between $V_t' = V_1' + V_2'$ and the horizontal [001] crystallographic direction. Top view on (110).

and

$$V_t'^2 = V_1'^2 + V_2'^2 + V_1'V_2'cos\alpha \tag{A.3}$$

with α the angle between both intersection lines. The trajectory angle, ϕ, (which is the angle between V_t' and the horizontal [001] direction) is given by

$$\sin\phi = \frac{V_2}{V_t'} \tag{A.4}$$

or

$$(\sin\phi)^{-1} = \frac{V_t'}{V_2} = \frac{(V_1'^2 + V_2'^2 + V_1'V_2'\cos\alpha)^{1/2}}{V_2}. \tag{A.5}$$

Rewriting equation 5.5, using equations 5.2 gives:

$$\frac{\sin^2\alpha}{\sin^2\phi} = {\Gamma_{12}^l}^2 + 2\Gamma_{12}^l\cos\alpha + 1 \tag{A.6}$$

with $\Gamma_{12}^l = \frac{V_1}{V_2}$ the ratio of the two intersection line displacement velocities. Expressed in

the ratio of the growth velocities of the side planes, $\Gamma_{12}^{p} = \frac{R_1}{R_2}$ one obtains

$$\Gamma_{12}^{p\,2}(\frac{\sin\beta_2}{\sin\beta_1})^2 + 2\Gamma_{12}^{p}(\frac{\sin\beta_2}{\sin\beta_1} * \cos\alpha) - \frac{\sin^2\alpha}{\sin^2\phi} + 1 = 0. \tag{A.7}$$

Now, using the HEWL values $\beta_1 = 72.21^o$, $\beta_2 = 90^o$ and $\alpha = 108.72^o$, one obtains the quadratic equation:

$$1.1029\Gamma_{12}^{p\,2} - 0.6740\Gamma_{12}^{p} + (-\frac{0.8970}{\sin^2\phi} + 1) = 0 \tag{A.8}$$

Solving this equation gives the expression of the relative growth rates of the adjacent faces $(1\bar{1}0)$ and (101) as a function of sector boundary slope ϕ

$$\frac{R_{101}}{R_{110}} = 0.3056 + \sqrt{\frac{0.8133}{sin^2\varphi} - 0.8133} \tag{A.9}$$

Hypothesis for the complete rejection of F-BSA from BSA crystals

For some reason, covalently bonded fluorophores to F-BSA suppresses the interaction between native BSA and F-BSA.

BSA is a negatively charged protein at pH $>$ 4.7. During the labelling (at pH 8.3), the negativity of BSA is relatively (pI 4.3). In addition, BSA molecules were shown earlier to possess a positively charged residue adjacent to its hydrophobic binding site. Furthermore, BSA binds anions more tightly than cations or neutral molecules with similar hydrophobic groups, even when the overall charge on the protein is negative [123]. All these features are expected to enhance the interaction of the negatively charged fluorophore with BSA molecules, which is reflected on the high labelling efficiency, as confirmed by the MALDI-TOF and Spectrophotometric measurements.

Moreover, the applied crystallisation conditions (pH 6.5-7) allowed both native and labeled BSA to maintain their net higher negative charge, while the latter possesses an extra negatively charged *pulp* on its surface due to the three sulfonate groups of the fluorophore (Fig. 5.6).

In our experiments, we used fatty acid-free BSA and therefore the 7 available fatty acid (FA) pockets are essentially FA-free in our experiments (Fig. A.4).

It was shown that during BSA crystallisation, PEG fragments and sulfate groups occupy fatty acid pockets on "A" subdomains in the macromolecule [122]. The FA1, which lies on the upper side of the molecule in IB subdomain, is thus the only possible *major* free

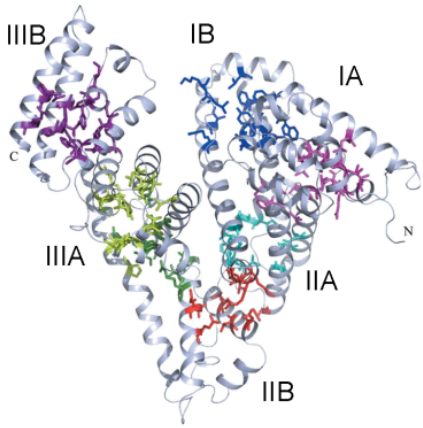

Figure A.4: BSA monomer with the main domains I, II and III and A and B subdomains of each. FA pockets coloured FA1, blue; FA2, pink; FA3, green; FA4, light green; FA5, violet; FA6, red; FA7, cyan. (Reproduced with permission of the International Union of Crystallography ([122])

position for binding with the fluorophore [121]. The unit cell of BSA crystals was shown to have an asymmetric unit of 2 BSA monomers that lie head to head. This means that an F-BSA with a fluorophore hanging at that side not only increases the local negative charge and causes repulsion, but also perturbs the packing within the crystal lattice.

Chapter 6

Ceiling Growth cell for Convection-free Protein Crystallization[1]

Abstract

A growth cell has been designed for an easy application of the ceiling crystallisation method. The growth cell allows for diffusion-limited crystal growth with a total volume down to 10 μl per trial and air-tight sealing for any type of protein sample. The ceiling crystals grow to sufficient size for diffraction experiments.

[1]The content of this chapter is to be submitted as: Alaa Adawy, Wil Corbeek, Erik de Ronde, Willem de Grip, Willem van Enckevort and Elias Vlieg

6.1 Introduction

In macromolecular crystallography, the growth of high quality crystals is a prerequisite for the determination of the structure of biological macromolecules. There is ample evidence generated in a large amount of studies by research groups worldwide that diffusion-limited growth conditions can result in the growth of better crystals compared to those grown under otherwise identical conditions [69, 33, 25, 86]. The merit of diffusion limited growth is that it allows protein crystals to grow from an initially highly supersaturated solution, which after nucleation undergoes a steady decrease in its supersaturation with no fluctuations. Also, the incorporation of sediments and impurities is highly suppressed. Diffusion-limited growth is attained in space microgravity conditions [44], but can also be accomplished under terrestrial conditions using magnetic fields [49], micro-capillaries [47] and gels [48]. This insight led to the development of commercially available equipment facilitating crystal growth of macromolecules through diffusive mass transport [124].

Despite the advantages of diffusion-limited growth, most protein crystallisation experiments are performed using the vapour diffusion and micro-batch methods, because they allow a small sample volume per trial ($<10\ \mu l$) and are thus easily automated and often yield good results. We have recently developed a simple diffusion-limited crystallisation method in which crystals grow at the very top (ceiling) of a vial overfilled with batch crystallisation solution [68]. Such ceiling crystals diffracted X-rays to high resolution limits [69]. This is mainly due to the development of a depletion zone around the growing crystals, which is not disrupted by convection currents [87]. The ceiling method is not intended for high throughput crystallisation screening [125] or miniaturisation, owing to the relatively large volume of the used crystallisation solution per trial. Vapour diffusion or micro-batch can be used for that. Yet, once the optimum growth conditions are known, the ceiling method is a convenient way to optimise the resultant crystal quality. Here, we report our "ceiling crystallisation kit", which we have recently developed. Our aim is to make the method widely available and further expand its potential, so that it may become one of the standard methods used by protein crystallographers.

6.2 Design considerations

We developed the ceiling method using commercially available micro-centrifuge tubes and micro- and nano-plates, with which we scaled the required solution volume from 1.8 ml down to 10 μl. In all these setups, ceiling crystals heterogeneously nucleate on the cover slips [126]. Because the ceiling method does not rely on solution evaporation, tight sealing is required to avoid any solution or air leakage out of or into the growth cell at the cover

slip-vial interface. Unlike vapour diffusion, for which vacuum grease or petroleum jelly can be easily used, the ceiling method in its original set-up [69] leads to solution-grease contact. It was shown earlier that grease does not act as an impurity for proteins [127], yet we have seen in our experiments a preferential nucleation of protein crystals at the grease side. Although microscopic inspections reveal that the crystals exhibit very good optical quality, fishing the crystals for cryo-protection and subsequent data collection is too difficult to be accomplished without contaminant portions of the sealant on the crystal surface. This is because the applied thin bead of grease or any other sealant tends to diffuse towards the very limited area for ceiling crystal growth (small diameters $<$ $4mm^2$ in nano-plates) and therefore, eventually interferes with the growing crystals. This affects the final diffraction quality of the crystals. Moreover, applying grease adversely influences attempts to crystallise membrane proteins which require detergents for their crystallisation.

Earlier, screw-capped wells on a plate (EasyXtal 15-Well Tools) have become commercially available for the hanging drop vapour diffusion method. For the ceiling method, this design would provide not only an alternative for the vacuum grease and all its consequences (air bubbles and solution leakage), but also the possibility of transferring the ceiling crystals from one condition to another, so that one can decouple the phases of nucleation and growth [128]. However, in case of the ceiling method, this decoupling is generally not required, because of the development of the depletion zone around the ceiling crystals. In addition, screwing the cap all the way down, is by itself a possible source of air leakage. We, therefore, have developed a design using a clamped rubber O-ring for an air-tight sealing. The design further facilitates microscopic inspection of the growing crystals.

6.3 The apparatus: The ceiling crystallisation kit

A ceiling crystallisation kit consists of a growth cell, mounting plate, cover slip, rubber O-ring and Teflon clamping plate (Fig. A.1).

A schematic diagram of the growth cell is given in Fig. A.2. The cells are made from optically clear and (preferably) hydrophobic materials. We used Perspex (after surface treatment), but polystyrene and polypropylene are even better, because mostly they do not need surface treatment. For convenient handling, the outer size of these cells (ϕ 6 mm) is the same as that of the cylindrical cavities in the mounting plate. The cells are milled to have cone shaped wells with a total volume of 8 μl, but other shapes and volumes are also possible. At the upper edge of each well, a groove is made to embed a rubber O-ring

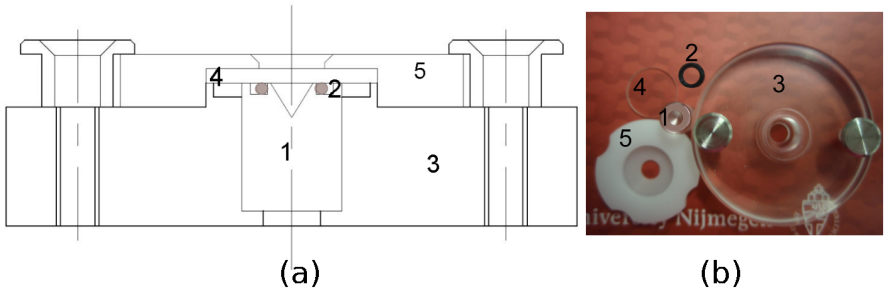

Figure A.1: A cross section (a) of a mounted assembly and a photograph (b) of its components: growth vial (1), rubber ring (2), mounting plate (3), cover slip (4) and Teflon clamping plate (5). The crystallisation solutions overfills the wedge-shaped volume in the growth cell. The protein crystals should grow underneath the cover slip.

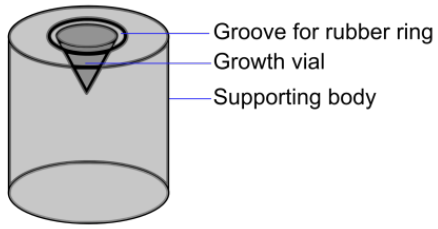

Figure A.2: Schematic diagram of the growth cell.

(NBR 36624 3.5 × 1, ERIKS) for watertight sealing. The cell can then be inserted in its cavity in the mounting plate.

The growth cell can easily be inserted into and removed from the optically clear Perspex mounting plate, which can be used repeatedly (Fig. A.3). On the top of this plate, two stainless steel pins are mounted to hold the Teflon clamping plate. The Teflon plate has a hole in its centre to allow for microscopic inspection and a groove to embed a siliconised glass cover slip (ϕ12 mm, 1.2 mm thick, HR8-088, Hampton Research) (Fig. A.4). The clamping plate has 4 circular notches for an easy and tight lock (Fig. A.5). For convenience, 12 growth cells can be mounted on a plate of the standard dimensions (130 × 90 × 8 mm^3) with cylindrical cavities for each complete assembly (Fig. A.6).

Figure A.3: The mounting plate with an inserted growth cell.

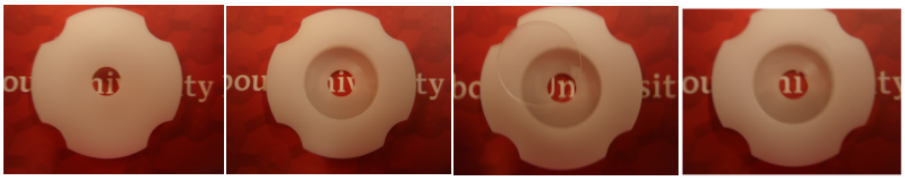

Figure A.4: Teflon clamping plate: outer view (a), inner view (b), a glass cover slip can be inserted into the inner groove (c, d).

6.4 Application

For every growth vial, 10 μl of the protein crystallisation solution is prepared using the same protocol for setting (micro-)batch crystallisation trials. In case the protein under test has been crystallised by vapour diffusion, instructions for converting vapour diffusion to batch method and vice versa are available elsewhere [11]. The clean growth cell is inserted into the mounting plate and the rubber O-ring is positioned. On the inner side of the clamping plate, a thick glass cover slip is inserted. The vial is then overfilled with the mother liquor and directly covered, excluding any air bubbles. During the experiment, the cell should be kept under temperature-controlled and vibration-free conditions. This setup can easily be inspected using a microscope with working distance down to 10 mm. After growth of the protein crystals to their final size, the clamping plate is unlocked and turned upside-down, exposing the ceiling crystals which are attached to the cover slip. The crystals will be wet with a small amount of adhering solution and the addition of the cryoprotectant (if needed) will be easy, as is fishing the crystals on silicon loops for data collection.

Figure A.5: The set up provides an easy and tight lock by rotating the Teflon plate.

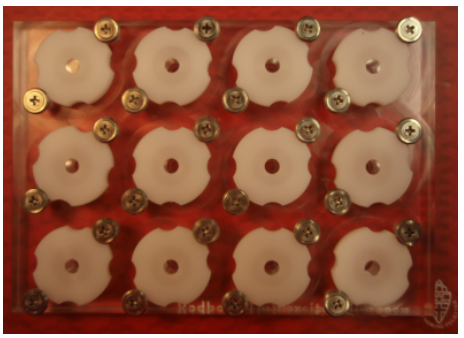

Figure A.6: A plate of 4 × 3 cells for ceiling crystallisation.

6.5 Results

We used this kit to grow crystals from a model protein (Hen egg white lysozyme, HEWL) as well as a confidential (proprietary) enzyme, which we obtained as a purified sample in a scientific collaboration with NTRC[2]. HEWL was crystallised into tetragonal crystals as described elsewhere [69]. The resultant crystals were compared to others grown in microtubes, which provide a total volume 100 × larger than which our crystallisation kit provides per trial. As shown in Fig. A.7, the enzyme crystals have grown in the ceiling kit to optimum sizes for XRD measurements. Ceiling tetragonal HEWL crystals also grew to an optimum size for diffraction measurements, and were about 2 × larger than a batch crystal that grew at the bottom of the cell (Fig. A.8).

6.6 Discussion and Conclusion

In our view, ceiling crystallisation is not a replacement for the currently used screening methods. For this commercial kits are available for efficient and flexible screening of crystallisation conditions for proteins, peptides, nucleic acids, macromolecular complexes

[2]Netherlands Translational Research Center, Oss, the Netherlands

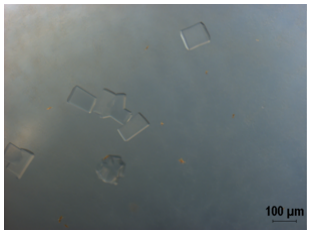

Figure A.7: Micrograph of the enzyme ceiling crystals grown using the ceiling crystallisation kit.

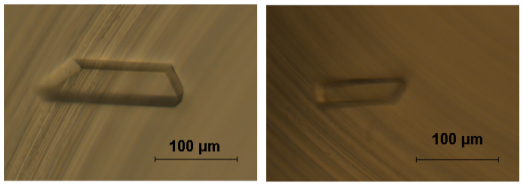

Figure A.8: Micrographs of ceiling (a) and batch (b) tetragonal HEWL crystals grown in the ceiling crystallisation kit.

and water soluble small molecules. But once the appropriate conditions are found (usually from crystallisation conditions that were statistically most successful in yielding protein crystals suitable for X-ray diffraction), the ceiling method could improve the crystal final quality, because of its convection-free crystallisation environment [69].

The designed cell is easy to use and does not really require automation, because mostly few (<30) crystallisation trials are sufficient at this late stage of optimisation. The kit has the following advantages:

1. It allows a total sample volume down to 10 μl per trial; but larger volumes are possible. This may be required for 10 $\times$ larger crystals, which are required for neutron crystallography;

2. Through the rubber O-ring, it provides mechanical air-tight sealing and there is no need to use vacuum grease or petroleum jelly which are a possible source of contamination, and are, moreover, incompatible with detergent-solubilised membrane proteins. The cell is thus suitable for the crystallisation of any type of protein;

3. It facilitates microscopic inspection, which is required for an easy follow-up for the experimental results;

4. It can be used with commercially available cover slips. In case nucleation needs to

be enhanced, these slips can be surface treated or a nucleant can be applied.

5. It facilitates fishing of the resultant protein crystals.

In conclusion, we designed a dedicated ceiling crystallisation kit, which is easy to use and suitable for any type of protein solutions. We hope that this kit will encourage the crystallisation community to use the ceiling method and we encourage researchers to contact us for discussing the application of this hardware.

Summary

A large of studies have been conducted on proteins to determine their structures. For that, many research groups are used to growing protein crystals, but less are interested in understanding the physical factors which affect this process. This thesis focuses on the these factors and how they can improve the crystal final quality. Because protein crystals are grown from solution, the rate limiting step can be the transport of the solute to the crystal surface (diffusion control) or the addition of solute to the crystal surface (interface control). In unstirred stagnant solution, diffusion control dominates and crystals can grow relatively large and perfect. Therefore, sources of convection should be avoided. A number of attempts were made in order to accomplish convection-free crystallisation conditions, yet the application of these methods is often quite complex. In this thesis, I have studied the possibility of growing protein crystals using an efficient setup based on an up-side down configuration, in which the protein crystals nucleate and grow downwards from the *ceiling* of a growth cell overfilled with crystallisation solution. This allows for exploiting the gravitational force to effectuate diffusion-limited crystal growth, which is far simpler than, for instance, using microgravity conditions.

This approach, dubbed the ceiling crystallisation method, is described in chapter two. Ceiling crystallisation results in a significant improvement of X-ray diffraction resolution for a number of model protein crystals. Their resolution exceeded the current world records realised using other growth methods. Also, the ceiling crystals are larger, purer and resulted in higher resolution compared to their batch counterparts grown at the bottom of the same growth cells.

The time evolution of the solute concentration in the vicinity of the crystals is reported in chapter three. This is studied using a combination of microscopic and interferometric experiments and numerical simulations. This synergy provides a comprehensive view of the direct effects of solution movement and depletion and how this can directly affect the ceiling and batch crystal growth. While the microscopic inspections provide details about the external morphology of the crystals, the Mach-Zehnder interferometer provides a tool to monitor the spatial changes in solute concentration and flows in the crystallisation solution. Combining and processing a number of consecutive interferograms, phase-shifted with

respect to each other, allow the determination of the spatial changes in the refractive index. Using the relation between solute concentration and refractive index, the concentration profiles are estimated with high precision. The concentration profile for crystal growth and dissolution at the ceiling and the bottom of growth cells were validated by numerical simulation using FLEX software suite. The results show the progression of the depletion zone during ceiling crystal growth, while convection plumes are rising from the batch crystals. The development of the depletion zone depends on growth cell dimensions, supersaturation and diffusion coefficient of the crystallising solutes.

In chapter four, a systematic study is presented on the influence of impurities on protein crystallisation in the presence and absence of convection currents, by comparing ceiling and batch crystals growing simultaneously in the same vials. The incorporation of impurities is determined by both the so-called segregation coefficients of impurities and the mass transport. For most studied impurities, the difference between ceiling and batch crystals follows the expected behaviour. Ceiling crystallisation is especially favourable for impurities that are preferentially incorporated. I have found, in contrast to previous reports, that the low growth rate during ceiling crystallisation results in very much reduced incorporation of large heterogeneous impurities. In addition, ceiling crystals beat others grown under convection currents in their structural resolution in all the studied cases.

By exploiting fluorescent labelled proteins as additives during protein growth, chapter five reports the possibility of monitoring the crystal growth history and symmetry through studying the optical properties of protein crystals by polarisation and laser confocal fluorescence microscopy. I present this new microscopic approach perspective to protein crystallographers which not only allows distinguishing protein crystals from salt crystals, but also shows their detailed growth behaviour. It is found that the optical properties, incorporation and distribution of the fluorescently labelled proteins in the various protein crystals differ significantly for the different additive-host systems. This shows that impurity segregation is indeed a complex issue.

Finally, I report on our ceiling crystallisation kit in chapter six. This technical development is meant to facilitate the application of the ceiling method. The set-up prevents solvent evaporation and allows the crystals to grow large enough for optimal diffraction experiments.

Gravity is often blamed for hindering the growth of large and high quality crystals, because it drives convection currents. Through experiments and simulations, this thesis demonstrates the positive effect of gravity on protein crystal growth, provided that the correct configuration of ceiling growth is chosen. I show here that the convection current dilemma can be overcome, if we use the ceiling method and have an "opposite" perspective to the gravitational force. If I would define a key phrase for the concept elaborated in this thesis, it would be "keep it simple!".

Samenvatting

Tijdens de afgelopen decennia is er veel onderzoek verricht aan eiwitkristallisatie om de structuur van deze biomoleculen te achterhalen. Hoewel een groot aantal onderzoeksgroepen geinteresseerd was in de groei van eiwitkristallen, kregen de fysische factoren die dit proces bepalen relatief weinig aandacht. Dit proefschrift richt zich juist op deze factoren met het oog op een verbetering van de uiteindelijke kristalkwaliteit. Omdat eiwitkristallen groeien vanuit een oplossing, kan de snelheidsbeperkende stap hetzij het transport van de opgeloste stof naar het kristaloppervlak zijn (diffusiebepaald) hetzij de aanhechting van de opgeloste stof aan het kristaloppervlak (oppervlaktekinetiek bepaald). In ongeroerde, stilstaande oplossingen zal diffusie domineren, waardoor kristallen kunnen uitgroeien tot relatief grote en perfecte exemplaren. Daarom moet elke bron van convectie worden vermeden. Verschillende pogingen hiertoe zijn al gedaan, maar helaas zijn de toegepaste methoden vaak erg ingewikkeld. In dit proefschrift heb ik de mogelijkheid onderzocht om eiwitkristallen te groeien met behulp van een eenvoudige opstelling die diffusiebepaalde groei mogelijk maakt. In deze configuratie is alles als het ware omgekeerd, waarbij het eiwit kiemt en uitgroeit bovenin een afgesloten groeicel die tot aan de top is gevuld met de kristallisatieoplossing. Deze "ceiling" (= plafond) kristallisatiemethode maakt gebruik van de zwaartekracht om diffusie tijdens de kristalgroei uit te sluiten, wat stukken eenvoudiger is dan bijvoorbeeld gebruik te maken van microgravitatie. Deze *ceiling* aanpak, heb ik gedetailleerd beschreven in hoofdstuk twee. Toepassing van de kristallisatiemethode voor een aantal model-eiwitkristallen resulteerde in een significante verbetering van de resolutie gemeten met behulp van röntgendiffractie. In enkele gevallen werd zelfs het huidige wereldrecord verbroken. Ook zijn de ceilingkristallen groter, zuiverder en hebben ze een betere röntgendiffractiekwaliteit dan hun *batch* tegenhangers gegroeid op de bodem van de cel. Hoofdstuk drie behandelt de tijdsafhankelijke verandering van het concentratieprofiel van de opgeloste stof tijdens de groei van kristallen. Dit heb ik onderzocht door gebruik te maken van microscopische en interferometrische experimenten gecombineerd met numerieke simulaties. Deze synergie geeft een gedetailleerd inzicht in de convectiestromen en depletie van de oplossing en hun invloed op de groei van zowel de ceiling als de batch kristallen. Terwijl de microscopische waarneming informatie geeft over de

vorm van de gegroeide kristallen, geeft het gebruik van een Mach-Zehnder interferometer inlichting over de tijd- en plaatsafhankelijke veranderingen van de concentratie opgeloste stof in de oplossing tijdens hun groei. Door een aantal opeenvolgende interferogrammen, ieder met een faseverschuiving van een kwart golflengte opgenomen, te verwerken met een geschikt algoritme wordt de ruimtelijke verdeling van de brekingsindex van de oplossing berekend. Gebruikmakend van het verband tussen brekingsindex en concentratie volgt hieruit nauwkeurig het concentratieprofiel. De gemeten concentratieprofielen, voor kristallen, zowel bovenin als onderin de groeicel, werden gevalideerd met behulp van numerieke simulaties waarbij gebruik werd gemaakt van het FLEX softwarepakket. De resultaten tonen de ontwikkeling en expansie van de stagnante depletiezone bij ceilinggroei, terwijl convectiepluimen omhoogstijgen vanaf de batchkristallen. De ontwikkeling van de depletiezone is afhankelijk van de afmetingen van de groeicel, de oververzadiging en de diffusiecoëfficient van de te kristalliseren stof. Hoofdstuk vier omvat een systematische studie van de invloed van onzuiverheden op eiwitkristallisatie zowel in aanwezigheid als in afwezigheid van convectiestromen. Dit gebeurde door ceiling- en batchkristallen gelijktijdig gegroeid in dezelfde cel te vergelijken. De inbouw van onzuiverheden in een kristal wordt zowel bepaald door hun segregatiecoefficiënt als door het massatransport in de oplossing. Voor de meeste van de onderzochte onzuiverheden was het verschil tussen de ceiling- en de batchkristallen zoals verwacht. Ceilingkristallisatie bleek vooral gunstig voor onzuiverheden die gemakkelijk inbouwen in het kristal. In tegenstelling tot wat vaak in de literatuur wordt aangenomen, vond ik dat de lage groeisnelheid tijdens de ceilinggroei resulteerde in een veel geringere inbouw van grote, heterogene, onzuiverheidmoleculen. Bovendien waren de ceilingkristallen in alle onderzochte gevallen qua rÃűntgendiffractiekwalitateit beter dan hun batch tegenhangers gegroeid in aanwezigheid van convectiestromen. Door fluorescent-gelabelde eiwitmonomeren als additief toe te voegen tijdens de groei van diverse soorten eiwitkristallen kon hun groeigeschiedenis en symmetrie worden vastgelegd door hun optische eigenschappen te registreren met behulp van polarisatiemicroscopie en confocale fluorescentiemicroscopie. Dit heb ik beschreven in hoofdstuk vijf. Voor eiwitkristallografen is dit belangrijk omdat ze met deze methoden gemakkelijk onderscheid kunnen maken tussen eiwitkristallen en zoutkristallen in dezelfde oplossing. Daarnaast geeft deze aanpak gedetailleerde informatie over het groeigedrag van de kristallen en de verdeling van de onzuiverheden in de kristallen. We vonden dat de optische eigenschappen, de inbouw en verdeling van de fluorescent-gelabelde additieven in de eiwitkristallen sterk varieerde voor de verschillende additief-gastheer systemen. Hieruit blijkt dat de inbouw van onzuiverheden in kristallen een verre van eenvoudige kwestie is. Tenslotte beschrijf ik in hoofdstuk zes een praktische kit die het toepassen van de ceilingmethode vergemakkelijkt. Ondanks het heel kleine volume van de oplossing per experiment, voorkomt de opstelling verdamping van het oplosmiddel en kunnen kristallen van voldoende grootte gegroeid worden, zodat ze optimaal geschikt zijn voor röntgen-

diffractieonderzoek. Zwaartekracht wordt altijd als schuldige beschouwd die de groei van grote en perfecte macromoleculaire kristallen bemoeilijkt, omdat ze convectiestromen veroorzaakt. Dit proefschrift toont door middel van experimenten en simulaties aan dat de zwaartekracht een positieve uitwerking kan hebben op de groei van eiwitkristallen, mits men de ceilingconfiguratie op de juiste wijze gebruikt. Ik laat hier zien dat het dillemma van de convectiestromen kan worden overwonnen door gebruik te maken van de ceiling methode die van de vijand "gravitatie" een vriend maakt. Als ik het concept uitgewerkt in dit proefschrift in één zin zou samenvatten, luidt het: "*hou het eenvoudig*".

Bibliography

[1] JC Kendrew, G Bodo, HM Dintzis, RG Parrish, H Wyckoff, DC Phillips, and et al. A three-dimensional model of the myoglobin molecule obtained by x-ray analysis. *Nature*, 181(4610):662–666, 1958.

[2] D Henry, N Eby, J Goodge, and D Mogk. X-ray reflection in accordance with bragg's law, 2012.

[3] PM B Piccoli, TF Koetzle, and AJ Schultz. Single crystal neutron diffraction for the inorganic chemist a practical guide. *Comments on Inorganic Chemistry*, 28(1-2):3–38, 2007. doi: 10.1080/02603590701394741.

[4] J Kern, R Alonso-Mori, R Tran, J Hattne, RJ. Gildea, and et al. Simultaneous femtosecond x-ray spectroscopy and diffraction of photosystem ii at room temperature. *Science*, 340(6131):491–495, 2013.

[5] L Redecke, K Nass, DP DePonte, TA. White, D Rehders, and et al. Natively inhibited trypanosoma brucei cathepsin b structure determined by using an x-ray laser. *Science*, 339(6116):227–230, 2013.

[6] G Rhodes. *Crystallography Made Crystal Clear*. Academic Press, 1 edition, 1993.

[7] AGW Leslie. imosflm, version 1.0. 4. *MRC-LMB, Cambridge, UK*, 2009.

[8] MD Winn, CC Ballard, KD Cowtan, EJ Dodson, P Emsley, PR Evans, RM Keegan, EB Krissinel, AGW Leslie, and A McCoy. Overview of the ccp4 suite and current developments. *Acta Crystallographica Section D: Biological Crystallography*, 67(4):235–242, 2011.

[9] P Emsley, B Lohkamp, WG Scott, and K Cowtan. Features and development of coot. *Acta Crystallographica Section D: Biological Crystallography*, 66(4):486–501, 2010.

[10] A McPherson. *Crystallization of Biological Macromolecules*. Cold Spring Harbor Laboratory Press, New York, 1999.

[11] NE Chayen. Comparative studies of protein crystallization by vapour diffusion and microbatch techniques. *Acta Crystallogr. D*, 54:8–15, 1998.

[12] A Hampel, M Labanauskas, PG Connors, L Kirkegard, UL Rajbhandary, PB Sigler, and RM Bock. Single crystals of transfer rna from formylmethionine and phenylalanine transfer rna's. *Science (New York, NY)*, 162(860):1384, 1968.

[13] JD Bernal and D Crowfoot. X-ray photographs of crystalline pepsin. *Nature*, 133(3369):794–795, 1934.

[14] A McPherson. Current approaches to macromolecular crystallization. *European Journal of Biochemistry*, 189(1):1–23, 2005.

[15] BR Thomas, AA Chernov, PG Vekilov, and DC Carter. Distribution coefficients of protein impurities in ferritin and lysozyme crystals self-purification in microgravity. *Journal of Crystal Growth*, 211(1):149–156, 2000.

[16] PWG Poodt. *Suppression of convection during protein crystal growth*. PhD thesis, Radboud University Nijmegen, 2008.

[17] DG Vlachos and KF Jensen. The roles of supersaturation, terrace width, and impurities on the formation of macrosteps on crystal surfaces using the terrace-ledge-kink model. *Surface Science*, 262(3):359–370, 1992.

[18] PG Vekilov, BR Thomas, and F Rosenberger. Effects of convective solute and impurity transport in protein crystal growth. *The Journal of Physical Chemistry B*, 102(26):5208–5216, 1998.

[19] YI Kwon, B Dai, and JJ Derby. Assessing the dynamics of liquid-phase solution growth via step growth models: From bcf to fem. *Progress in Crystal Growth and Characterization of Materials*, 53(3):167–206, 2007.

[20] BR Thomas and AA Chernov. Acetylated lysozyme as impurity in lysozyme crystals: constant distribution coefficient. *Journal of crystal growth*, 232(1):237–243, 2001.

[21] F Rosenberger, PG Vekilov, M Muschol, and BR Thomas. Nucleation and crystallization of globular proteins: what we know and what is missing. *Journal of crystal growth*, 168(1):1–27, 1996.

[22] W Littke and C John. Materials: protein single crystal growth under microgravity. *Science (New York, NY)*, 225(4658):203, 1984.

[23] A McPherson. Virus and protein crystal growth on earth and in microgravity. *Journal of Physics D: Applied Physics*, 26(8B):B104, 1993.

[24] A Yonath, J Müssig, and HG Wittmann. Parameters for crystal growth of ribosomal subunits. *Journal of cellular biochemistry*, 19(2):145–155, 1982.

[25] F Otalora, JA Gavira, JD Ng, and JM Garcia-Ruiz. Counterdiffusion methods applied to protein crystallization. *Progress in Biophysics and Molecular Biology*, 101(1-3):26–37, 2009.

[26] C Biertumpfel, J Basquin, D Suck, and C Sauter. Crystallization of biological macromolecules using agarose gel. *Acta Crystallographica Section D: Biological Crystallography*, 58(10):1657–1659, 2002.

[27] TY Miller, X He, and DC Carter. A comparison between protein crystals grown with vapor diffusion methods in microgravity and protein crystals using a gel liquid-liquid diffusion ground-based method. *Journal of Crystal Growth*, 122(1):306–309, 1992.

[28] LJ DeLucas, MM Long, KM Moore, WM Rosenblum, TL Bray, and et al. Recent

results and new hardware developments for protein crystal growth in microgravity. *Journal of Crystal Growth*, 135(1):183–195, 1994.

[29] NI Wakayama. Effects of a strong magnetic field on protein crystal growth. *Crystal growth & design*, 3(1):17–24, 2003.

[30] N Ramachandran and FW Leslie. Using magnetic fields to control convection during protein crystallizationanalysis and validation studies. *Journal of Crystal Growth*, 274(1):297–306, 2005.

[31] PWG Poodt, MCR Heijna, K Tsukamoto, WJ de Grip, PCM Christianen, and et al. Suppression of convection using gradient magnetic fields during crystal growth of $niso_4$ $6h_2o$. *Applied Physics Letters*, 87(21), 2005. 985FM.

[32] PWG Poodt, MCR Heijna, PCM Christianen, WJP van Enckevort, WJ de Grip, K Tsukamoto, JC Maan, and E Vlieg. Using gradient magnetic fields to suppress convection during crystal growth. *Crystal Growth & Design*, 6(10):2275–2280, 2006. 091LR.

[33] MCR Heijna, PWG. Poodt, K Tsukamoto, WJ de Grip, PCM Christianen, JC Maan, JLA Hendrix, WJP van Enckevort, and E Vlieg. Magnetically controlled gravity for protein crystal growth. *Applied Physics Letters*, 90(26), 2007. 184FC.

[34] DE McRee. *Practical Protein Crystallography*. Academic Press, San Diego, 1993.

[35] NE Chayen, PD Shaw Stewart, and DM Blow. Microbatch crystallization under oil: a new technique allowing many small-volume crystallization trials. *Journal of Crystal Growth*, 122(1):176–180, 1992.

[36] B Rupp and J Wang. Predictive models for protein crystallization. *Methods*, 34(3):390–407, 2004.

[37] R Savino and R Monti. Oscillatory marangoni convection in cylindrical liquid bridges. *Physics of Fluids*, 8:2906, 1996.

[38] EH Snell, A Cassetta, JR Helliwell, TJ Boggon, NE Chayen, and et al. Partial improvement of crystal quality for microgravity-grown apocrustacyanin c1. *Acta Crystallographica Section D: Biological Crystallography*, 53(3):231–239, 1997.

[39] P Baldock, V Mills, and PS Stewart. A comparison of microbatch and vapour diffusion for initial screening of crystallization conditions. *Journal of Crystal Growth*, 168(1):170–174, 1996.

[40] PWG Poodt, MCR Heijna, A Schouten, P Gros, WJP Van Enckevort, and E Vlieg. Simple geometry for diffusion limited protein crystal growth: harnessing gravity to suppress convection. *Crystal Growth and Design*, 9(2):885–888, 2008.

[41] R Giege, AC Dock, D Kern, B Lorber, JC Thierry, and D Moras. The role of purification in the crystallization of proteins and nucleic-acids. *Journal of Crystal Growth*, 76(3):554–561, 1986. E4727.

[42] BR Thomas, PG Vekilov, and F Rosenberger. Heterogeneity determination and purification of commercial hen egg-white lysozyme. *Acta Crystallographica Section*

D: Biological Crystallography, 52(4):776–784, 1996.

[43] A McPherson, A Greenwood, and J Day. The effect of microgravity on protein crystal growth. *Adv. Space Res.*, 11:343– 356, 1991.

[44] EH Snell and JR Helliwell. Macromolecular crystallization in microgravity. *Reports on Progress in Physics*, 68(4):799, 2005.

[45] T Reichhardt. Expensive space crystal programme has produced little of scientific value, says panel. *Nature*, 404:114., 2000.

[46] LJ De Lucas. Protein crystallization - is it rocket science? *Drug Discov. Today*, 6:734–744, 2001.

[47] MM Roberts, JYY Heng, and DR Williams. Protein crystallization by forced flow through glass capillaries: Enhanced lysozyme crystal growth. *Crystal Growth & Design*, 10(3):1074ï£¡1083, 2010.

[48] J M Garcia-Ruiz. The uses of crystal growth in gels and other diffusing-reacting systems. *Key Eng. Mater.*, 58:87–106, 1991.

[49] SX Lin, M Zhou, A Azzi, G.-J Xu, NI Wakayama, and M Ataka. Magnet used for protein crystallization: Novel attempts to improve the crystal quality. *Biochem. Biophys. Res. Commun.*, 275:274–278, 2000.

[50] I Rayment. Small-scale batch crystallization of proteins revisited: An underutilized way to grow large protein crystals. *Structure*, 10:147–151, 2002.

[51] I Reviakine, DK Georgiou, and PG Vekilov. Capillarity effects on crystallization kinetics: insulin. *Journal of the American Chemical Society*, 125(38):11684–11693, 2003.

[52] Number 4 Collaborative Computational Project. The ccp4 suite: programs for protein crystallography. *Acta Crystallogr. D*, 50:760–763, 1994.

[53] AJ McCoy, RW Grosse-Kunstleve, PD Adams, MD Winn, LC Storoni, and RJ Read. Phaser crystallographic software. *J. Appl. Cryst.*, 40:658–674, 2007.

[54] K Waizumi, M Plomp, and WJP van Enckevort. Atomic force microscopy studies on growing surfaces of bovine insulin crystals. *Colloids and Surf. B: Biointerfaces*, 30:73–86, 2003.

[55] CM Yip, MR Defelippis, BH Frank, Brader ML, and MD Ward. Structural and morphological characterization of ultralente insulin crystals by atomic force microscopy: Evidence of hydrophobically driven assembly. *Biophys. J.*, 75:1172–1179, 1998.

[56] GD Smith, WA Pangborn, and RH Blessing. The structure of t6 bovine insulin. *Acta Crystallogr. D*, 61:1476–1482, 2005.

[57] CG Frankaer, MV Knudsen, K Noren, E Nazarenko, K Stahl, and P Harris. The structures of t6, t3r3 and r6 bovine insulin: combining x-ray diffraction and absorption spectroscopy. *Acta Crystallographica Section D: Biological Crystallography*, 68(10):1259–1271, 2012.

[58] C Sauter, F Otalora, JA Gavira, O Vidal, R Giege, and JM Garcia-Ruiz. Structure

of tetragonal hen egg-white lysozyme at 0.94 a from crystals grown by the counter-diffusion method. *Acta Crystallographica Section D: Biological Crystallography*, 57(8):1119–1126, 2001.

[59] RFP Grimbergen, ES Boek, H Meekes, and P Bennema. Explanation for the supersaturation dependence of the morphology of lysozyme crystals. *Journal of crystal growth*, 207(1):112–121, 1999.

[60] K Harata and T Akiba. Structural phase transition of monoclinic crystals of hen egg-white lysozyme. *Acta Crystallogr. D*, 62:375–382, 2006.

[61] K Harata, Y Abe, and M Muraki. Crystallographic evaluation of internal motion of human alpha-lactalbumin refined by full-matrix least-squares method. *J. Mol. Biol.*, 287:347–358, 1999.

[62] C Vonrhein, C Flensburg, P Keller, A Sharff, O Smart, W Paciorek, T Womack, and G Bricogne. Data processing and analysis with the auto proc toolbox. *Acta Crystallogr. D*, 67:293–302, 2011.

[63] B Dam and WJP van Enckevort. On the formation of etch grooves around stress fields due to inhomogeneous impurity distribution in kdp single crystals. *Journal of Crystal Growth*, 51(3):607–623, 1981.

[64] T Kuroda. The marangoni effect and its artistic applicaton. *Forma*, 15:203–204, 2000.

[65] RM Bill, PJ Henderson, S Iwata, ER Kunji, H Michel, R Neutze, and et al. Overcoming barriers to membrane protein structure determination. *Nat. Biotechnol.*, 29:335–340, 2011.

[66] AA Chernov and EI Givargizov. *Modern crystallography III: crystal growth*, volume 169. Springer-Verlag Berlin, 1984.

[67] Hong Lin, Dimiter N Petsev, S-T Yau, Bill R Thomas, and Peter G Vekilov. Lower incorporation of impurities in ferritin crystals by suppression of convection: modeling results. *Crystal Growth & Design*, 1(1):73–79, 2001.

[68] PWG Poodt, M Heijna, A Schouten, P Gros, WJP van Enckevort, and E Vlieg. Simple geometry for diffusion limited protein crystal growth: Harnessing gravity to suppress convection. *Cryst. Growth & Design*, 9:885–888, 2009.

[69] A Adawy, E Rebuffet, S Tornroth-Horsefield, de Grip WJ, WJP van Enckevort, and E Vlieg. High resolution protein crystals using an efficient convection-free geometry. *Crystal Growth & Design*, 13:775–781, 2013.

[70] G Dhanaraj, K Byrappa, V Prasad, and M Dudley. Crystal growth techniques and characterization: An overview. *Springer Handbook of Crystal Growth*, pages 759–794, 2010.

[71] FA Jenkins and HE White. Fundamentals of optics: Fourth edition; bearing dates of 1937, 1950, 1957, and 1976; isbn: 0-07-032330-5, 1976.

[72] S. Verma and PJ Shlichta. Imaging techniques for mapping solution parameters,

growth rate, and surface features during the growth of crystals from solution. *Progress in Crystal Growth and Characterization of Materials*, 54(1-2):1–120, 2008.

[73] A-V Lugt. Signal detection by complex spatial filtering. *Information Theory, IEEE Transactions on*, 10(2):139–145, 1964.

[74] J Schmit and K Creath. Extended averaging technique for derivation of error-compensating algorithms in phase-shifting interferometry. *Applied Optics*, 34(19):3610–3619, 1995.

[75] L Duan and JZ Shu. The convection during naclo< sub> 3</sub> crystal growth observed by the phase shift interferometer. *Journal of Crystal Growth*, 223(1):181–188, 2001.

[76] T Kambe. *Elementary fluid mechanics*. World Scientific Pub Co Inc, 2007.

[77] TM FlexPDE. Finite element software, 2010.

[78] FCG De Marco, CR De Andrade, and EL Zaparoli. The no-slip boundary condition in the stream function-vorticity formulation using the penalty method. *International communications in heat and mass transfer*, 30:495–504, 2003.

[79] PWG Poodt, PCM Christianen, WJP Enckevort, JC Maan, and E Vlieg. The critical rayleigh number in low gravity crystal growth from solution. *Crystal Growth and Design*, 8(7):2194–2199, 2008.

[80] RA Judge, EL Forsythe, and ML Pusey. The effect of protein impurities on lysozyme crystal growth. *Biotechnology and Bioengineering*, 59(6):776–785, 1998. 110TL.

[81] CL Caylor, I Dobrianov, C Kimmer, and RE Throne. Two photon fluorescence imaging of impurity distribution in protein crystals. *Physical review E*, 59(4):3831–3834, 1999.

[82] C. P. Lee and A. A. Chernov. Solutal convection around growing protein crystals and diffusional purification in space. *Journal of Crystal Growth*, 240(3ï£¡4):531–544, 2002.

[83] N Cabrera and DA Vermilyea. The growth of crystals from solution. *Growth and perfection of crystals*, pages 393–410, 1958.

[84] M Plomp, A McPherson, and AJ Malkin. Repair of impurity-poisoned protein crystal surfaces. *Proteins: Structure, Function, and Bioinformatics*, 50(3):486–495, 2003.

[85] K Kurihara, S Miyashita, G Sazaki, T Nakada, SD Durbin, H Komatsu, T Ohba, and K Ohki. Incorporation of impurity to a tetragonal lysozyme crystal. *Journal of crystal growth*, 196(2):285–290, 1999.

[86] A Vergara, B Lorber, C Sauter, R Giegé, and A Zagari. Lessons from crystals grown in the advanced protein crystallisation facility for conventional crystallisation applied to structural biology. *Biophysical chemistry*, 118(2):102–112, 2005.

[87] A Adawy, K Marks, WJ de Grip, WJP van Enckevort, and E Vlieg. The development of the depletion zone during ceiling crystallization: phase shifting interferometry and simulation results. *CrystEngComm*, 2013.

[88] RN Hall. Segregation of impurities during the growth of germanium and silicon. *The Journal of Physical Chemistry*, 57(8):836–839, 1953.

[89] JA Burton, RC Prim, and WP Slichter. The distribution of solute in crystals grown from the melt. part i. theoretical. *The journal of chemical physics*, 21:1987, 1953.

[90] JA Burton, ED Kolb, WP Slichter, and JD Struthers. Distribution of solute in crystals grown from the melt. part ii. experimental. *The journal of chemical physics*, 21:1991, 1953.

[91] D. C. Carter, K. Lim, J. X. Ho, B. S. Wright, P. D. Twigg, T. Y. Miller, J. Chapman, K. Keeling, J. Ruble, P. G. Vekilov, B. R. Thomas, F. Rosenberger, and A. A. Chernov. Lower dimer impurity incorporation may result in higher perfection of hewl crystals grown in microgravity - a case study. *Journal of Crystal Growth*, 196(2-4):623–637. 161YY.

[92] AA Chernov. Protein crystals and their growth. *Journal of structural biology*, 142(1):3–21, 2003. 675TJ.

[93] L Rong, H Komatsu, and S Yoda. Control of heterogeneous nucleation of lysozyme crystals by using poly-l-lysine modified substrate. *Journal of crystal growth*, 235(1):489–493, 2002.

[94] L Rong, T Yamane, and N Niimura. Measurement and control of the crystal growth rate of tetragonal hen egg-white lysozyme imaged with an atomic force microscope. *Journal of crystal growth*, 217(1):161–169, 2000.

[95] T. Geoff G. Battye, Luke Kontogiannis, Owen Johnson, Harold R. Powell, and Andrew G. W. Leslie. *iMOSFLM*: a new graphical interface for diffraction-image processing with *MOSFLM*. *Acta Crystallographica Section D*, 67(4):271–281, Apr 2011.

[96] Brian R Baker, Azim N Laiwalla, Jeong-Yeol Yoon, Javier Caï£¡avate, and Robin L Garrell. Adhesion and cohesion of mussel adhesive protein on glass and gold through protein removal studies. *Polym Mater Sci Eng*, 85:115–6, 2001.

[97] RA Judge, EL Forsythe, and ML Pusey. The effect of protein impurities on lysozyme crystal growth. *Biotechnology and bioengineering*, 59(6):776–785, 2000.

[98] EL Forsythe, A Nadarajah, and ML Pusey. Growth of (101) faces of tetragonal lysozyme crystals: measured growth-rate trends. *Acta Crystallographica Section D: Biological Crystallography*, 55(5):1005–1011, 1999.

[99] MCR Heijna, MJ Theelen, WJP van Enckevort, and E Vlieg. Spherulitic growth of hen egg-white lysozyme crystals. *The Journal of Physical Chemistry B*, 111(7):1567–1573, 2007.

[100] T Sawaura, D Fujii, M Shen, Y Yamamoto, K Wako, K Kojima, and M Tachibana. Characterization of dislocations in monoclinic hen egg-white lysozyme crystals by synchrotron monochromatic-beam x-ray topography. *Journal of Crystal Growth*, 318(1):1071–1074, 2011.

[101] Joseph R Lakowicz and Barry R Masters. *Principles of fluorescence spectroscopy*.

Springer, 3rd edition, 2008.

[102] RF Chen. Limited reaction of lysozyme with a fluorescent labeling agent. *Biochemical and Biophysical Research Communications*, 40(5):1117–1124, 1970.

[103] E Forsythe, A Achari, and Marc L Pusey. Trace fluorescent labeling for high-throughput crystallography. *Acta Crystallographica Section D*, 62(3):339–346, 2006.

[104] Y Iimura, I Yoshizaki, H Nakamura, S Yoda, and H Komatsu. Development of fluorescence label and con-focal laser scanning microscopy method for non-destructive local impurity distribution analysis in protein crystals. *Jpn. J. Appl. Phys.*, 42:5831–5836, 2003.

[105] T Matsui, G Sazakia, H Hondohc, Y Matsuurad, T Nakadac, and K Nakajimaa. Impurity effects of lysozyme molecules specifically labeled with a fluorescent reagent on the crystallization of tetragonal and monoclinic lysozyme crystals. *Journal of Crystal Growth*, 293:415–422, 2006.

[106] AES Van Driessche, G Sazaki, F Otalora, FM Gonzalez-Rico, P Dold, K Tsukamoto, and K Nakajima. Direct and noninvasive observation of two-dimensional nucleation behavior of protein crystals by advanced optical microscopy. *Crystal Growth Design*, 7(10):1980–1987, 2007. 217KZ.

[107] JP Sumida, EL Forsythe, and ML Pusey. Preparation and preliminary characterization of crystallizing fluorescent derivatives of chicken egg white lysozyme. *Journal of Crystal Growth*, 232(1):308–316, 2001.

[108] ZS Derewenda. Rational protein crystallization by mutational surface engineering. *Structure*, 12(4):529–535, 2004.

[109] AES Van Driessche, G Sazaki, G Dai, F Otalora, JA Gavira, T Matsui, I Yoshizaki, K Tsukamoto, and K Nakajima. Direct observation of adsorption sites of protein impurities and their effects on step advancement of protein crystals. *Crystal Growth and Design*, 9(7):3062–3071, 2009.

[110] SJ Wright and G Schatten. Confocal fluorescence microscopy and three-dimensional reconstruction. *Journal of electron microscopy techniques*, 18(1):2–10, 1991.

[111] S Sugio, A Kashima, S Mochizuki, M Noda, and K Kobayashi. Crystal structure of human serum albumin at 2.5 ÃĚ resolution. *Protein engineering*, 12(6):439–446, 1999.

[112] SD Durbin and G Feher. Crystal growth studies of lysozyme as a model for protein crystallization. *Journal of Crystal Growth*, 76(3):583–592, 1986.

[113] A Cvetkovic, AJJ Straathof, DN Hanlon, S Van der Zwaag, R Krishna, and LAM Van der Wielen. Quantifying anisotropic solute transport in protein crystals using 3d laser scanning confocal microscopy visualization. *Biotechnology and Bioengineering*, 86(4):389–398, 2004.

[114] F Dismer and J Hubbuch. A novel approach to characterize the binding orientation of lysozyme on ion-exchange resins. *Journal of Chromatography A*, 1149(2):312–320,

2007.

[115] P Dold, E Ono, K Tsukamoto, and G Sazaki. Step velocity in tetragonal lysozyme growth as a function of impurity concentration and mass transport conditions. *Journal of Crystal Growth*, 293(1):102–109, 2006.

[116] SD Durbin, WE Carlson, and MT Saros. In situ studies of protein crystal growth by atomic force microscopy. *Journal of Physics D: Applied Physics*, 26(8B):B128, 1993.

[117] MCR Heijna, WJP van Enckevort, and E Vlieg. Growth inhibition of protein crystals: A study of lysozyme polymorphs. *Crystal Growth and Design*, 8(1):270–274, 2007.

[118] H Hondoh, G Sazaki, S Miyashita, SD. Durbin, K Nakajima, and Yi Matsuura. Macrobond analysis of the macro- and micromorphology of monoclinic lysozyme crystal. *Crystal Growth Design*, 1(4):327–332, 2001.

[119] A Adawy, E van der Heijden, J Hekelaar, WJ De Grip, W van Enckevort, and E Vlieg. A comparative study of the impurity effects on protein crystallization using the ceiling method:diffusive *versus* convective crystal growth. to be published, 2013.

[120] L Bergeron, LF Filobelo, O Galkin, and PG Vekilov. Thermodynamics of the hydrophobicity in crystallization of insulin. *Biophysical journal*, 85(6):3935–3942, 2003.

[121] KA Majorek, PJ Porebski, A Dayal, MD Zimmerman, K Jablonska, AJ Stewart, M Chruszcz, and W Minor. Structural and immunologic characterization of bovine, horse, and rabbit serum albumins. *Molecular Immunology*, 52(3):174–182, 2012.

[122] A Bujacz. Structures of bovine, equine and leporine serum albumin. *Acta Crystallographica Section D: Biological Crystallography*, 68(10):0–0, 2012.

[123] CA Haskard and ECY Li-Chan. Hydrophobicity of bovine serum albumin and ovalbumin determined using uncharged (prodan) and anionic (ans-) fluorescent probes. *Journal of Agricultural and Food Chemistry*, 46(7):2671–2677, 1998.

[124] JM Garcia-Ruiz, LA Gonzalez-Ramirez, JA Gavira, and F Otalora. Granada crystallisation box: a new device for protein crystallisation by counter-diffusion techniques. *Acta Crystallographica Section D: Biological Crystallography*, 58(10):1638–1642, 2002.

[125] RC Stevens. High-throughput protein crystallization. *Current Opinion in Structural Biology*, 10(5):558–563, 2000.

[126] S Stolyarova, E Baskin, NE Chayen, and Y Nemirovsky. Possible model of protein nucleation and crystallization on porous silicon. *Physica Status Solidi a-Applications and Materials Science*, 202(8):1462–1466, 2005. 941HW.

[127] M Maruyama, N Shimizu, S Sugiyama, Y Takahashi, H Adachi, K Takano, S Murakami, T Inoue, H Matsumura, and Y Mori. Estimated effects of silicone glue on protein crystal growth. *Journal of Crystal Growth*, 312(19):2771–2774, 2010.

[128] NE Chayen. Methods for separating nucleation and growth in protein crystallisation.

Progress in Biophysics and Molecular Biology, 88(3):329–338, 2005.

List of Scientific Contributions

List of publications

1. Adawy A, Rebuffet E, Tornroth-Horsefield S, DeGrip WJ, van Enckevort WJP and Vlieg E, High resolution protein crystals using an efficient convection-free geometry. Cryst Growth Des 13:775-781 (2013).

2. Adawy A, Marks K, de Grip WJ, Van Enckevort W and Vlieg E, The development of the depletion zone during ceiling crystallization: phase shifting interferometry and simulation results. CrystEngComm 15:2275-2286 (2013).

3. Adawy A and Abdel-Fattah WI, An efficient biomimetic coating methodology for a prosthetic alloy. Materials Science and Engineering: C 33:1813-1818 (2013).

4. Adawy A, El-Bassyouni GT, Ibrahim M and Abdel-Fattah WI, Bio nano material: the third alternative, in Nanotechnology, ed by Govil JN. Studium Press LLC, Houston, pp. 27-49 (2012).

5. Abdel-Fattah WI, El-Sayed M, Talaat MS and Adawy A, Comparativestudy of Sr and Zn incorporation in the biomimetic coating of a prosthetic alloy. The open biomaterial journal 3:4-13 (2011).

6. Adawy A, Abdel-Fattah W, Talaat MS and E. E-SM, Biomimetic coating of a pre-calcified Ti-6Al-4V alloy. Open Medical devices 1:19-28 (2009).

To be submitted

7. Adawy A, van der Heijden E, Hekelaar J, De Grip WJ, van Enckevort W and Vlieg E, A Comparative study of the impurity effect on protein crystallization under diffusive and convective crystal growth.

8. Adawy A, van Enckevort W, de Grip WJ and Vlieg E, Illuminating protein crystal growth using fluorescent-labelled protein monomers.

9. Adawy A, Corbeek W, de Ronde E, de Grip WJ, van Enckevort W and Vlieg E, Ceiling kit for optimizing protein crystallization.

List of oral presentations

1. Diffusive or Convective Protein Crystal Growth? Does it really matter?! Belgian Symposium on Crystal Growth and Crystallization of Organic Compounds. 31/05/2013, Université Catholique de Louvain, Louvain-la-Neuve, Belgium.

2. Protein Crystal Growth on the Ceiling: A Terrestrial Alternative. In proceeding of: NWO CW Study group meeting Chemistry in Relation to Physics and Materials Sciences, Netherlands Organisation for Scientific Research. 04/03/2013, Veldhoven, The Netherlands.

3. An Efficient Convection-Free Geometry Effectuates the Growth of High Resolution Protein Crystals. 14*th* International Conference on the Crystallization of Biological Macromolecules. 23/09/2012, Huntsville, Alabama, USA.

4. Higher Resolution Protein Crystals using an Efficient Convection-Free Geometry. 4*th* European Conference on Crystal Growth (ECCG4) Crystallisation in Focus: from fundamentals to applications. 19/06/2012, University of Strathclyde, Glasgow, UK.

5. Growing the Best Protein Crystals. IMM colloquium. 28/02/2012, Radboud University Nijmegen, The Netherlands.

6. Towards High Resolution Protein Crystal Growth in Microgravity-Resembling Conditions. Jaarvergaderingen NVK/NVKG: A Structural View on Crystallization. 04/11/2011, Utrecht, The Netherlands.

7. Fast biomimetic coating of stainless steel implants. The 3*rd* international conference on environmental engineering (ASCEE-3). 14-16/04/ 2009, Faculty of engineering Ain Shams university, Cairo, Egypt.

List of poster presentations

1. HERCULES School, Grenoble, France 27/02/2014

2. RAMC meeting, Strasbourg, France, 8-11/09/2013
3. The international conference for crystallization of biological macromolecules 14, Huntsville, Alabama, USA, 23-29/09/2012
4. The international school of crystallography : macromolecular crystallography, Erice, Italy, 31/05-10/06/2012
5. CHAINS 2011, De Fabrique, Utrecht, The Netherlands, 28-30/11/2011
6. BACG 2011, University College London, United Kingdom, 10-12/07/2011
7. IMM symposium 2011, University Auditorium, Radboud University Nijmegen, The Netherlands, 16-17/05/2011
8. Scientific meeting on Chemistry related to Physics Material Sciences / Dutch Polymer Days, 14-15/03/2011
9. 1*st* Alexandria International Congress on Tissue Engineering, Bibliotheca Alexandrina, Alexandria, Egypt, 13-16/02/2009
10. New Curriculum for Management of Maxillofacial Deformities, Tempus Dental Day, Faculty of Dentistry, Ain Shams university, Cairo, Egypt, 20-21/01/2009
11. The Role of physics in the applications of the nanotechnology, British University in Cairo, Egypt, 17/01/2008
12. The interdisciplinary Italian/Egyptian workshop. Future Aspects of biomaterials in relation to tissue engineering. 13-15/02/2007
13. Environmental Biophysics, Cairo Satellite Meeting, Azhar Conference centre, Cairo, Egypt, 4-5/09/2005

Highlights

1. Ceiling Crystallization: A terrestrial alternative for microgravity protein crystal growth. IMM annual report 2011.

   http://www.ru.nl/publish/pages/526338/imm_annual_report_2011.pdf
2. Laat ze hangen die kristallen, dan groeien ze beter. 19/12/2012.

   http://www.ru.nl/actueel/nieuws-0/vm/laat-hangen/?IdxIdt=813549

3. Geen ballen maar kristallen. 21/12/2012.
   http://www.voxweb.nl
4. Suspend the Crystals, and They Grow Better 21/12/2012.
   http://www.sciencedaily.com/releases/2012/12/121221113949.htm
5. Hanging crystals grow without flaws. 28/12/2012.
   http://why.knovel.com/all-engineering-news/2152-hanging-crystals-grow-without-flaws.html
6. Met rust krijg je de fijnste kristalletjes. 12/01/2013. De Volkskrant, Wetenschap, Chemie, Reportage V5.

Biography

Alaa Adawy is an Egyptian academic researcher, who currently works at Radboud University Nijmegen. She was born in Al-Dammam, Kingdom of Saudi Arabia, in which she spent three years of her early childhood, before she returned with her family to their home country, Egypt. Alaa earned all her school and undergraduate education in Cairo[3], Egypt[4]. She completed her primary, preparatory and secondary education at English schools (Orman language school and later Yousuf El-Sebaie language school) in Heliopolis[5]. In September 1999, She started her undergraduate B.Sc. education at the Faculty of Science, Ain shams University[6], from which she graduated with honours (excellent 86.38%) in Biophysics, ranking the first among her colleagues in May 2003. For that she was awarded the medal of honour from the Egyptian ministry of higher Education and scientific research in March 2004, the certificate of appreciation from the Egyptian syndicate of scientific professions in August 2003 and the medal of the faculty of Science, Ain Shams University in April 2004. In September 2003, she started her academic career at the same University, where she got a permanent position as an academic assistant. In November 2003, she started a postgraduate programme in medical biophysics. To improve her teaching and soft skills, she attended several interpersonal skills courses, including effective communication and "the seven habits for more effective people". In 2006, she started her Master thesis project. In Egyptian Universities, the postgraduate student is responsible for writing the research project and propose it to possible supervisors, who may then approve the proposal and accept the student registration for M.Sc or PhD thesis's. Her thesis, entitled "surface modification and biophysical characterisation of a prosthetic alloy" was a research study on bio-mimetic coating of metallic implants, which are used in joint replacement. In 2008, she defended her master thesis in public and she got promoted to assistant lecturer. In July 2009, She relocated to Nijmegen, the Netherlands, where

[3] http://wikitravel.org/en/Cairo
[4] http://wikitravel.org/en/Egypt
[5] http://en.wikipedia.org/wiki/Heliopolis_(Cairo_Suburb)
[6] http://www.shams.edu.eg/

she started a PhD project at the Institute for Molecules and Materials, Radboud University. The project, described in this thesis, was an interdisciplinary research combining crystal growth, biochemistry, physical optics and numerical simulations. Thanks to the open-minded Dutch scientific atmosphere, she collaborated with other research groups in the Netherlands, as well as in Spain and Sweden.

"Science" is definitely not the entire life of Alaa. She spends her free time with her family and friends. She also enjoys very much reading Arabic poetry and has her humble attempts into this field[7]. She also has other hobbies such as singing, knitting, crochet and sewing.

[7] http://alaa2000s.wordpress.com/